Doctoral Dissertation

Pectate-Based Eco-Friendly Polymer as a High-performing Binder for Lithium-Ion Battery Electrodes

Li Ze

Supervisor: Noriyoshi Matsumi

Graduate School of Advanced Science and Technology

Japan Advanced Institute of Science and Technology

Materials Science

September 2025

Abstract

Li Ze (2220418)

The ongoing global transition toward sustainable energy has intensified research efforts into high-performance and environmentally benign energy storage systems. Lithium-ion batteries (LIBs), with their superior energy density and long cycling life, remain the dominant technology for a wide range of applications, including consumer electronics, electric vehicles (EVs), and grid-scale storage. However, the widespread use of environmentally harmful, non-water-soluble electrode binders, such as poly(vinylidene fluoride) (PVDF), raises significant concerns due to their toxicity, high processing costs, and limited recyclability. In response, the development of water-soluble, biodegradable binder materials has become a critical focus for high electrochemical performance of next-generation LIBs.

This research begins by establishing the foundational background of LIBs, emphasizing the crucial role of binders in ensuring electrode cohesion, structural integrity, and stable electrochemical behavior during long cycling. Traditional binders are reviewed in detail, followed by an in-depth discussion of recent advancements. The limitations of current binder materials motivate the development of pectate-based PIL binders proposed in this thesis.

1-allyl-3-methylimidazolium pectate ([AMIm][Pectate]) is synthesized by neutralizing polygalacturonic acid (pectic acid) with [AMIm][OH]. The obtained binder exhibits strong interfacial adhesion due to the abundant hydroxyl (-OH) groups on the pectate polymer backbone, which interact favorably with both graphite and conductive additives. Meanwhile, the imidazolium cation enhances Li^+ mobility, contributing to improved charge-transfer kinetics. Electrochemical testing of graphite anodes assembled with [AMIm][Pectate] demonstrates enhanced cycling stability and capacity retention compared to PVDF-based controls. Scanning electron microscopy (SEM) and X-Ray photoelectron spectroscopy (XPS) further confirm the binder's ability to maintain electrode integrity over long cycling.

The synthesis of [Choline][Pectate] is via the neutralization of pectic acid with choline hydroxide ([Choline][OH]). This binder is evaluated under even more demanding conditions, including high current densities (1 C, 2 C, 5 C) and full-cell configurations pairing graphite anodes with $LiNi_{1/3}Co_{1/3}Mn_{1/3}O_2$ (NCM) cathode. Compared to CMC-SBR binder, [Choline][Pectate] exhibits superior rate capability and coulombic efficiency, attributed to its enhanced ionic conductivity and mechanical robustness. Post-mortem analyses of cycled electrodes reveal minimal delamination and stable solid electrolyte interphase (SEI) formation, further validating its practical viability.

Finally, these findings not only demonstrate the electrochemical viability of [AMIm][Pectate] and [Choline][Pectate] as sustainable alternatives to non-water-soluble binders but also establish a versatile platform for ongoing binder innovation. The integration of pectate-derived polymer backbones with tunable ionic liquid components offers a promising pathway for the development of next-generation binder systems. Moreover, this work makes a significant contribution to the field of LIB materials by introducing a green, scalable, and high-performance binder strategy aligned with global sustainability objectives.

Keywords: Lithium-ion battery, Graphite anode, Binder, Water soluble, High electrochemical performance.

Referee-In-Chief: Professor Noriyoshi Matsumi
Japan Advanced Institute of Science and Technology

Referees: Professor Toshiaki Taniike
Japan Advanced Institute of Science and Technology

Professor Kazuma Gotoh
Japan Advanced Institute of Science and Technology

Professor Kosuke Okeyoshi
Japan Advanced Institute of Science and Technology

Professor Akinori Takasu
Nagoya Institute of technology

Acknowledgements

As I stand at the completion of my doctoral journey, memories of my early days in Japan remain vivid. Arriving amid an epidemic, with limited knowledge of Japanese, I was filled with uncertainty and apprehension. Yet, thanks to the immense support I received from many individuals in JAIST, I was able to find stability and gradually adapt to this new chapter of life.

First and foremost, I would like to express my deepest gratitude to my supervisor, Professor Matsumi. His insightful guidance shaped the direction of my research, and his patience extended even to the smallest concerns, always offering thoughtful solutions. Professor Matsumi's gentle and supportive mentorship transformed my view of research: what once felt like a series of tedious tasks and a mere academic requirement evolved into a meaningful and passionate pursuit. The academic freedom he granted me inspired deep reflection on my field, my future, and my life aspirations.

I am sincerely thankful to my lab members: Zhou Lihang for his generous transportation assistance, Liu Zhaohan for experimental collaboration, Anusha for easing my transition into lab life, Patra for technical support, Sumala for introducing me to Indian cuisine, Bharat for mentoring my experiments and publications, Sameer for his constant encouragement, and Sai for his timely expertise. To all my lab colleagues – even those with whom I interacted less frequently – your kindness and willingness to help are deeply appreciated.

I would also like to thank my friends in JAIST: Luo Yufeng, Xu Xiujuan, Ke Bingchen, Yuan Chenyuhe, Thanh, and Tan Yanqiu. The experiences we shared and the joyful memories from our travels will remain cherished forever.

Finally, I extend my heartfelt gratitude to my family for their unwavering support throughout this academic journey. Your love and encouragement have been my foundation and strength.

Li Ze

Graduate School of Advanced Science and Technology

Japan Advanced Institute of Science and Technology

September 2025

Content

Chapter 1 General Introduction

1.1 Introduction to the background and influence of energy storage device-lithium-ion battery (LIB)

Energy storage plays a crucial role in modern energy systems, supporting a wide range of renewable energy sources, including hydropower, wind, solar, geothermal, and biomass energy.[1,2] To transform these intermittent and unstable energy sources into reliable, continuous 24-hour electricity supplies,[3] various energy storage technologies have been widely applied in both everyday life and commercial applications.[4] These technologies include batteries, hydrogen storage, supercapacitors, thermal storage, and pumped hydro storage. Among these, batteries stand out as essential electrochemical energy storage systems due to their high energy density and exceptional scalability,[5,6] making them more critical than ever in enabling efficient, flexible, and sustainable energy solutions.[7] The chronological evolution of battery development began with lead-acid and followed by nickel-cadmium (Ni-Cd), nickel-metal hydroxide (Ni-MH), lithium-ion, sodium-sulfur (Na-S), flow, and sodium-nickel-chloride ($NaNiCl_2$) batteries.[8]

(1) Lead-acid battery

Lead-acid battery, invented by Gaston Planté in 1860, marked a major milestone in energy storage technology. Planté's early design involved two lead (Pb) plate electrodes submerged in sulfuric acid, with energy storage achieved through the redox reactions of Pb and PbO_2.[9] Over the next century, incremental advancements enhanced their functionality, although large-scale adoption remained limited. However, the 1960s and 1970s saw key breakthroughs in battery sealing and maintenance technology, which significantly improved performance and reliability,

paving the way for widespread applications.[10] Lead-acid batteries became popular due to their low production and maintenance costs, robust safety profile, and stable electrochemical performance. Despite these strengths, challenges persist, particularly those related to Pb/Pb-alloy corrosion, which affects electrode longevity and battery efficiency. Addressing this corrosion remains critical to optimizing the long-term viability of lead-acid systems, especially as they continue to play a significant role in applications ranging from automotive to grid-scale energy storage.[11]

(2) Ni-Cd battery

Ni-Cd battery was invented by Waldemar Jungner in 1899. His design utilized nickel hydroxide as cathodes and metallic Cd as anodes, with alkaline electrolytes to facilitate charge-discharge reactions. This invention marked a significant advancement in battery technology, making it possible to power various portable electronic devices in everyday life. However, during the early 20th century, the widespread application of Ni-Cd batteries was hindered by their high production cost and the toxic nature of Cd, which posed environmental and health risks.[12] It was not until the 1980s that Ni-Cd battery market expanded rapidly, driven by improvements in manufacturing techniques, excellent charge-discharge efficiency, and reliable specific capacity. In recent years, increasing attention has been directed toward the recycling and safe disposal of Ni-Cd batteries due to growing environmental concerns.[13] In 2006, European Union established regulations with a target to recycle 75% of used Ni-Cd batteries by 2016.[14] Meanwhile, Ni-Cd market has been gradually declining, as Ni-MH batteries and LIBs have gained popularity due to their higher energy density, reduced environmental impact, and the absence of "memory effect" that affects Ni-Cd batteries.

(3) Ni-MH battery

Ni-MH battery was first commercialized in the 1980s, with the primary goal of replacing the toxic Cd electrode used in Ni-Cd batteries. This development was based on the discovery that certain metal alloys could effectively store hydrogen, enabling a safer and more environmentally friendly alternative.[15] Ni-MH batteries are known for their ability to maintain high capacity and long cycling endurance, even under harsh conditions. Although they are less cost-competitive compared to lead-based batteries, Ni-MH batteries offer distinct advantages, including fast charging capability and stable discharge performance, which lead-based batteries cannot match.[16] Today, Ni-MH batteries are widely used in electric vehicles (EVs) and hybrid electric vehicles (HEVs). Their popularity in these applications is attributed to their flexible cell packaging, and high operational voltage, which make them well-suited for automotive power systems.[17]

(4) LIB

The first-generation LIB could date back to the 1970s when Whittingham[18] utilized titanium disulfide (TiS_2) as the cathode and lithium metal as the anode. After nearly two decades of development, Sony[19] successfully commercialized LIBs in 1991, replacing the positive electrode with lithium cobalt oxide ($LiCoO_2$). LIBs offer several advantages, including high energy density, long cycle life, lightweight design, and no memory effect-unlike Ni-Cd batteries. These benefits have led to their widespread adoption in EVs. By 2016, the global LIB market had surpassed USD 20 billion and was projected to reach USD 60 billion by 2025.[20] However, due to their high capacity and energy absorption, LIBs are susceptible to thermal runaway, posing safety risks. Consequently, research efforts are now focused on developing LIBs with safer and more environmentally friendly materials to enhance sustainability and security.[21]

(5) Na-S battery

The foundation of Na-S batteries was laid by Joe Kummer and Neil Weber in 1966 with the goal of reducing dependence on fossil fuels and lowering energy storage costs.[22] These batteries operate at high temperatures between 300 °C and 350 °C, where sulfur cathodes undergo electrochemical transformations into Na_2S, Na_2S_2 and Na_2S_3, each with different energy storage capacities.[23] Na-S batteries are composed of earth-abundant materials, making them environmentally friendly and economically advantageous. Due to these benefits, they are considered a promising alternative to other battery types and deserve further research and development.[24] Although NaS batteries have a high theoretical capacity of 1672 mAh/g, their elevated operating temperature limits their application in EVs and electrical grids. As a result, current research efforts focus on enabling operation at room temperature while maintaining high-capacity stability and efficiency.[25]

(6) Flow battery

The first flow battery, utilizing an iron-chromium redox system for energy storage, was proposed by Lawrence H. Thaller of NASA.[26,27] Later, in 1986, Maria Skyllas-Kazacos and her team patented the all-vanadium redox flow battery, which significantly improved efficiency and service life while preventing electrolyte cross-contamination.[28] Unlike traditional batteries, flow batteries store and convert energy using active materials contained in external electrolyte tanks rather than within solid electrodes.[29] This working mechanism allows flow batteries to achieve megawatt-hour (MWh)-scale energy storage, with capacity determined by the size of electrolyte tanks.[26] Despite their potential for large-scale power grid applications, flow batteries face challenges such as high costs and low energy density, limiting their widespread industrialization. Therefore, developing cost-effective alternative materials to replace existing components is significant for advancing these batteries from laboratory research to practical applications.[30]

(7) $NaNiCl_2$ battery

$NaNiCl_2$ battery, commonly known as ZEBRA battery, was developed in South Africa in the 1970s with the goal of enabling vehicle electrification at high operating temperatures.[31] The charge-discharge process occurs through an electrochemical reaction involving a molten sodium anode, a porous cathode structure containing NaCl and Ni, and solid ceramic electrolytes. Since Na is an abundant element on Earth, Na-based batteries offer cost-effective alternatives for next-generation energy storage systems.[32] Moreover, due to their suitable redox potential and long cycling stability, $NaNiCl_2$ batteries have become attractive candidates for replacing other battery technologies. However, high temperature cycling leads to the formation of resistance layers on the electrode surface, hindering battery performance and further development.[33] Addressing these challenges is crucial for enhancing the efficiency and scalability of $NaNiCl_2$ batteries for practical applications.

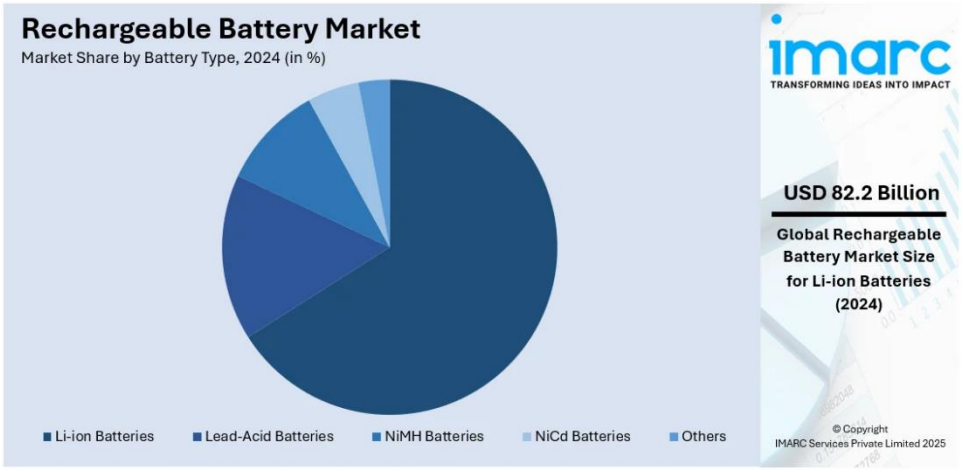

Figure 1.1. Market share of rechargeable batteries by type in 2024.[34]

In 2024, the market share of rechargeable batteries follows this order: lithium-ion, lead-acid, Ni-MH, Ni-Cd, and other types of batteries, as shown in **Figure 1.1**. Notably, the market dominance of LIBs not only exceeded expectations but also reached USD 82.2 billion, driven by approximately 35 years of exponential growth. LIBs now hold the largest market share at

65.8%, primarily due to their increasing capacity and portability.[34] Therefore, research focused on enhancing the efficiency and sustainability of LIBs has become more important than ever.

1.2 Important components in LIBs

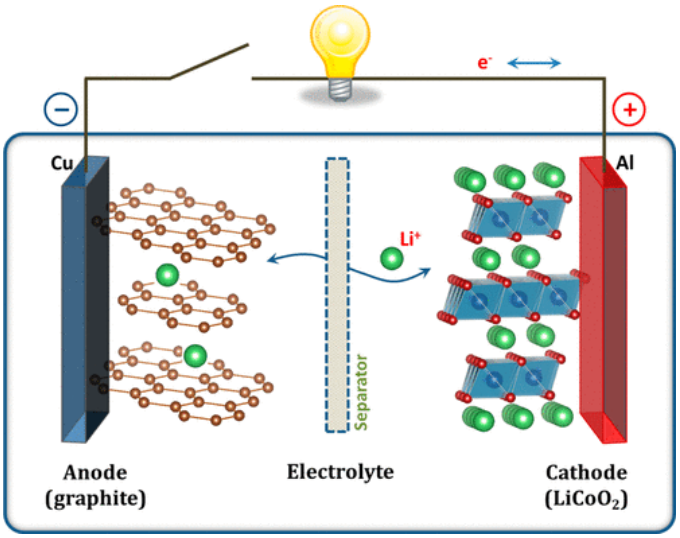

Figure 1.2. Illustration of the first LIB ($LiCoO_2$/Li^+ electrolyte/graphite).[35]

Typically, LIBs mainly consist of cathode, anode, electrolyte, separator, and current collectors (copper (Cu) and aluminum (Al)), as shown in **Figure 1.2**. Their working mechanism relies on an electrolyte that helps Li ion (Li^+) movement between the anode (reductant electrode) and the cathode (oxidant electrode), enabling the conversion of chemical energy within the cell and electrical energy outside the cell. During this process, current collectors provide a conductive pathway for electrons.[35] The separator plays a crucial role in preventing direct contact between the positive and negative electrodes, thereby avoiding short circuits. Its porous structure allows only Li^+ to pass through during charge-discharge process.[36] With the increasing global energy demand and the goal of achieving Net Zero emissions by 2050, the selection and application of recyclable and environmentally friendly materials in battery production are becoming increasingly urgent for the future of energy storage.[37]

1.2.1 Cathode

Transition metal oxides $LiMO_2$ (M = Co, Mn, Ni), are widely used as cathode materials in laboratory research due to their layered structure, which facilitates fast Li^+ mobility. However, challenges in cathode materials for LIB are still existing primarily due to limitations in low potential window, capacity, and stability.[38]

The commercialization of $LiCoO_2$ by Sony in 1991 marked a breakthrough, achieving a high energy density of 253 Wh/L. Following this, research efforts mainly focused on reducing material degradation at high potentials (e.g., 4.2 V).[39] $LiMnO_2$ is considered an environmentally friendly cathode material, but its structural instability and rapid capacity fading hinder its long cycling performance. To address this issue, current research focuses on structural modifications to enhance its durability.[40] Although $LiNiO_2$ offers lower cost and toxicity compared to $LiMnO_2$, its synthesis remains challenging, and Ni can influence Li^+ motion.[41] As a result, the industrial adoption of $LiNiO_2$ has been limited compared to $LiCoO_2$ and $LiMnO_2$.

To reduce production costs, lithium iron phosphate ($LiFePO_4$) was developed as a primary cathode material. While its specific capacity and ionic conductivity are not ideal, its superior safety and long service life have made it a key choice in EVs market.[42] Balancing cost, cycling life, safety, and stability has led to the development and commercialization of Ni-rich layered materials such as $LiNi_xMn_yCo_zO_2$ (NMC, x > 60%) and $LiNi_{0.8}Co_{0.1}Al_{0.1}O_2$ (NCA). Their widespread adoption has significantly contributed to the growth and advancement of LIB industry.[43,44]

1.2.2 Anode

Graphite, with theoretical capacity of 372 mAh/g, remains the dominant commercial anode material due to its unique hierarchical structure, which provides insertion sites for Li^+

and helps mitigate volume changes.[45] While graphite meets the energy storage needs of certain 3C devices, it no longer satisfies the growing demand for higher energy density and fast charge-discharge.[46] In order to achieve greater capacity, some researchers have turned their attention to silicon (Si), which has a remarkable theoretical capacity of 3,597 mAh/g. Despite its superior lithium storage ability, Si undergoes a drastic volume expansion of up to 300% during lithiation, leading to severe structural degradation and poor cycling stability. To address these challenges, various strategies have been explored, such as incorporating Si with low-expansion materials, downsizing Si to the nanoscale, and applying surface coatings to improve stability and performance.[47]

Lithium titanate ($Li_4Ti_5O_{12}$) was once considered as a promising anode material due to its excellent cycling stability and safety features. However, its adoption has declined over time by cause of its low energy density, which limits its suitability for high-energy applications.[48] Meanwhile, nanostructured metal oxide-based anodes, such as SnO_2, TiO_2, and transition metal oxides, have demonstrated specific capacities in the range of 800~1000 mAh/g, but they face challenges similar to those of Si.[49] Current research focuses not only on carbon-based materials, such as graphene, hard carbon and soft carbon, but also on improving existing anodes through innovative approaches. These include integrating Si with graphite, developing diverse nanostructured anodes, and optimizing binders and electrolytes for improved compatibility and performance.[50]

1.2.3 Electrolyte

The most common electrolyte composition in LIBs consists of dissolving Li salts-such as lithium hexafluorophosphate ($LiPF_6$), lithium tetrafluoroborate ($LiBF_4$), lithium perchlorate ($LiClO_4$)-into organic solvents like ethylene carbonate (EC), dimethyl carbonate (DMC), diethyl carbonate (DEC), and ethyl methyl carbonate (EMC). While this combination offers

high ionic conductivity, it suffers from low thermal stability and high flammability, leading to safety hazards that have resulted in loss of life and significant economic damage.[51] To enhance safety, researchers have introduced solid electrolyte interface (SEI)-forming additives, overcharge protection agents, and flame-retardant additives into liquid electrolytes. Additionally, alternative electrolytes have been explored, including gel polymer electrolytes (GPEs), solid-state electrolytes, and ionic liquids (ILs), which offer improved thermal stability and safety.[52]

GPEs combine the high ionic conductivity of liquid electrolytes with the mechanical robustness of polymers, offering improved safety.[53] While poly(ethylene oxide) (PEO) was the first-generation gel polymer, recent research has shown promising results with alternative materials such as polymethyl methacrylate (PMMA), poly(acrylic anhydride-2-methyl-acrylic acid-2-oxirane-ethyl ester-methyl methacrylate (PAMM), and cyanoethyl poly(vinyl alcohol) (PVA-CA).[54] Furthermore, inorganic Li^+ conductors, polymer/Li salt complexes, and organic-inorganic hybrid electrolytes have also demonstrated excellent performance.[55] ILs, composed of organic cations and organic/inorganic anions, offer high ionic conductivity at room temperature and low flammability, making them attractive alternatives to traditional electrolytes.[56] Despite significant progress in developing safer and more efficient electrolytes, achieving low-cost commercialization remains a major challenge.

1.2.4 Separator

Polyethylene (PE), polypropylene (PP), and PE/PP multilayer membranes are widely used as commercial separator materials due to their excellent mechanical strength and ease of production. However, they suffer from poor thermal stability (degrading above 150 °C) and vulnerability to Li dendrite penetration over long cycling, which can lead to fire hazards or explosions. To ensure separator integrity at high temperatures, researchers are focusing on

strategies to prevent shrinkage and mechanical failure.[57] These approaches include: (a) coating or blending polymer membranes with thermostable inorganic particles, (b) directly modifying polymer materials to enhance thermal resistance, and (c) developing solid-state electrolyte separators for improved safety. In addition to thermal stability, environmental sustainability and advanced manufacturing techniques are becoming increasingly influential in separator development. For instance, researchers have explored hydroxyapatite nanowires (HAP NW) for improved stability, nanocellulose fiber (NCF)/polypyrrole (PPy) composites for enhanced mechanical strength, and electrospun fiber membranes made from Poly(vinylidene fluoride) (PVDF) or PMMA, offering high porosity and improved electrolyte wettability.[58] These innovations aim to create safer, more efficient, and eco-friendly separators for next-generation LIBs.

1.2.5 Current collector

Current collectors are primarily composed of materials such as Cu, Al, Ni, Ti, stainless steel, and carbon fiber papers, and each selected based on their specific properties. Cu is commonly used for anodes, while Al is preferred for cathodes due to their high electrical conductivity, electrochemical stability, and cost-effectiveness. Ni is utilized for anodes, Ti is integrated into emerging electrode designs, and stainless steel is employed in Fe-containing anodes. Additionally, carbon-based materials are applied in specialized cases, such as Shafiei and Alpas-coated Sn anodes. While Cu and Al continue to dominate the global market as standard materials in conventional LIBs, new materials are under active investigation for next-generation applications, including solid-state and high-temperature batteries. The exploration of alternative current collectors aims to enhance durability, and adaptability to advanced energy storage technologies.[59]

Over the past three decades, researchers, scholars, and manufacturers have been working toward a common goal: developing next-generation LIBs with higher energy storage and conversion efficiency, lower costs, and enhanced stability. Moreover, as global energy demands continue to rise and sustainability becomes a key focus. Ongoing advancements in original materials and technologies will play a vital role in shaping the future of energy storage solutions.

1.3 Binders in anodes

Generally, traditional anodes in LIBs are composed of active material, conductive additive, and binder. The ratio of these components varies depending on the type of active material used, with the conductive additive and binder typically comprising only a small fraction of total composition. Common active materials include graphite, Si, and metal oxides, which serve as Li^+ storage hosts.[60] To enhance electron transport across the anode, conductive additives such as carbon black, carbon nanotubes, and graphene are incorporated-except in cases like LTO which inherently exhibits high conductivity.[61]

The binder plays a crucial role in maintaining anode integrity by holding active material and conductive additive together, ensuring structural stability even after prolonged cycling. Despite its small proportion in the anode, the binder significantly enhances mechanical strength, electrochemical performance, and specific capacity, ultimately contributing to the overall efficiency and durability of LIBs.[62] The following subsections discuss the characteristics and properties of both traditional and next-generation binders based on recent research advancements.

1.3.1 Traditional binders

(1) PVDF

For graphite anodes, PVDF, as a traditional binder, has long been the industrial standard in numerous studies. Its excellent electrochemical stability, thermal stability, and mechanical strength make it a preferred choice for LIB manufacturers.[63,64] However, despite its advantages, PVDF also has several drawbacks: (a) PVDF can undergo dehydrofluorination, leading to the release of hydrogen fluoride (HF), which poses safety and performance concerns, (b) PVDF can react with metallic lithium, causing undesirable side reactions and high enthalpy changes during lithiation-delithiation cycles, (c) The processing of PVDF-based anodes typically requires toxic and environmentally harmful solvents such as N-Methyl-2-Pyrrolidone (NMP) and dimethylformamide (DMF) for slurry preparation, (d) The presence of F in PVDF complicates the recycling process of waste LIBs, making sustainable disposal more difficult.[65] Given these limitations, rather than modifying PVDF, researchers are increasingly focusing on water-soluble binders that eliminate harmful elements and offer eco-friendly processing alternatives.

(2) Polyacrylonitrile (PAN)

PAN exhibits high conductivity, flame resistance, and strong chemical stability. Although, like PVDF, it requires organic solvents for mixing with electrode materials, it has not been as widely used as PVDF in anode applications.[63] Research by Zhang and Jow[66] on PAN as a binder revealed that its high crystallinity hindered effective adhesion of electrode materials to current collectors. To address this limitation, they blended PAN with other polymers to enhance its physical properties, making it more suitable for electrode applications. Piper et al.[67] explored the use of cyclized-PAN in nano-Si anodes. While the specific capacity remained above 2000 mAh/g after 150 cycles at 0.1 C and 0.05 C, the capacity retention declined significantly.

Moreover, the study did not provide data on the binder's performance under fast charge-discharge conditions, which is a crucial factor for the future development of high-performance.

(3) Polytetrafluorethylene (PTFE)

PTFE is widely used in the battery industry due to its thermal, chemical, and electrochemical stability, as well as its low friction properties. When subjected to shear force, PTFE can fibrillate, facilitating electrode processes without the need for solvents. This solvent-free approach provides a sustainable alternative, reducing the reliance on toxic solvents and contributing to the development of a more sustainable society.[68] Zhang et al. fabricated PTFE binder with graphite, hard carbon, and soft carbon for solvent-free anodes, and compared these anodes to conventional slurry-casting anodes. The results revealed that graphite anode experienced the largest volume expansion compared to hard/soft carbon, and it failed to maintain stability due to degradation reactions occurring at low potentials.[69] Additionally, because of the high electronegativity of F in polymer chains, van der Waals forces are very weak, which is unfavorable for the connection of electrode materials with current collectors.[70]

(4) Carboxymethyl cellulose (CMC)

CMC, a water-soluble binder rich in hydroxyl (-OH) groups, is considered as a promising alternative to PVDF due to its strong adhesion properties and low cost. Additionally, CMC contributes to the stable formation of SEI, which enhances cycling performance.[71] In one study, Jagau et al.[72] investigated the impact of different molecular weights of CMC in graphite anodes, finding that higher molecular weight CMC improved both elasticity and adhesion strength, ultimately enhancing the anode's electrochemical performance. However, CMC also has certain drawbacks, including low electrical conductivity, insufficient mechanical strength, and potential degradation over long cycling.[73] For example, Wei et al.[74] employed CMC as a binder for Si anode. After 100 cycles at 0.1 C, the specific capacity decreased by more than 50%.

Upon disassembling the CMC-based cell, they observed cracks on SEI film caused by the volume expansion of Si.

(5) Poly(acrylic acid) (PAA)

PAA, a water-soluble binder containing abundant carboxyl (-COOH) groups, can form hydrogen bonds with hydroxyl groups, making it suitable for use Si anodes.[75] Urbanski et al.[76] demonstrated that PAA exhibits strong adhesion strength, which helps mitigate the rapid expansion of Si during lithiation and delithiation. However, despite its potential, several limitations have hindered the commercialization of PAA. While its highly polar nature enables strong binding with Si particles, it shows poor adhesion to non-polar Cu current collector. Additionally, when PAA is mixed with other electrode materials, the drying process often results in uneven material distribution, increasing the risk of particle breakage.[77]

As LIB technology continues to progress, binder materials are transitioning from non-water-soluble to water-soluble systems. To address the limitations of conventional water-soluble binders, researchers are exploring a variety of strategies to enhance their performance and compatibility.

1.3.2 New generation binders

(1) CMC-Styrene-Butadiene Rubber (SBR)

To improve the performance of CMC binder in anodes, water-soluble SBR was combined with CMC as a binder system. Chang et al.[78] studied the distribution of CMC and SBR in a practical graphite anode using various analytical techniques. The results showed that CMC tended to accumulate on the surface of the electrode, while SBR was more concentrated at the bottom. The flexibility of SBR played a key role in improving the adhesion between the electrode and current collector. In another study, Müllner et al.[79] applied CMC-SBR binder system to Si-rGO composites, where the anode maintained good structural integrity after 50

cycles. However, the capacity did not meet the requirements for future advancements in LIB development. Despite these challenges, CMC-SBR binder has transitioned from laboratory research to commercialization at present.[80]

(2) Chitosan

Chitosan is derived from chitin, a naturally abundant biopolymer found in organisms. While chitosan itself is not water-soluble, it can dissolve in aqueous acetic acid, forming a positively charged form of glucosamine units ($R\text{-}NH^{3+}$) that interact effectively with Si surface.[65] Its structure is similar to that of cellulose, and it is biodegradable and non-toxic, making it an environmentally friendly option that aligns with the goals of sustainable development.[81] However, research has shown some limitations. In a study by Lee et al.[82], it was found that chitosan-based Si anode could not maintain performance after 100 cycles at a current density of 1000 mA/g due to insufficient mechanical strength. Similarly, in the work by Chen et al.[83], chitosan-based Si/CS-GA anode exhibited a significant drop in specific capacity, decreasing from 2500 mAh/g to under 1500 mAh/g after just 100 cycles at a current density of 500 mA/g.

(3) Alginate

Alginate, a water-soluble polysaccharide, is a naturally derived biopolymer produced by certain strains of bacteria and extracted primarily from brown seaweed. Widely studied in applications such as wound healing and tissue engineering, alginate's biocompatibility and gel-forming ability have inspired its use as a self-healing binder for Si anodes in LIBs.[84] Its abundant hydroxyl groups enable the formation of extensive hydrogen bonding networks, which help to suppress the volume expansion of anodes during lithiation and delithiation. When assembled into cells, alginate-based anodes exhibit electrochemical performance comparable to that of chitosan, particularly in terms of charge-discharge cycling.[85,86] Furthermore, Wu et

al. investigated the performance of various metal alginate binders (M-alginate, where M = Al, Ba, Mn, Zn) in Si anodes. All variants demonstrated high-capacity retention and structural integrity over 200 cycles, attributed to the improved mechanical properties.[86]

(4) Poly(ionic liquid) (PIL)

PILs, which integrate the polymeric backbone of polymers with the functional characteristics of ILs, have attracted significant attention across various fields due to their thermal stability, high ionic conductivity, and mechanical robustness.[87] Initially, PILs were investigated as solid-state electrolytes in LIBs, capitalizing on high ionic conductivity of ILs and structural stability of polymers.[88] However, over the past decade, increasing research efforts have explored the use of PILs as alternative binders in LIB anodes, aiming to replace conventional binders like PVDF.[89]

1.4 Strategies in binders for high performance LIBs

Compared to modifying traditional non-water-soluble binders, recent research has increasingly focused on improving water-soluble binders such as CMC and PAA to enhance the overall performance of LIBs. For next-generation binders, scholars often concentrate on optimizing the properties of existing bio-based materials to balance sustainability with electrochemical performance. In the case of PILs, improvement strategies typically involve rational molecular design to develop tailor-made binders that meet the specific mechanical, chemical, and ionic transport requirements of anode materials.

1.4.1 Strong adhesion and binding interactions

Binders with low surface energy often exhibit poor connection with active materials and current collectors, leading to weak electrode integrity. To address these challenges, polymers

containing polar functional groups such as -COOH and -OH are often blended with low surface energy binders to enhance interfacial adhesion. These functional groups facilitate stronger interactions with both the active materials and the current collector, thereby improving the mechanical stability of electrodes. In addition to blending strategies, some polymers are chemically modified or treated to increase these polar groups, further enhancing their adhesive properties.

Several studies have demonstrated the effectiveness of these strategies. For example, Sung et al.[70] introduced PAA as a co-binder with PTFE in dry electrode fabrication. The incorporation of PAA enhanced adhesion between the electrode and current collector. Compared to the electrode using PTFE alone, the anode utilizing PAA/PTFE hybrid binder exhibited improved electrolyte wettability and maintained a more stable electrode structure over 300 cycles at 0.1 C. A similar focus on interfacial enhancement was explored by Hu et al.[90], who utilized an interface-adaptive triblock polymer as a binder for Si/graphite anodes. This binder not only formed hydrogen bonds with Si but also enabled π···π stacking interactions with graphite, thereby addressing the interfacial incompatibility arising from the different water contact angles of Si and graphite particles. For modification of active materials, Jung et al.[91] pretreated Si particles using a piranha solution at 180 °C, introducing additional -OH groups on the surface. These groups enabled strong covalent bonding with PAA binder. The resulting electrode effectively suppressed delamination, maintaining structural integrity over 500 cycles at a current density of 1000 mA/g. Guo et al.[92] reported Si nanoparticles with SiO_2 layer and utilized konjac glucomannan (KGM), a natural polymer rich in -OH groups, as the binder., which is rich in -OH groups. The KGM binder provided abundant contact sites with SiO_2 layer, significantly improving mechanical strength and buffering volume changes of Si during cycling.

1.4.2 Composite binder systems

For anode materials such as Si and graphite, conventional single-component binders often fail to effectively accommodate structural changes and ensure electrochemical performance. To address these challenges, some studies have focused on developing multifunctional composite binders that offer enhanced mechanical strength, ionic conductivity, and stability during cycling. Methods include the use of biodegradable polymers with high van der Waals interactions, the integration of conductive components, and the incorporation of Li-containing moieties. These approaches aim to not only improve the physical cohesion of the electrode but also to facilitate Li^+ transport, ultimately enhancing overall battery performance.

For instance, Hapuarachchi et al.[93] developed a biodegradable composite binder using tapioca starch incorporated with polyethylene glycol (PEG) for Si anodes. The introduction of PEG enhanced the elasticity and hardness of starch binder, while the abundant -OH groups in starch facilitated strong interactions with Si nanoparticles. This combination not only improved mechanical integrity but also contributed to better Li^+ transport. Compared to conventional PVDF and CMC binders, starch-PEG composite demonstrated superior ionic conductivity and mechanical strength, highlighting its potential for sustainable and high-performance anodes. Wang et al.[94] introduced a ternary composite binder consisting of PVDF, PMMA, and poly(lithium methacrylate) (PMALi) for graphite anodes. This design leveraged the electrochemical stability of PVDF, the ionic conductivity of PMMA, and the additional Li^+ transport pathways provided by PMALi. The synergistic effect of these components resulted in improved rate performance and extended cycling life of graphite porous electrode, showcasing the effectiveness of integrating multifunctional polymers to address the limitations of PVDF. Shao et al.[95] proposed a conductive composite binder by combining water-soluble CMC with poly(3,4-ethylenedioxythiophene):poly(styrenesulfonate) (PEDOT:PSS) for Si

anodes. Compared to electrodes using CMC alone, PEDOT:PSS/CMC-based electrode exhibited significantly enhanced electrochemical performance, achieving a high specific discharge capacity of 1834 mAh/g with minimal loss in coulombic efficiency over 100 cycles. The incorporation of the conductive polymer PEDOT:PSS facilitated efficient Li^+ transport and reinforced electrode stability.

1.4.3 Self-healing binders

Si anodes are highly attractive for next-generation LIBs due to their high theoretical capacity. However, their practical application is hindered by severe volume expansion during lithiation and delithiation, which often results in electrode cracking, particle isolation, and rapid capacity degradation. To mitigate these issues, self-healing binders have emerged as a promising solution. These advanced binders are engineered to restore structural integrity by repairing micro-cracks and maintaining electrical connectivity within electrodes. Self-healing binders are typically derived from natural polymers and incorporate dynamic covalent or supramolecular interactions. These features not only enhance mechanical toughness but also confer benefits in environmental sustainability and cost efficiency.

Extensive research has highlighted the potential of self-healing binders. Wu et al.[85] developed a self-healing porous scaffold binder composed of alginate and carboxymethyl chitosan for Si/graphite anodes. Compared to conventional PVDF binder, this biopolymer-based binder is more cost-effective and environmentally friendly. Its self-healing ability stems from electrostatic interactions between carboxylate groups ($-COO^-$) in alginate and protonated amine groups ($-NH_3^+$) in carboxymethyl chitosan. These dynamic ionic bonds allow the electrode to tolerate high current densities by repairing structural damage during cycling, thereby supporting the development of fast-charging, high-capacity LIBs. Similarly, Rajeev et al.[96] utilized Schiff base chemistry to construct a three-dimensional (3D) self-healing network

by crosslinking glycol chitosan with oxidized alginate. The formation of dynamic imine bonds between amino and aldehyde groups allowed the binder to self-recover under mechanical stress, thereby maintaining the structural integrity of electrodes. When applied to Si and Si/graphite anodes, the binder maintained high specific capacities even at elevated current densities, underscoring its potential for commercial applications. In another approach, Sun et al.[97] employed a supramolecular binder system based on β-cyclodextrin and 1-vinylimidazole for carbon/Si anodes. These two components formed reversible host-guest interactions, further reinforced by dynamic hydrogen bonding. This interaction allowed the binder to repair electrode cracks during cycling, resulting in improved structural stability and electrochemical performance.

1.4.4 Crosslinked polymer networks

Crosslinked polymer network binders share many characteristics with self-healing binders, and their primary focus is on reinforcing the mechanical and electrochemical stability of Si anodes. This makes them a promising strategy for overcoming the challenges associated with volume expansion and structural degradation in high-capacity LIBs.

Yu et al.[98] developed a simple method for preparing a 3D conductive PAA/polyaniline (PANI) interpenetrating polymer network (IPN) gel binder for Si anodes. This 3D network structure tightly encapsulates Si nanoparticles and creates efficient channels for electron and ion transport. As a result, the binder significantly improved the charge transfer rate and capacity of Si anode. Hu et al.[99] synthesized a highly crosslinked binder through esterification reaction between oxidized starch and PAA. Compared to PAA alone, oxidized starch-PAA binder exhibited not only enhanced electrolyte wettability but also excellent flexibility. These improvements led to higher ionic conductivity, reduced charge transfer resistance, and more stable formation of SEI on Si surface. You et al.[100] introduced a 3D oxidized starch-CMC

binder for Si anodes. This binder demonstrated improved thermal and chemical stability compared to CMC, contributing to enhanced durability of the electrode during cycling process. Xie et al.[101] designed a novel crosslinked binder by reacting commercial PAA with hydroxypropyl polyrotaxane (HPR) via reversible boronic ester bonds, resulting in PAA-B-HPR network. This enabled the binder to self-repair microcracks generated during cycling, thereby preserving electrode stability and prolonging battery life.

1.4.5 PIL binders

For PIL binders, researchers typically followed two main synthesis routes: either synthesizing the polymer chain first and subsequently grafting it, or initially producing the IL monomers and then polymerizing them to obtain the final binder product. The primary goal of these strategies has been to strengthen Li^+ mobility and electrochemical properties within electrodes, thereby mitigating the rapid degradation of electrodes. Although the application of PIL binders in LIBs is still in early stages and not yet widely explored, they offer a promising avenue for improving electrodes' performance.

For instance, Jayakumar et al.[102] synthesized poly(vinylbenzylallylimidazolium chloride) (PVBCAImCl) by reacting allylimidazole (AIm) with poly(vinylbenzyl chloride) (PVBC). They then replaced the chloride anions in PVBCAImCl with bis(trifluoromethylsulfonyl)imide ($TFSI^-$) anions to obtain the final PIL binder, PVBCAImTFSI. Electrochemical testing demonstrated that PVBCAImTFSI-based graphite electrode exhibited lower SEI resistance and higher Li^+ diffusion coefficients compared to conventional PVDF binder, ultimately resulting in enhanced charge-discharge capacity. Similarly, Li et al.[103] developed a water-soluble PIL binder by decorating the IL 1-vinyl-3-ethylimidazolium hexafluorophosphate ([ViEtIm][PF_6]) on poly((ethylene glycol) methyl ether methacrylate)-co-(acrylic acid)-co-(1-vinyl-3-ethylimidazolium hexafluorophosphate). Applied to Si/graphite anode, this binder facilitated

the rapid formation of a stable SEI, contributing to improved rate capability and extended cycling performance. Grygiel et al.[104] pursued a similar strategy by first synthesizing vinylthiazolium-based IL monomers containing either tetrafluoroborate (BF_4^-) or $TFSI^-$ anions. These monomers were then polymerized via radical polymerization to produce thiazolium-type PILs for the use within $LiFePO_4$ cathodes. The results showed that the PIL containing $TFSI^-$ anions outperformed its BF_4^- counterpart, particularly in terms of long cycling performance at 1 C. In a related study, Lee et al.[105] also investigated a series of imidazolium-based PIL binders for $LiFePO_4$ cathodes. They observed that these binders not only offered efficient Li^+ transport but also exhibited excellent electrochemical stability under high-voltage conditions, further validating the potential of PILs.

1.5 Selection of ionic liquids and polymer backbone of PIL

For the selection of ionic liquids, [AMIm][OH] and [Choline][Pectate] are chosen for reacting with polymer backbone in this research. For [AMIm] based ionic liquids, incorporating allyl groups into imidazolium cations to form AMIm-based cations helps suppress crystallization, increase ionic conductivity, and reduce the viscosity of the resulting salts. Also, AMIm-based poly(ionic liquid) binders have been applied in graphite anodes, where they mitigate electrolyte degradation and facilitate lithium-ion transport. When introduced into LIB electrodes, these binders have also enabled high discharge capacities and excellent capacity retention during extended cycling.[106-108] For [Choline] based ionic liquids, they offer advantages such as low cost in industry scale, thermal stability, non-toxicity, and biocompatibility, reducing the overall cost of battery cycling. Additionally, choline-based ionic

liquids exhibit excellent ionic conductivity, wide electrochemical stability window, and thermal stability. Moreover, -OH groups in $[Choline]^+$ cations can increase the interaction between active materials and conductive materials and improve the wetting ability of anode in liquid electrolyte.[109-111]

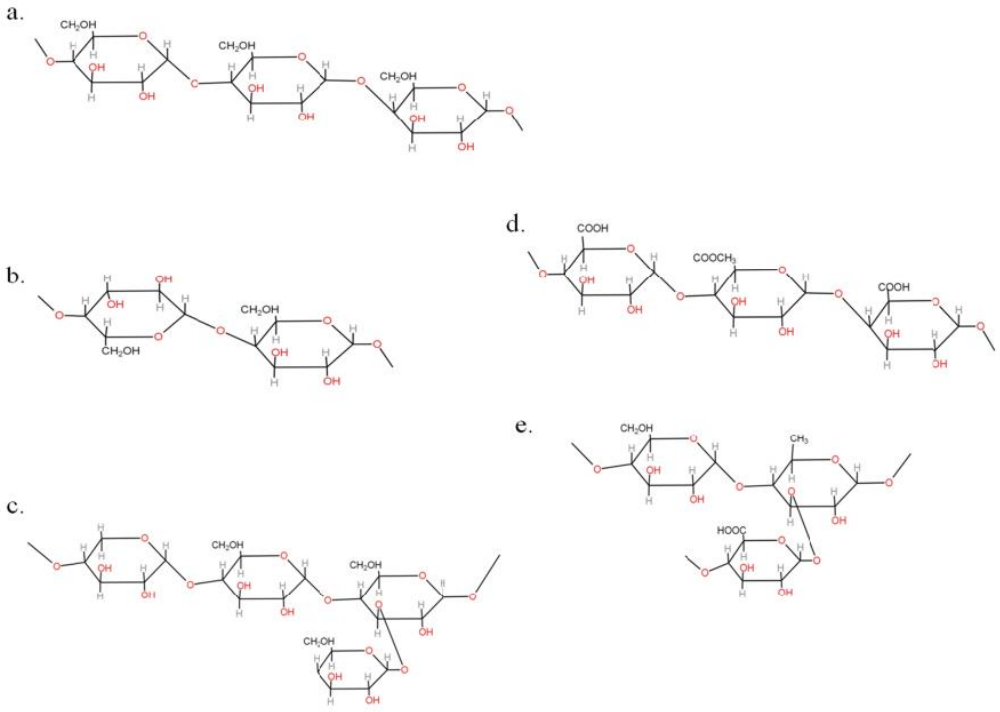

Figure 1.3. Structure of (a) starch, (b) cellulose, (c) hemicellulose, (d) pectin, (e) mucilage.

The polymer backbone materials are focused on plant-derived polysaccharides due to their renewability, abundance, and environmental compatibility. Common examples include starch, cellulose, hemicellulose, pectin, and mucilage, with their structures illustrated in **Figure 1.3**.[112] CMC/cellulose contain abundant $-COO^-$ groups, which can interact with $[AMIm]^+$ or $[Choline]^+$. The resulting materials may benefit from enhanced mechanical strength due to the

linear and crystalline nature of cellulose, as well as excellent water dispersibility, leading to a uniform electrode slurry. However, compared to pectate-based poly(ionic liquids), cellulose-derived binder may exhibit lower ionic conductivity, since CMC is less flexible and less ionically mobile. In the case of starch, the polymer chains are rich in -OH groups, which may form ionic interactions with $[Choline]^+$ or $[AMIm]^+$. Modified starch is inexpensive, biodegradable, and may offer improved ionic conductivity depending on its degree of substitution. It is particularly suited for sustainable or disposable battery applications. However, its mechanical strength is generally inferior to that of cellulose-based materials due to the branched structure of starch. Hemicellulose, composed of various sugar units with reactive -OH groups, can also be functionalized with ionic liquids. Its amorphous and flexible nature results in softer binders, which may enhance ion transport and elasticity. However, it is often more effective when blended with rigid polysaccharides like cellulose to balance flexibility and mechanical strength. Alginate, another anionic polysaccharide, contains abundant $-COO^-$ groups, making it particularly well-suited for ionic crosslinking with $[AMIm]^+$ or $[Choline]^+$. Like pectate-based PILs, alginate-based systems may exhibit high ionic conductivity due to the formation of mobile ion pairs. In addition, alginate shows gel-forming behavior, which may impart self-healing properties, mechanical flexibility, and improved tolerance to volume changes in electrode materials. However, its thermal stability may be lower than that of cellulose- or pectate-based systems.

Pectic acid, a demethylated form of pectin, was identified as the most suitable candidate of polymer backbone. Composed primarily of galacturonic acid units (**Figure 1.4**).[113] It

contains a high density of free carboxylic acid groups (-COOH), which are easily ionized or functionalized to introduce ionic sites. It also possesses abundant hydroxyl groups (-OH), which can enhance interactions with graphite layers in lithium-ion battery (LIB) anodes. Furthermore, pectic acid is easily sourced from fruit industry waste (e.g., citrus peels), and it can be isolated in a purer form compared to other polysaccharides. Its degradation product, galacturonic acid, is non-toxic and biocompatible, making it especially attractive for applications in biomedical and environmental fields.[114] Considering these advantages, pectic acid was selected as the polymer backbone for the synthesis of poly(ionic liquid)s in this work.

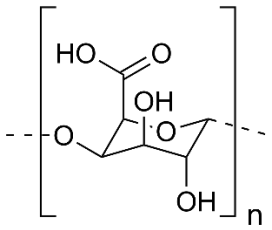

Figure 1.4. Structure of pectic acid.

1.6 Aims of thesis

The primary objective of this thesis is to develop a water-soluble PIL binder as a sustainable alternative to the widely used but environmentally unfriendly, non-water-soluble PVDF. While water-soluble binders such as CMC-SBR and PAA have been explored, they often suffer from poor electrochemical stability. During charge-discharge cycles, these materials tend to increase internal resistance, accelerating electrode degradation. In light of these limitations and the growing emphasis on sustainable materials, this thesis investigates

polygalacturonic acid (pectic acid) as a biodegradable backbone for the synthesis of novel PIL binders for LIB electrodes.

In **Chapter 2**, the IL 1-Allyl-3-methylimidazolium chloride ([AMIm][Cl]) is first converted to [AMIm][OH], which is then reacted with pectic acid to synthesize [AMIm][Pectate] binder. The stable chain structure and abundant -OH groups of $[Pectate]^-$ cations facilitate strong binding with active and conductive materials. Meanwhile, the incorporation of $[AMIm]^+$ anions enhances Li^+ transport and reduces internal resistance, thereby improving the overall electrochemical performance of batteries. A comparative analysis with PVDF is conducted to validate the potential and feasibility of [AMIm][Pectate] binder.

In **Chapter 3**, pectic acid is directly reacted with [Choline][OH] to prepare [Choline][Pectate]. Building on the results of [AMIm][Pectate], [Choline][Pectate] is evaluated in anodic half-cells under high current densities (1 C, 2 C, and 5 C), and its performance is compared to that of CMC-SBR binder. Furthermore, its applicability is assessed in full-cell configurations using $LiNi_{1/3}Co_{1/3}Mn_{1/3}O_2$ (NCM) as the cathode material.

Based on the performance of both [AMIm][Pectate] and [Choline][Pectate], the potential for further development of pectate-based PIL binders through neutralization of pectic acid with other ILs could be discussed in the future. Given the demonstrated stability and electrochemical performance, these binders also show promise for use in high-capacity anode materials, such as Si/graphite anodes.

Reference

(1) Panwar, N. L.; Kaushik, S. C.; Kothari, S. Role of Renewable Energy Sources in Environmental Protection: A Review. *Renewable and Sustainable Energy Reviews*. **2011**, 15 (3), 1513-1524. https://doi.org/10.1016/j.rser.2010.11.037.

(2) Rybár, R.; Kudelas, D.; Beer, M. Selected problems of classification of energy sources – What are renewable energy sources. *Acta Montanistica Slovaca*. **2015**, *20* (3), 172-180. https://doi.org/10.3390/ams20030172.

(3) Dincer, I. Renewable Energy and Sustainable Development: A Crucial Review. *Renewable Energy and Sustainable Energy Reviews.* **2000**, *4* (2), 157-175. https://doi.org/10.1016/S1364-0321(99)00011-8

(4) Rahman, M. M.; Oni, A. O.; Gemechu, E.; Kumar, A. Assessment of Energy Storage Technologies: A Review. *Energy Conversion and Management*. **2020**, *223*, 113295. https://doi.org/10.1016/j.enconman.2020.113295.

(5) Rolison, D. R.; Nazar, L. F. Electrochemical Energy Storage to Power the 21st Century. *MRS Bulletin*. **2011**, *36* (7), 486-493. https://doi.org/10.1557/mrs.2011.136.

(6) Doughty, D. H.; Butler, P. C.; Akhil, A. A.; Clark, N. H.; Boyes, J. D. Batteries for Large-Scale Stationary Electrical Energy Storage. *The Electrochemical Society Interface*. **2010**, *19* (49). https://iopscience.iop.org/article/10.1149/2.F05103if.

(7) Boicea, V. A. Energy Storage Technologies: The Past and the Present. *Proceedings of the IEEE*. **2014**, *102* (11), 1777-1794. https://doi.org/10.1109/JPROC.2014.2359545.

(8) Šimić, Z.; Knežević, G.; Topić, D.; Pelin, D. Battery Energy Storage Technologies Overview. *International Journal of Electrical and Computer Engineering Systems*. **2021**, *12* (1), 53-65. https://doi.org/10.32985/IJECES.12.1.6.

(9) Kurzweil, P. Gaston Planté and His Invention of the Lead-Acid Battery-The Genesis of the First Practical Rechargeable Battery. *Journal of Power Sources*. **2010**, *195* (14), 4424-4434. https://doi.org/10.1016/j.jpowsour.2009.12.126.

(10) McKeon, B. B.; Furukawa, J.; Fenstermacher, S. Advanced Lead-Acid Batteries and the Development of Grid-Scale Energy Storage Systems. *Proceedings of the IEEE*. **2014**, *102* (6), 951-963. https://doi.org/10.1109/JPROC.2014.2316823.

(11) Zhang, Y.; Zhou, C. G; Yang, J.; Xue, S. C.; Gao, H. L.; Yan, X. H.; Huo, Q. Y.; Wang, S. W.; Cao, Y.; Yan, J.; Gao, K. Z.; Wang, L. X. Advances and Challenges in Improvement of the Electrochemical Performance for Lead-Acid Batteries: A Comprehensive Review. *Journal of Power Sources*. **2022**, *520*, 230800. https://doi.org/10.1016/j.jpowsour.2021.230800.

(12) Eguro, T. Ni-Cadmium Batteries. *Encyclopedia of Applied Electrochemistry*. **2014**. https://doi.org/10.1007/978-1-4419-6996-5_147

(13) Zhang, L. Batteries, Rechargeable. *Encyclopedia of Materials: Science and Technology*. **2001**, 463-483. https://doi.org/https://doi.org/10.1016/B0-08-043152-6/00092-9.

(14) Dobrowolski, Z.; Sułkowski, Ł.; Danielak, W. Management of Waste Batteries and Accumulators: Quest of European Union Goals. *Energies*. **2021**, *14* (19), 6273. https://doi.org/10.3390/en14196273.

(15) Hariprakash, B.; Shukla, A. K.; Venugoplan, S. SECONDARY BATTERIES – NICKEL SYSTEMS | Nickel – Metal Hydride: Overview. *Encyclopedia of Electrochemical Power Sources*. **2009**, 494-501. https://doi.org/10.1016/B978-044452745-5.00158-1.

(16) Bäuerlein, P.; Antonius, C.; Löffler, J.; Kümpers, J. Progress in High-Power Nickel-Metal Hydride Batteries. *Journal of Power Sources*. **2008**, *176* (2), 547-554. https://doi.org/10.1016/j.jpowsour.2007.08.052.

(17) Ovshinsky, S. R.; Fetcenko, M. A. Development of High Catalytic Activity Disordered Hydrogen-Storage Alloys for Electrochemical Application in Nickel-Metal Hydride Batterie. *Applied Physics A*. **2001**, *72* (2), 239-244. https://doi.org/10.1007/s003390100776.

(18) Whittingham, M. S. Electrical Energy Storage and Intercalation Chemistry. *Science*. **1976**, *192* (4244), 1126-1127. https://doi.org/10.1126/science.192.4244.1126.

(19) Blomgren, G. E. The Development and Future of Lithium Ion Batteries. *Journal of The Electrochemical Society*. **2017**, *164* (1), A5019-A5025. https://doi.org/10.1149/2.0251701jes.

(20) He, B.; Zheng, H.; Tang, K.; Xi, P.; Li, M.; Wei, L.; Guan, Q. A Comprehensive Review of Lithium-Ion Battery (LiB) Recycling Technologies and Industrial Market Trend Insights. *Recycling*. **2024**, *9* (1), 9. https://doi.org/10.3390/recycling9010009.

(21) Dunn, J. B.; Gaines, L.; Kelly, J. C.; James, C.; Gallagher, K. G. The Significance of Li-Ion Batteries in Electric Vehicle Life-Cycle Energy and Emissions and Recycling's Role in Its Reduction. *Energy & Environmental Science*. **2015**, *8* (1), 158-168. https://doi.org/10.1039/c4ee03029j.

(22) Brodd. R. J. Applications-portable | Notebooks: Batteries. *ENCYCLOPEDIA OF ELECTROCHEMICAL POWER SOURCES*. **2009**, 22-28. https://doi.org/10.1016/B978-044452745-5.00359-2.

(23) Kumar, D.; Rajouria, S. K.; Bahniwal, S. B.; Kanchan, D. K. Progress and Prospects of Sodium-Sulfur Batteries: A Review. *Solid State Ionics*. **2017**, *312*, 8-16. https://doi.org/10.1016/j.ssi.2017.10.004.

(24) Wang, L.; Wang, T.; Peng, L.; Wang, Y.; Zhang, M.; Zhou, J.; Chen, M.; Cao, J.; Fei, H.; Duan, X.; Zhu, J.; Duan, X. The Promises, Challenges and Pathways to Room-Temperature Sodium-Sulfur Batteries. *National Science Review*. **2015**, *9* (3). https://doi.org/10.1093/nsr/nwab050

(25) Wang, Y. X.; Zhang, B.; Lai, W.; Xu, Y.; Chou, S. L.; Liu, H. K.; Dou, S. X. Room-Temperature Sodium-Sulfur Batteries: A Comprehensive Review on Research Progress and Cell Chemistry. *Advanced Energy Materials*. **2017**, *7* (24). https://doi.org/10.1002/aenm.201602829.

(26) Wang, W.; Luo, Q.; Li, B.; Wei, X.; Li, L.; Yang, Z. Recent Progress in Redox Flow Battery Research and Development. *Advanced Functional Materials*. **2013**, *23* (8), 970-986. https://doi.org/10.1002/adfm.201200694.

(27) Thaller, L. H. Recent advances in redox flow cell storage systems. *Intersoc. Energy Conversion Eng. Conf.* **1979**. https://ntrs.nasa.gov/search.jsp?R=19790018334.

(28) Skyllas-Kazacos, M.; Chakrabarti, M. H.; Hajimolana, S. A.; Mjalli, F. S.; Saleem, M. Progress in Flow Battery Research and Development. *Journal of The Electrochemical Society*. **2011**, *158*, R55-R79. https://doi.org/10.1149/1.3599565.

(29) Zhang, H.; Lu, W.; Li, X. Progress and Perspectives of Flow Battery Technologies. *Electrochemical Energy Reviews*. **2019**, *2*, 492-506. https://doi.org/10.1007/s41918-019-00047-1.

(30) Yuan, Z.; Yin, Y.; Xie, C.; Zhang, H.; Yao, Y.; Li, X. Advanced Materials for Zinc-Based Flow Battery: Development and Challenge. *Advanced Materials*. **2019**, *31* (50). https://doi.org/10.1002/adma.201902025.

(31) Schossig, P.; Droege, P.; Riemer, A.; Speer, M. Peer-Review Statements. *Proceedings of the International Renewable Energy Storage Conference*. **2023**, 2589-4943. https://doi.org/10.2991/978-94-6463-156-2_1.

(32) Xiong, G.; Wu, M.; Wu, X.; Wen, Z. Improvement of Rate Capability and Cycle Life of Na-$NiCl_2$ Battery via Designing a Graphene Anchoring Porous Nickel Nanostructures as Cathode. *Chemical Engineering Journal*. **2024**, *497*, 154444. https://doi.org/10.1016/j.cej.2024.154444.

(33) Zhan, X.; Li, M. M.; Weller, J. M.; Sprenkle, V. L.; Li, G. Recent Progress in Cathode Materials for Sodium-Metal Halide Batteries. *Materials*. **2021**, *14* (12), 3260. https://doi.org/10.3390/ma14123260.

(34) Rechargeable Battery Market Size, Share, Trends and Forecast by Battery Type, Capacity, Application, and Region, 2025-2033. *Imarc: Transforming Ideas into Impact*. Retrieved from https://www.imarcgroup.com/rechargeable-battery-market.

(35) Goodenough, J. B.; Park, K. S. The Li-Ion Rechargeable Battery: A Perspective. *Journal of the American Chemical Society*. **2013**, *135* (4), 1167-1176. https://doi.org/10.1021/ja3091438.

(36) Deng, D. Li-Ion Batteries: Basics, Progress, and Challenges. *Energy Science and Engineering*. **2015**, *3* (5), 385-418. https://doi.org/10.1002/ese3.95.

(37) Zubi, G.; Dufo-López, R.; Carvalho, M.; Pasaoglu, G. The Lithium-Ion Battery: State of the Art and Future Perspectives. *Renewable and Sustainable Energy Reviews*. **2018**, *89*, 292-308. https://doi.org/10.1016/j.rser.2018.03.002.

(38) Mohamed, N.; Allam, N. K. Recent Advances in the Design of Cathode Materials for Li-Ion Batteries. *RSC Advances*. **2020**, *37*, 21662-21685. https://doi.org/10.1039/d0ra03314f.

(39) Lyu, Y.; Wu, X.; Wang, K.; Feng, Z.; Cheng, T.; Liu, Y.; Wang, M.; Chen, R.; Xu, L.; Zhou, J.; Lu, Y.; Guo, B. An Overview on the Advances of $LiCoO_2$ Cathodes for Lithium-Ion Batteries. *Advanced Energy Materials*. **2020**, *11* (2). https://doi.org/10.1002/aenm.202000982.

(40) Zhu, X.; Meng, F.; Zhang, Q.; Xue, L.; Zhu, H.; Lan, S.; Liu, Q.; Zhao, J.; Zhuang, Y.; Guo, Q.; Liu, B.; Gu, L.; Lu, X.; Ren, Y.; Xia, H. $LiMnO_2$ Cathode Stabilized by Interfacial Orbital Ordering for Sustainable Lithium-Ion Batteries. *Nature Sustainability.* **2021**, *4*, 392-401. https://doi.org/10.1038/s41893-020-00660-9.

(41) Yoon, C. S.; Jun, D. W.; Myung, S. T.; Sun, Y. K. Structural Stability of $LiNiO_2$ Cycled above 4.2 V. *ACS Energy Letters*. **2017**, *2* (5) 1150-1155. https://doi.org/10.1021/acsenergylett.7b00304.

(42) Ilabija. C. O.; Kehinde, T. O.; Ishiwu, J. I.; Ojo, O. T.; Ogunkanmi, S. A.; Salman. M. B.; Bello, A. R. Advances in Nanomaterials for Lithium-Ion Batteries: Enhancing Energy Density and Lifespan. *World Journal of Advanced Engineering Technology and Sciences*. **2024**, *13* (2), 560-588. https://doi.org/10.30574/wjaets.2024.13.2.0631.

(43) Bi, Y.; Liu, M.; Xiao, B.; Jiang, Y.; Lin, H.; Zhang, Z.; Chen, G.; Sun, Q.; He, H.; Huang, F.; Sun, X.; Wang, D.; Zhang, J. G. Highly Stable Ni-Rich Layered Oxide Cathode Enabled by a Thick Protective Layer with Bio-Tissue Structure. *Energy Storage Materials*. **2020**, *24*, 291-296. https://doi.org/10.1016/j.ensm.2019.08.006.

(44) Julien, C. M.; Mauger, A. NCA, NCM811, and the Route to Ni-Richer Lithium-Ion Batteries. *Energies*. **2020**, *13* (23), 6363. https://doi.org/10.3390/en13236363.

(45) Nzereogu, P. U.; Omah, A. D.; Ezema, F. I.; Iwuoha, E. I.; Nwanya, A. C. Anode Materials for Lithium-Ion Batteries: A Review. *Applied Surface Science Advances*. **2022**, *9*, 100233. https://doi.org/10.1016/j.apsadv.2022.100233.

(46) Chang, H.; Wu, Y. R.; Han, X.; Yi, T. F. Recent Developments in Advanced Anode Materials for Lithium-Ion Batteries. *Energy Materials*. **2022**, *1* (1), 100003. https://doi.org/10.20517/energymater.2021.02.

(47) Ashuri, M.; He, Q.; Shaw, L. L. Silicon as a Potential Anode Material for Li-Ion Batteries: Where Size, Geometry and Structure Matter. *Nanoscale*. **2016**, *1*, 74-103. https://doi.org/10.1039/c5nr05116a.

(48) Sandhya, C. P.; John, B.; Gouri, C. Lithium Titanate as Anode Material for Lithium-Ion Cells: A Review. *Ionics*. **2014**, *20*, 601-620. https://doi.org/10.1007/s11581-014-1113-4.

(49) Wu, H. B.; Chen, J. S.; Hng, H. H.; Lou, X. W. Nanostructured Metal Oxide-Based Materials as Advanced Anodes for Lithium-Ion Batteries. *Nanoscale*. **2012**, *8*, 2526-2542. https://doi.org/10.1039/c2nr11966h.

(50) Mekonnen, Y.; Sundararajan, A.; Sarwat, A. I. A Review of Cathode and Anode Materials for Lithium-Ion Batteries. *SoutheastCon*. **2016**, 1-6. https://doi.org/10.1109/SECON.2016.7506639.

(51) Liu, Y. K.; Zhao, C. Z.; Du, J.; Zhang, X. Q.; Chen, A. B.; Zhang, Q. Research Progresses of Liquid Electrolytes in Lithium-Ion Batteries. *Small*. **2023**, *19* (8). https://doi.org/10.1002/smll.202205315.

(52) Kalhoff, J.; Eshetu, G. G.; Bresser, D.; Passerini, S. Safer Electrolytes for Lithium-Ion Batteries: State of the Art and Perspectives. *ChemSusChem*. **2015**, *8* (13), 2154-2175. https://doi.org/10.1002/cssc.201500284.

(53) Liang, S.; Yan, W.; Wu, X.; Zhang, Y.; Zhu, Y.; Wang, H.; Wu, Y. Gel Polymer Electrolytes for Lithium Ion Batteries: Fabrication, Characterization and Performance. *Solid State Ionics*. **2018**, *318*, 2-18. https://doi.org/10.1016/j.ssi.2017.12.023.

(54) Ma, C.; Cui, W.; Liu, X.; Ding, Y.; Wang, Y. In Situ Preparation of Gel Polymer Electrolyte for Lithium Batteries: Progress and Perspectives. *InfoMat*. **2022**, *4* (2). https://doi.org/10.1002/inf2.12232.

(55) Zhao, W.; Yi, J.; He, P.; Zhou, H. Solid-State Electrolytes for Lithium-Ion Batteries: Fundamentals, Challenges and Perspectives. *Electrochemical Energy Reviews*. **2019**, *2*, 574-605. https://doi.org/10.1007/s41918-019-00048-0.

(56) Niu, H.; Wang, L.; Guan, P.; Zhang, N.; Yan, C.; Ding, M.; Guo, X.; Huang, T.; Hu, X. Recent Advances in Application of Ionic Liquids in Electrolyte of Lithium Ion Batteries. *Journal of Energy Storage*. **2021**, *40*, 102659. https://doi.org/10.1016/j.est.2021.102659.

(57) Wang, F.; Ke, X.; Shen, K.; Zhu, L.; Yuan, C. A Critical Review on Materials and Fabrications of Thermally Stable Separators for Lithium-Ion Batteries. *Advanced Materials Technologies*. **2022**, *7* (5). https://doi.org/10.1002/admt.202100772.

(58) Dai, X.; Zhang, X.; Wen, J.; Wang, C.; Ma, X.; Yang, Y.; Huang, G.; Ye, H. M.; Xu, S. Research Progress on High-Temperature Resistant Polymer Separators for Lithium-Ion Batteries. *Energy Storage Materials*. **2022**, *51*, 638-659. https://doi.org/10.1016/j.ensm.2022.07.011.

(59) Zhu, P.; Gastol, D.; Marshall, J.; Sommerville, R.; Goodship, V.; Kendrick, E. A Review of Current Collectors for Lithium-Ion Batteries. *Journal of Power Sources*. **2021**, *485*, 229321. https://doi.org/10.1016/j.jpowsour.2020.229321.

(60) Korthauer, R. *Lithium-Ion Batteries: Basics and Applications*; **2018**. https://doi.org/10.1007/978-3-662-53071-9.

(61) Higgins, T. M.; Park, S. H.; King, P. J.; Zhang, C.; McEvoy, N.; Berner, N. C.; Daly, D.; Shmeliov, A.; Khan, U.; Duesberg, G.; Nicolosi, V.; Coleman, J. N. A Commercial Conducting Polymer as Both Binder and Conductive Additive for Silicon Nanoparticle-Based Lithium-Ion Battery Negative Electrodes. *ACS Nano*. **2016**, *10* (3), 3702-3713. https://doi.org/10.1021/acsnano.6b00218.

(62) Li, J.; Daniel, C.; Wood, D. Materials Processing for Lithium-Ion Batteries. *Journal of Power Sources*. **2011**, *196* (5), 2452-2460. https://doi.org/10.1016/j.jpowsour.2010.11.001.

(63) Lee, S.; Koo, H.; Kang, H. S.; Oh, K. H.; Nam, K. W. Advances in Polymer Binder Materials for Lithium-Ion Battery Electrodes and Separators. *Polymers*. **2023**, *15* (23), 4477. https://doi.org/10.3390/polym15234477.

(64) Zhang, S. S.; Xu, K.; Jow, T. R. Evaluation on a Water-Based Binder for the Graphite Anode of Li-Ion Batteries. *Journal of Power Sources*. **2004**, *138* (1-2), 226-231. https://doi.org/10.1016/j.jpowsour.2004.05.056.

(65) Srivastava, M.; R. A. K. M.; Zaghib, K. Binders for Li-Ion Battery Technologies and Beyond: A Comprehensive Review. *Batteries*. **2024**, *10* (8), 268. https://doi.org/10.3390/batteries10080268.

(66) Zhang, S. S.; Jow, T. R. Study of Poly(Acrylonitrile-Methyl Methacrylate) as Binder for Graphite Anode and $LiMn_2O_4$ Cathode of Li-Ion Batteries. *Journal of Power Sources*. **2002**, *109* (2), 422-426. https://doi.org/10.1016/S0378-7753(02)00107-6.

(67) Piper, D. M.; Yersak, T. A.; Son, S. B.; Kim, S. C.; Kang, C.; Oh, K. H.; Ban, C.; Dillon, A. C.; Lee, S. H. Conformal Coatings of Cyclized-PAN for Mechanically Resilient Si Nano-Composite Anodes. *Advanced Energy Materials*. **2013**, *3* (6), 697-702. https://doi.org/10.1002/aenm.201200850.

(68) Sudhakaran, S.; Bijoy, T. K. A Comprehensive Review of Current and Emerging Binder Technologies for Energy Storage Applications. *ACS Applied Energy Materials*. **2023**, *6* (23), 11773-11794. https://doi.org/10.1021/acsaem.3c02218.

(69) Zhang, Y.; Huld, F.; Lu, S.; Jektvik, C.; Lou, F.; Yu, Z. Revisiting Polytetrafluorethylene Binder for Solvent-Free Lithium-Ion Battery Anode Fabrication. *Batteries*. **2022**, *8* (6), 57. https://doi.org/10.3390/batteries8060057.

(70) Sung, K. E.; Hwang, I.; Choi, J.; Jung, S. K.; Yoon, J. Enhanced Adhesion in PTFE-Based Dry Electrodes with Hydrogen Bonding Co-Binder Integration for Advanced Lithium-Ion Batteries. *Chemical Engineering Journal*. **2025**, *511*, 161789. https://doi.org/10.1016/j.cej.2025.161789.

(71) Park, J. H.; Kim, S. H.; Ahn, K. H. Role of Carboxymethyl Cellulose Binder and Its Effect on the Preparation Process of Anode Slurries for Li-Ion Batteries. *Colloids and Surfaces A: Physicochemical and Engineering Aspects*. **2023**, *664*, 131130. https://doi.org/10.1016/j.colsurfa.2023.131130.

(72) Jagau, R.; Huttner, F.; Mayer, J. K.; Cavers, H.; Scheffler, S.; Brokmann, J.; Kwade, A. Influence of Different Alginate and Carboxymethyl Cellulose Binders on Moisture Content, Electrode Structure, and Electrochemical Properties of Graphite-Based Anodes for Lithium-Ion Batteries. *Energy Technology*. **2023**, *11* (5). https://doi.org/10.1002/ente.202200871.

(73) Li, S.; Liu, Y. M.; Zhang, Y. C.; Song, Y.; Wang, G. K.; Liu, Y. X.; Wu, Z. G.; Zhong, B. H.; Zhong, Y. J.; Guo, X. D. A Review of Rational Design and Investigation of Binders Applied in Silicon-Based Anodes for Lithium-Ion Batteries. *Journal of Power Sources*. **2021**, *485*, 229331. https://doi.org/10.1016/j.jpowsour.2020.229331.

(74) Wei, L.; Chen, C.; Hou, Z.; Wei, H. Poly (Acrylic Acid Sodium) Grafted Carboxymethyl Cellulose as a High Performance Polymer Binder for Silicon Anode in Lithium Ion Batteries. *Sci. Rep*. **2016**, *6*, 19583. https://doi.org/10.1038/srep19583.

(75) Shen, H.; Wang, Q.; Chen, Z.; Rong, C.; Chao, D. Application and Development of Silicon Anode Binders for Lithium-Ion Batteries. *Materials*. **2023**, *16* (12), 4266. https://doi.org/10.3390/ma16124266.

(76) Urbanski, A.; Omar, A.; Guo, J.; Janke, A.; Reuter, U.; Malanin, M.; Schmidt, F.; Jehnichen, D.; Holzschuh, M.; Simon, F.; Eichhorn, K. J.; Giebeler, L.; Uhlmann, P. An Efficient Two-Polymer Binder for High-

Performance Silicon Nanoparticle-Based Lithium-Ion Batteries: A Systematic Case Study with Commercial Polyacrylic Acid and Polyvinyl Butyral Polymers. *Journal of The Electrochemical Society*. **2019**, *166* (3), A5275-A5286. https://doi.org/10.1149/2.0371903jes.

(77) Yoon, J.; Lee, J.; Kim, H.; Kim, J.; Jin, H. J. Polymeric Binder Design for Sustainable Lithium-Ion Battery Chemistry. *Polymers*. **2024**, *16* (2), 254. https://doi.org/10.3390/polym16020254.

(78) Chang, W. J.; Lee, G. H.; Cheon, Y. J.; Kim, J. T.; Lee, S. Il; Kim, J.; Kim, M.; Park, W. Il; Lee, Y. J. Direct Observation of Carboxymethyl Cellulose and Styrene-Butadiene Rubber Binder Distribution in Practical Graphite Anodes for Li-Ion Batteries. *ACS Applied Materials & Interfaces*. **2019**, *11* (44), 41330-41337. https://doi.org/10.1021/acsami.9b13803.

(79) Müllner, S.; Michlik, T.; Reichel, M.; Held, T.; Moos, R.; Roth, C. Effect of Water-Soluble CMC/SBR Binder Ratios on Si-RGO Composites Using Mm- and Nm-Sized Silicon as Anode Materials for Lithium-Ion Batteries. *Batteries*. **2023**, *9* (5), 248. https://doi.org/10.3390/batteries9050248.

(80) Wang, W.; Yue, X.; Meng, J.; Wang, X.; Zhou, Y.; Wang, Q.; Fu, Z. Comparative Study of Water-Based LA133 and CMC/SBR Binders for Sulfur Cathode in Advanced Lithium-Sulfur Batteries. *The Journal of Physical Chemistry C*. **2019**, *123* (1), 250-257. https://doi.org/10.1021/acs.jpcc.8b10736.

(81) Hamzelui, N.; Linhorst, M.; Nyenhuis, G. M.; Haneke, L.; Eshetu, G. G.; Placke, T.; Winter, M.; Moerschbacher, B. M.; Figgemeier, E. Chitosan as Enabling Polymeric Binder Material for Silicon-Graphite-Based Anodes in Lithium-Ion Batteries. *Energy Technology*. **2023**, *11* (3). https://doi.org/10.1002/ente.202201239.

(82) Lee, S. H.; Lee, J. H.; Nam, D. H.; Cho, M.; Kim, J.; Chanthad, C.; Lee, Y. Epoxidized Natural Rubber/Chitosan Network Binder for Silicon Anode in Lithium-Ion Battery. *ACS Applied Materials & Interfaces*. **2018**, *10* (19), 16449-16457. https://doi.org/10.1021/acsami.8b01614.

(83) Chen, C.; Lee, S. H.; Cho, M.; Kim, J.; Lee, Y. Cross-Linked Chitosan as an Efficient Binder for Si Anode of Li-Ion Batteries. *ACS Applied Materials & Interfaces*. **2016**, *8* (4), 2658-2665. https://doi.org/10.1021/acsami.5b10673.

(84) Deng, Y.; Shavandi, A.; Okoro, O. V.; Nie, L. Alginate Modification via Click Chemistry for Biomedical Applications. *Carbohydrate Polymers*. **2021**, *270*, 118360. https://doi.org/10.1016/j.carbpol.2021.118360.

(85) Wu, Z. H.; Yang, J. Y.; Yu, B.; Shi, B. M.; Zhao, C. R.; Yu, Z. L. Self-Healing Alginate-Carboxymethyl Chitosan Porous Scaffold as an Effective Binder for Silicon Anodes in Lithium-Ion Batteries. *Rare Metals*. **2016**, *38*, 832-839. https://doi.org/10.1007/s12598-016-0753-0.

(86) Wu, Z. Y.; Deng, L.; Li, J. T.; Huang, Q. S.; Lu, Y. Q.; Liu, J.; Zhang, T.; Huang, L.; Sun, S. G. Multiple Hydrogel Alginate Binders for Si Anodes of Lithium-Ion Battery. *Electrochimica Acta*. **2017**, *245*, 371-378. https://doi.org/10.1016/j.electacta.2017.05.094.

(87) Qian, W.; Texter, J.; Yan, F. Frontiers in Poly(Ionic Liquid)s: Syntheses and Applications. *Chem. Soc. Rev.* **2017**, *46*. https://doi.org/10.1039/C6CS00620E.

(88) Yuan, J.; Mecerreyes, D.; Antonietti, M. Poly(Ionic Liquid)s: An Update. *Progress in Polymer Science*. **2013**, *38* (7), 1009-1036. https://doi.org/10.1016/j.progpolymsci.2013.04.002.

(89) Chauque, S.; Oliva, F. Y.; Cámara, O. R.; Torresi, R. M. Use of Poly[Ionic Liquid] as a Conductive Binder in Lithium Ion Batteries. *Journal of Solid State Electrochemistry*. **2018**, *22* (11), 3589-3596. https://doi.org/10.1007/s10008-018-4078-9.

(90) Hu, L.; Jin, M.; Zhang, Z.; Chen, H.; Ajdari, F. B.; Song, J. Interface-Adaptive Binder Enabled by Supramolecular Interactions for High-Capacity Si/C Composite Anodes in Lithium-Ion Batteries. *Advanced Functional Materials*. **2022**, *32* (26). https://doi.org/10.1002/adfm.202111560.

(91) Jung, C. H.; Kim, K. H.; Hong, S. H. Stable Silicon Anode for Lithium-Ion Batteries through Covalent Bond Formation with a Binder via Esterification. *ACS Applied Materials & Interfaces*. **2019**, *11* (30), 26753-26763. https://doi.org/10.1021/acsami.9b03866.

(92) Guo, S.; Li, H.; Li, Y.; Han, Y.; Chen, K.; Xu, G.; Zhu, Y.; Hu, X. SiO2-Enhanced Structural Stability and Strong Adhesion with a New Binder of Konjac Glucomannan Enables Stable Cycling of Silicon Anodes for Lithium-Ion Batteries. *Advanced Energy Materials*. **2018**, *8* (24). https://doi.org/10.1002/aenm.201800434.

(93) Hapuarachchi, S. N. S.; Wasalathilake, K. C.; Nerkar, J. Y.; Jaatinen, E.; O'Mullane, A. P.; Yan, C. Mechanically Robust Tapioca Starch Composite Binder with Improved Ionic Conductivity for Sustainable Lithium-Ion Batteries. *ACS Sustainable Chemistry & Engineering*. **2020**, *8* (26), 9857-9865. https://doi.org/10.1021/acssuschemeng.0c02843.

(94) Wang, Y.; Zhang, L.; Qu, Q.; Zhang, J.; Zheng, H. Tailoring the Interplay between Ternary Composite Binder and Graphite Anodes toward High-Rate and Long-Life Li-Ion Batteries. *Electrochimica Acta*. **2016**, *191*, 70-80. https://doi.org/10.1016/j.electacta.2016.01.025.

(95) Shao, D.; Zhong, H.; Zhang, L. Water-Soluble Conductive Composite Binder Containing PEDOT:PSS as Conduction Promoting Agent for Si Anode of Lithium-Ion Batteries. *ChemElectroChem*. **2014**, *1* (10), 1679-1687. https://doi.org/10.1002/celc.201402210.

(96) Rajeev, K. K.; Nam, J.; Jang, W.; Kim, Y.; Kim, T. H. Polysaccharide-Based Self-Healing Polymer Binder via Schiff Base Chemistry for High-Performance Silicon Anodes in Lithium-Ion Batteries. *Electrochimica Acta*. **2021**, *384*, 138364. https://doi.org/10.1016/j.electacta.2021.138364.

(97) Sun, Q.; Wu, X.; He, Z.; Xiong, K.; Cao, Q.; Hu, H.; Zheng, M.; Xiao, Y.; Liang, Y. A Self-Healing Binder Based on Host-Guest Interaction for Carbon-Silicon Anodes in Llithium Ion Batteries. *Journal of The Electrochemical Society*. **2025**, *172*, 010508. https://doi.org/10.1149/1945-7111/ad9d7e.

(98) Yu, X.; Yang, H.; Meng, H.; Sun, Y.; Zheng, J.; Ma, D.; Xu, X. Three-Dimensional Conductive Gel Network as an Effective Binder for High-Performance Si Electrodes in Lithium-Ion Batteries. *ACS Applied Materials & Interfaces*. **2015**, *7* (29), 15961-15967. https://doi.org/10.1021/acsami.5b04058.

(99) Hu, X.; Liang, K.; Li, J.; Ren, Y. A Highly Crosslinked Polymeric Binder for Silicon Anode in Lithium-Ion Batteries. *Materials Today Communications*. **2021**, *28*, 102530. https://doi.org/10.1016/j.mtcomm.2021.102530.

(100) You, R.; Han, X.; Zhang, Z.; Li, L.; Li, C.; Huang, W.; Wang, J.; Xu, J.; Chen, S. An Environmental Friendly Cross-Linked Polysaccharide Binder for Silicon Anode in Lithium-Ion Batteries. *Ionics*. **2019**, *25*, 4109-4118. https://doi.org/10.1007/s11581-019-02972-z.

(101) Xie, Z. H.; Rong, M. Z.; Zhang, M. Q. Dynamically Cross-Linked Polymeric Binder-Made Durable Silicon Anode of a Wide Operating Temperature Li-Ion Battery. *ACS Applied Material & Interfaces*. **2021**, *13* (24), 28737-28748. https://doi.org/10.1021/acsami.1c01472.

(102) Jayakumar, T. P.; Badam, R.; Matsumi, N. Allylimidazolium-Based Poly(Ionic Liquid) Anodic Binder for Lithium-Ion Batteries with Enhanced Cyclability. *ACS Applied Energy Materials*. **2020,** *3* (4), 3337-3346. https://doi.org/10.1021/acsaem.9b02376.

(103) Li, X.; Chen, H.; Chen, M.; Qi, J.; Chen, S.; Zhuo, H. Ionic Liquid-Decorated Copolymer Binders for Silicon/Graphite Anodes with Enhanced Rate Capability and Excellent Cycle Stability. *ACS Applied Energy Materials*. **2021**, *4* (11), 12709-12717. https://doi.org/10.1021/acsaem.1c02422.

(104) Grygiel, K.; Lee, J. S.; Sakaushi, K.; Antonietti, M.; Yuan, J. Thiazolium Poly(Ionic Liquid)s: Synthesis and Application as Binder for Lithium-Ion Batteries. *ACS Macro Letters.* **2015**, *4* (12), 1312-1316. https://doi.org/10.1021/acsmacrolett.5b00655.

(105) Lee, J. S.; Sakaushi, K.; Antonietti, M.; Yuan, J. Poly(Ionic Liquid) Binders as Li^+ Conducting Mediators for Enhanced Electrochemical Performance. *RSC Advances*. **2015**, *5* (104), 85517-85522. https://doi.org/10.1039/c5ra16535k.

(106) Mizumo, T.; Marwanta, E.; Matsumi, N.; Ohno, H. Allylimidazolium Halides as Novel Room Temperature Ionic Liquids. *Chemistry Letters.* **2004**, *33* (10), 1360-1361. https://doi.org/10.1246/cl.2004.1360.

(107) Jayakumar, T. P.; Badam, R.; Matsumi, N. Allylimidazolium-Based Poly(Ionic Liquid) Anodic Binder for Lithium-Ion Batteries with Enhanced Cyclability. *ACS Applied Energy Materials.* **2020**, *3* (4), 3337-3346. https://doi.org/10.1021/acsaem.9b02376.

(108) Patra, A.; Matsumi, N. Densely Imidazolium Functionalized Water Soluble Poly(Ionic Liquid) Binder for Enhanced Performance of Carbon Anode in Lithium/Sodium-Ion Batteries. *Advanced Energy Materials.* **2024**, *15* (5). https://doi.org/10.1002/aenm.202403071.

(109) Hernández-Sánchez, A.; Alcaraz-Espinoza, J. J.; Thomas, C. S.; Jiménez-Regalado, E.; Mayrén, A.; González, I.; Sánchez, G. R. Choline Based Poly-Ionic Liquid as Outstanding Binder for Li[Sbnd]S Batteries. *Journal of Energy Storage.* **2025**, *106*. 114746. https://doi.org/10.1016/j.est.2024.114746.

(110) Lee, T. H. W. *Thermophysical and Electrochemical Properties Measurements of Novel Choline-Based Ionic Liquids. THESIS*. **2025**, University of Nottingham Malaysia. https://eprints.nottingham.ac.uk/id/eprint/80023.

(111) Mobin, M.; Aslam, R.; Salim, R.; Kaya, S. An Investigation on the Synthesis, Characterization and Anti-Corrosion Properties of Choline Based Ionic Liquids as Novel and Environmentally Friendly Inhibitors for Mild Steel Corrosion in 5% HCl. *Journal of Colloid and Interface Science*. **2022**, *620* (1), 293-312. https://doi.org/10.1016/j.jcis.2022.04.036.

(112) Choudhury, A., Sarma, S., Sarkar, S., Kumari, M., & Dey, B. K. Polysaccharides Obtained from Vegetables: An effective source of alternative excipient. *Journal of Pharmacopuncture*. **2022**, *25* (4), 317-325. https://doi.org/10.3831/KPI.2022.25.4.317.

(113) Ozcan, B. E., Tetik, N., & Aloglu, H. S. Polysaccharides from fruit and vegetable wastes and their food applications: A review. *International Journal of Biological Macromolecules*. **2024**, 276, 134007. https://doi.org/10.1016/j.ijbiomac.2024.134007.

(114) El-Aassar, M. R., Ibrahim, O. M., Albogmi, R. G., Hussein, M. F., Alsirhani, A. M., Rafea, M. A., Zaki, M. E. A., Hassan, H. M. A., & Agwa, M. M. Capsaicin/silica-infused polygalacturonic acid/polyvinyl alcohol nano-matrix for enhanced wound healing in skin injuries. *International Journal of Biological Macromolecules*. **2024**, 282, 137319. https://doi.org/10.1016/j.ijbiomac.2024.137319.

Chapter 2 [AMIm][Pectate] Eco-Friendly Polymer as a High-Performing Binder for Lithium-Ion Battery Electrodes

2.1 Introduction

Lithium-ion batteries (LIBs), pivotal components within the realm of energy conversion and utilization, are expected to mitigate the reliance on fossil fuels in traditional transportation and the effects of climate change.[1,2] This significance is particularly pronounced under the background of net-zero goal set by over 140 nations for the year 2050. The global market for electric vehicles (EVs), driven by LIBs, has already surpassed USD 20 billion in sales in 2016 and is anticipated to approach USD 90 billion in 2050.[1,3,4] In striving for enhanced electrochemical performance and extended lifespans, researchers have made considerable efforts toward the refinement of conductive and active materials important to LIB electrodes.[5,6] Binders serve as a necessary part of electrodes preparation, functioning as adhesive substances to tightly bind conductive and active materials. Their role is significant in ensuring the mechanical integrity of electrodes while influencing on ionic diffusion thereof.[7] For instance, suitable binder selection benefits for alleviating graphite anode cracks during charging-discharging process to improve interparticle contacts and forming thinner solid electrolyte interface (SEI) to increase lithium-ion (Li^+) diffusion.[8]

Poly(vinylidene fluoride) (PVDF), renowned for its exceptional chemical and thermal stability, stands as the common non-aqueous binder utilized in the fabrication of LIB electrodes. Whereas it is noteworthy that the presence of fluorine element along PVDF polymer chain poses environmental challenges during producing and recovering processes. Also, the organic solvents employed in the mixture of electrode materials often exhibit toxicity and volatility, further accelerating environmental degradation. In consideration of practical application, the diminished ionic conductivity and inherent hydrophobicity of PVDF prevent batteries from achieving optimal performance.[9,10] Aqueous carboxymethyl cellulose (CMC)/styrene butadiene rubber (SBR), poly(acrylic acid) (PAA), chitosan, and alginates based polymer

binders with hydrogen groups (-OH) and carboxyl groups (-COOH) are promising alternatives to PVDF upon comprehensive evaluation of their advantages and drawbacks, however their limited chemical stability and reduced mechanical strength are still the challenges for further development.[11]

To address the challenges inherent in traditional binders, poly(ionic liquid)s (PILs) have recently garnered considerable scholarly interest owing to the combination of advantageous properties derived from both ILs and the chain structure characteristic of polymers. These properties encompass great chemical stability, high ionic conductivity, and broad electrochemical stability window.[12] The exploration of PILs has predominantly centered on imidazolium, thiazolium, and pyrrolidinium based ILs.[13–15] Noteworthy, there is one study elucidating the efficacy of imidazolium-based nanoparticles, which has been demonstrated dispersibility in a wide array of organic solvents. Additionally, their smaller binder particle size is advantageous for preventing graphite from detaching since these nanoparticles with the same mass fraction as traditional binder can provide more 'glue points'. After introduction into electrode, PILs exhibit improvements in coulombic efficiency and capacity retention within lithium batteries, surpassing those achievable with conventional PVDF.[16] Moreover, incorporating allyl groups into imidazolium cations to form AMIm-based cations reduces crystallization, enhances ionic conductivity, and lowers the viscosity of the corresponding salts.[17] Jayakumar et al.[18] synthesized an [AMIm]-based PIL binder for graphite anodes in LIBs, demonstrating reduced electrolyte degradation and enhanced lithium-ion transport. Similarly, Patra et al.[19] introduced an [AMIm]-based PIL binder into LIB and sodium-ion battery (SIB) electrodes, where the corresponding half-cells exhibited high discharge capacities and excellent capacity retention over prolonged cycling. However, it is imperative to acknowledge that some PILs are synthesized via monomer polymerization processes, particularly through radical polymerization. In such cases, the occurrence of side reactions and potential for halides

contamination may be problematic. Also, there exists a notable deficiency in the consideration of environmental impact and energy consumption associated with some polymerization process.[5]

In the context of the ongoing exploration of renewable materials for prospective application in LIBs, polygalacturonic acid (pectic acid), as one structure of bio-material pectin broadly existing in fruits and other plants emerges as a prominent candidate. Pectin consists of abundant α-(1,4)-linked D-galacturonic acid units and a handful of α-(1,2)-linked L-rhamnose units, but homopolymer pectic acid can be obtained via complete deacetylation. So far, it has been applied as dietary fibers, ophthalmic drugs, scaffold for cell growth, the component of admixture for diagnostic magnetic resonance imaging, and crop protection in food, pharmaceutical, and agricultural industries.[20–23] Despite the limited utilization of pectic acid in LIBs to date, Ankorta et al.[24] have undertaken pioneering work to fabricate gel electrolytes based on pectin, incorporating glycerol and $LiClO_4$. Their investigation yielded promising results for electrolytes in electrochromic devices, with the ionic conductivity of 10^{-5} S/cm.

On the other hand, this work employs 1-allyl-3-methylimidazolium chloride ([AMIm][Cl]) and non-water-soluble α-(1,4)-linked pectic acid to synthesize a PIL, [AMIm][Pectate], intended for utilization as an anodic binder within LIBs anodes. The synthesized [AMIm][Pectate] serves as an environmentally friendly alternative to traditional binders. Structural and physicochemical analysis are conducted to assess the composition and characteristics of this polygalacturonate before and after integrating into anode matrix. Also, electrochemical investigations are undertaken after binder materials are applied into half cells, facilitating a comparative analysis with PVDF. The objective of Chapter 2 is to develop a water-soluble binder with enhanced performance to replace the water-insoluble PVDF binder, whose polymeric chains impose environmental burdens during production and recycling. This also aims to reduce reliance on toxic volatile organic solvents required for electrode slurry

preparation. The following tests encompass the resistance assessment after SEI formation and charge-discharge properties of batteries, thereby elucidating the performance attributes of [AMIm][Pectate] binder.

2.2 Experimental

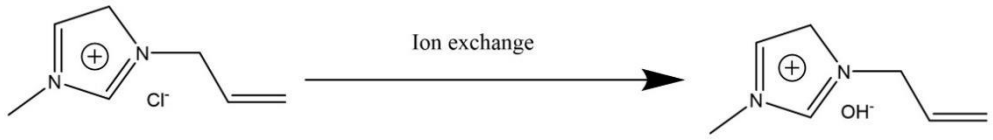

Scheme 2.1. Ion exchange of Cl^- to OH^- form using Amberlyte hydroxide resin.

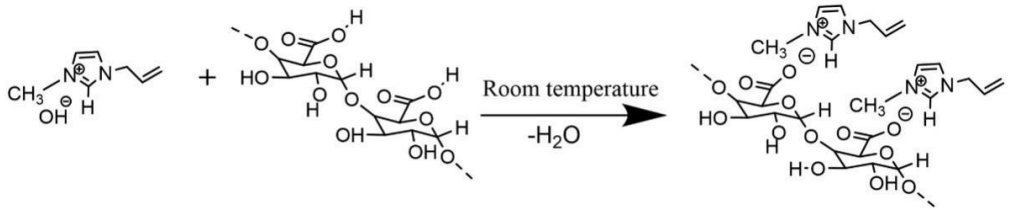

Scheme 2.2. Synthesis of [AMIm][Pectate] through the reaction between [AMIm][OH] and pectic acid.

Binder synthesis. A column was filled with Amberlyte hydroxide (Kanto Chemical CO., INC., Japan) submerged in distilled water. Subsequently, 2.0 g of [AMIm][Cl] (Tokyo Chemical Industry Co., LTD., Japan) was dissolved in 200 mL of distilled water. [AMIm][Cl] solution was directed through the ion exchange resin at a flow rate of 1 mL/min. After the completion of ion exchange process, resulting in conversion of [AMIm][Cl] to [AMIm][OH], as depicted in **Scheme 2.1**, the column was rinsed with additional 100 mL of distilled water. A small amount of [AMIm][OH] solution was introduced into $AgNO_3$ solution to ascertain the completeness of Cl^- displacement by OH^-. Following this, the eluent was gathered and

subjected to concentration using a rotary evaporator (N-1300, EYELA, Tokyo) at 70 °C to yield a brownish semi-solid substance. Subsequently, the product underwent drying treatment under vacuum at 80 °C overnight. A solution comprising 2.0 mmol of [AMIm][OH] dissolved in 30 mL of distilled water was prepared. After that, half of the equimolar quantity of pectic acid (M_r 25000-50000, Sigma-Aldrich, USA), amounting to 176.0 mg, was added to the solution and the neutralization process occurred, as illustrated in **Scheme 2.2**. Following this, the solvent, water, was removed under vacuum at 80 °C. The resultant product was washed with acetone to purify [AMIm][Pectate]. After drying under vacuum at 80 °C, 291 mg of brittle yellow solid material was obtained, and yield was 97.3%.

Characterization. ^{1}H-NMR and ^{13}C-NMR (Nuclear Magnetic Resonance) measurements were performed via Bruker Advance || -400 MHz and 100 MHz spectrometer respectively. Deuterium oxide (D_2O) was employed as solvent and standard. Chemical shifts in ^{1}H-NMR are 8.38 ppm (1H, N=N**H**-N), 7.38 ppm (2H, N-C**H**-C**H**-N), 5.96 ppm (1H CH_2-C**H**=CH_2), 5.35 ppm (2H, CH=C**H**$_2$), 4.83 ppm (2H, N-C**H**$_2$-CH), 3.83 ppm (3H, C**H**$_3$-N), 5.27 ppm (1H, O-C**H**-O), 5.0 ppm (1H, C-CH(O**H**)-C), 4.80 ppm (1H, C-C**H**(COO^-)-O), 4.34 ppm (1H, C-CH(O**H**)-C), 3.92 ppm (1H, C-C**H**(OH)-C), 3.87 ppm (1H, C-C**H**(OH)-C), 3.58 ppm (1H, C-C**H**(O)-C). Chemical shifts in ^{13}C-NMR are 174.35, 136.01, 130.59, 123.76, 120.96, 99.25, 78.07, 70.89, 68.09, 51.64, 35.89, and 11.38 ppm. The Fourier Transform Infrared (FT-IR) spectrum of [AMIm][Pectate] was acquired through PerkinElmer 100 instrument, with a resolution of 2 cm^{-1} for 10 scans in Attenuated Total Reflectance (ATR) mode. The peeling behavior of anode was evaluated through peeling test conducted by INSTRON 3365-L5 tensile testing machine. Scotch tape was used as the peeling medium at an angle of 180 degrees at a rate of 2 mm/min, under ambient conditions. Thermogravimetric analysis (TGA) was conducted using Hitachi STA 7200 instrument under a constant nitrogen flow of 150 MPa, with

a heating rate of 10 °C/min. Prior to TGA, the samples were preheated at 120 °C for 5 days to remove any residual moisture. The elemental distribution analysis of binders, both prior to their integration into cells and after charging-discharging cycles, was performed via S-probe TM 2803 X-ray Photoelectron Spectroscopy (XPS). The surface morphology of anode materials after charging-discharging was investigated via Hitachi S-4500 Scanning Electron Microscopy (SEM). Additionally, [AMIm][Pectate]-based anodes kept at 0.2 V, 0.4 V, and 2.1 V after lithiation were characterized by X-ray Diffraction (XRD) using Smart Lab X-ray Diffractometer (Rigaku) with Cu Kα radiation (λ = 0.154 nm). The measurements were conducted over a 2θ range of 5° to 50°, with a step size of 0.02°.

Anode preparation. 80 wt% of graphite anode powder (Sigma-Aldrich, USA), 10 wt% of super P (Alfa Aesar, US), 10 wt% of PVDF (Sigma-Aldrich, USA), and N-methyl-2-pyrrolidone (NMP) (Sigma-Aldrich, USA) were mixed via SK-350TII Kakuhunter planetary motion mixer to get PVDF-based anode slurry. 80 wt% of graphite, 10 wt% of super P, 10 wt% of [AMIm][Pectate], and distilled water were mixed via planetary motion mixer to get [AMIm][Pectate]-based anode slurry. After mixture completion, the slurry was coated on copper foil (thickness 0.02 mm, The Nilaco Corporation, Japan). PVDF and [AMIm][Pectate] based anodes were dried under vacuum at 80 °C for 8 hours and 2 hours, respectively.

Cell assembly. The anodes were fashioned into 15 mm diameter discs, each bearing a loading mass within 0.75-1.51 mg/cm^2; then, these anode discs were inserted into CR2025 coin cells. During the assembly procedure within Ar-filled glovebox, the separator was polypropylene (PP) (thickness 25 μm, Celgard 2500), the counter electrode was lithium metal (13 mm diameter, Honjo Chemical Corporation, Japan), and the liquid electrolyte (Sigma-Aldrich, USA) consisted of a solution comprising 1.0 M lithium hexafluorophosphate ($LiPF_6$) dissolved in a 1:1 volume ratio of ethylene carbonate (EC) and diethyl carbonate (DEC).

Electrochemical characterization. The cyclic voltammetry (CV) analysis was conducted

utilizing Bio-logic Science Instruments, at scan rates of 0.1, 0.2, 0.4, 0.6, 0.8, 1.0 mV/s across potential range from 0.1V to 2.1V. Prior to CV test, PVDF and [AMIm][Pectate]-based anodic half cells underwent 150 charge-discharge cycles at 0.5 C to ensure electrochemical stabilization. Linear sweep voltammetry (LSV) was also conducted using Bio-Logic Science Instruments to evaluate the electrochemical stability of synthesized binder, scanning from 2.5 V to 0.01 V at a rate of 0.2 mV/s. Potentiostatic electrochemical impedance spectroscopy (PEIS) and dynamic electrochemical impedance spectroscopy (DEIS) measurements were performed via VSP potentiostat electrochemical workstation (Bio-Logic Co. Ltd). PEIS measurements were undertaken within a frequency range of 1.0 MHz to 0.1 Hz, while DEIS investigations encompassed various potentials ranging from 0.1 V to 2.1 V at intervals of 0.1 V. Additionally, activation energy of charge transfer process was measured at different temperatures ranging from 20 °C to 60 °C, with increments of 10 °C. Charging-discharging was conducted through Electro Field ABE 1024 between 0.01 and 2.1 V in constant-current.

2.3 Result and discussion

The functional group analysis of [AMIm][Pectate] binder was conducted by FT-IR spectra of [AMIm][Cl], pectic acid, and [AMIm][Pectate], as depicted in **Figure 2.1**. The absorption band at 3390 cm^{-1} is attributed to the stretching vibration of -OH group, resulting from water absorption by [AMIm][Cl]. The peak detected at 3057 cm^{-1} corresponds to the saturated -CH stretching of imidazole ring, while those at 1565 cm^{-1} and 1170 cm^{-1} denote typical stretching and bending vibrations of imidazole ring. In addition, the peaks at 1647 cm^{-1} and 1426 cm^{-1} are indicative of C=C and -CH stretching vibrations of allyl group.[25,26] In the case of pectic acid, the peaks at 3400 cm^{-1} and 2930 cm^{-1} are associated with the stretching vibrations of -OH and -CH groups.[27,28] Furthermore, the peaks detected at 1734 cm^{-1} and 1626 cm^{-1}, which are

significant for identifying pectic acid, represent the stretching vibrations of ester and COO- groups. After synthesis, a significant decrease in peak intensity around 1600 cm^{-1} is noted, accompanied by a sharp increase in the intensity of COO^- peak. These observations provide convincing evidence of the successful neutralization reaction between [AMIm][OH] and pectic acid.

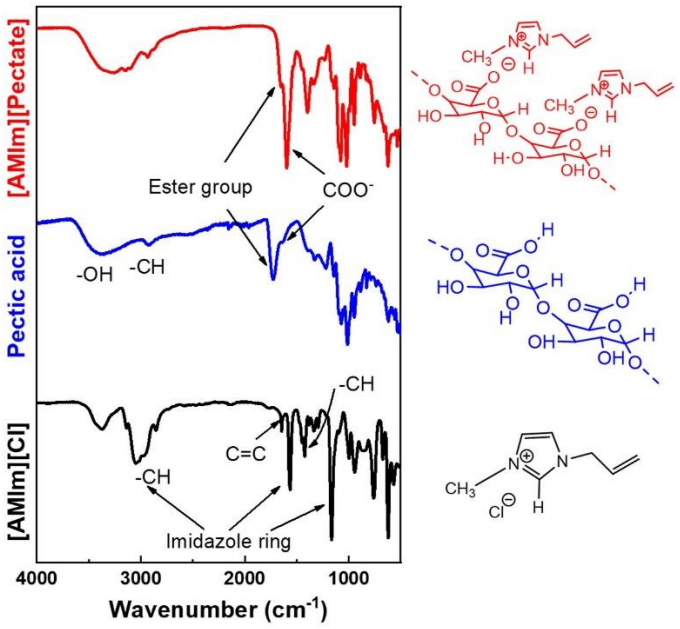

Figure 2.1. ATR-IR spectra of [AMIm][Cl], pectic acid, and [AMIm][Pectate].

The synthesized product, [AMIm][Pectate], was characterized using ^{1}H-NMR and ^{13}C-NMR in D_2O solvent, as depicted in **Figure 2.2a** and **2.2b**. By analyzing proton and carbon chemical shifts, the chemical groups present in the product were identified from a different perspective.[29–31] **Figure 2.2c** illustrates the integration of protons at positions 2, 7, 13, and 14, providing conclusive evidence that all -COOH groups present in pectic acid reacted with OH^- in [AMIm][OH]. Therefore, the obtained PIL maintains a 1:1 molar ratio between the ionic liquid $[AMIm]^+$ and the pectate anion $[Pectate]^-$. After dissolving [AMIm][Pectate] into distilled water, the pH value was measured at 7.04, as shown in **Figure 2.3**.

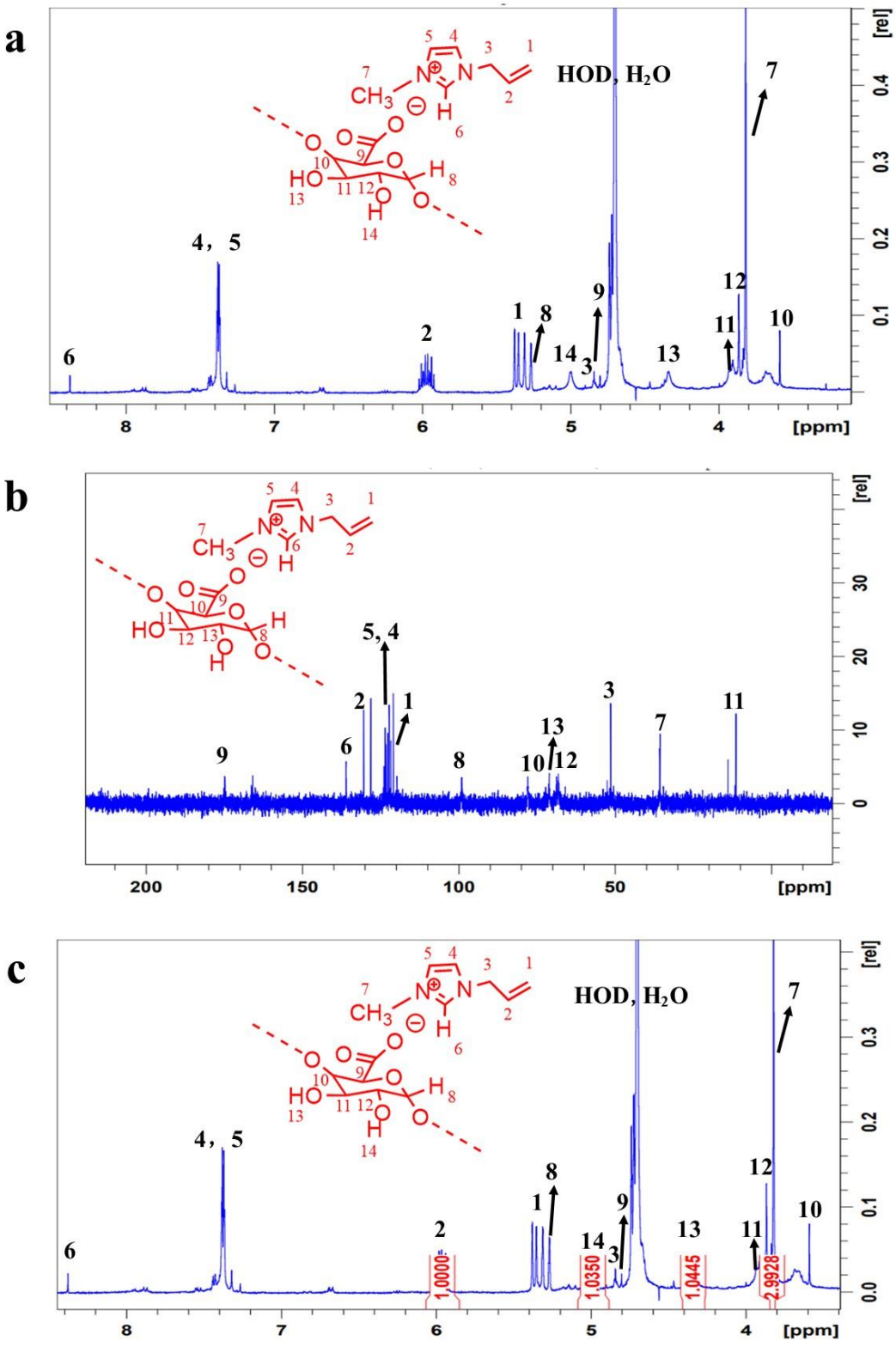

Figure 2.2. (a) ^{1}H-NMR, (b) ^{13}C-NMR of [AMIm][Pectate] in D_2O, and (c) Integration of protons at positions 2, 7, 13, and 14 of ^{1}H-NMR.

Figure 2.3. pH value of [AMIm][Pectate] dissolved in distilled water.

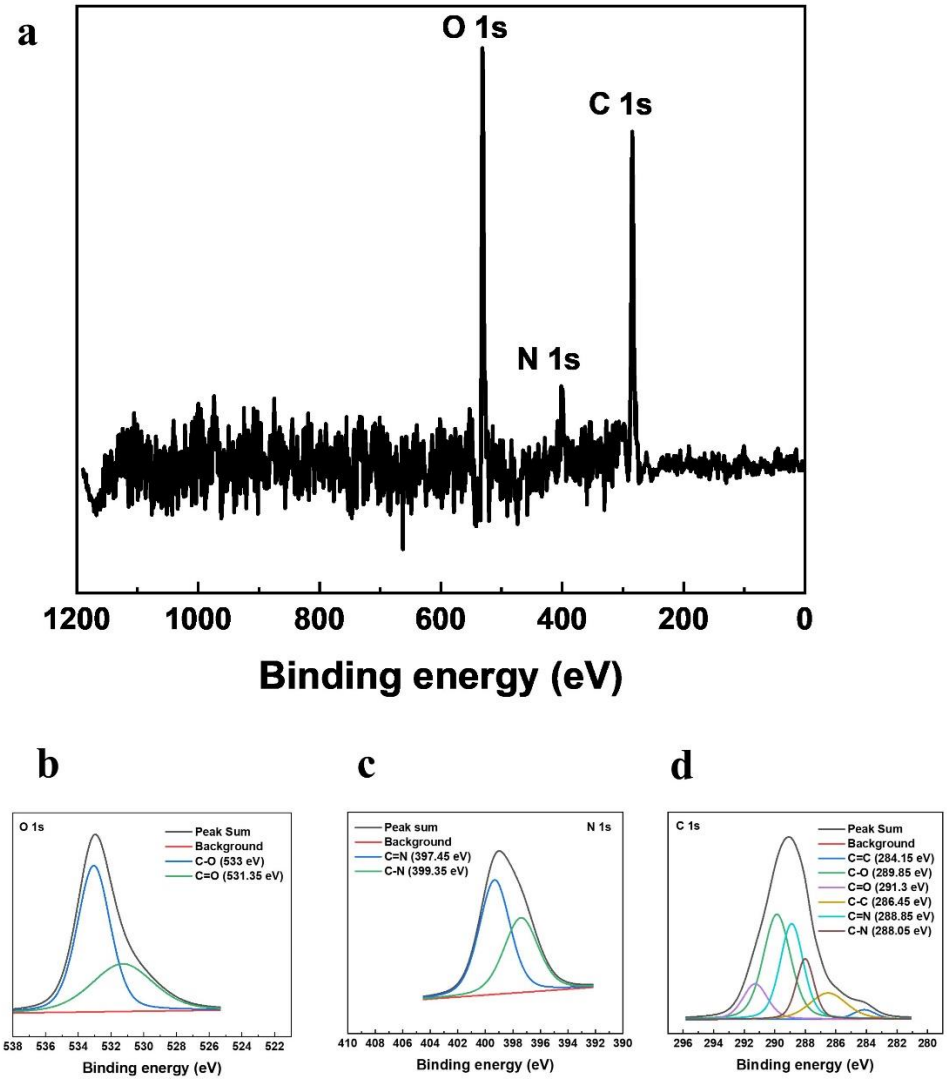

Figure 2.4. (a) XPS survey spectra of [AMIm][Pectate] and (b) O 1s, (c) N 1s, (d) C 1s analysis.

Additionally, XPS analysis of [AMIm][Pectate] sample, which covers the binding energy range from 0 to 1200 eV, was carried out as illustrated in **Figure 2.3a**. The elemental composition analysis revealed the presence of O, N, and C elements, while the absence of Cl is noted. The results confirmed the presence of key elements, including O, N, and C, while the absence of Cl indicated the complete exchange of Cl^- with OH^- during the ion exchange process. Furthermore, the fitting data obtained from XPS analysis (**Figure 2.3b-d**) elucidate the predominant chemical bonds, offering a supplementary explanation of the synthesized binder's structure.[32]

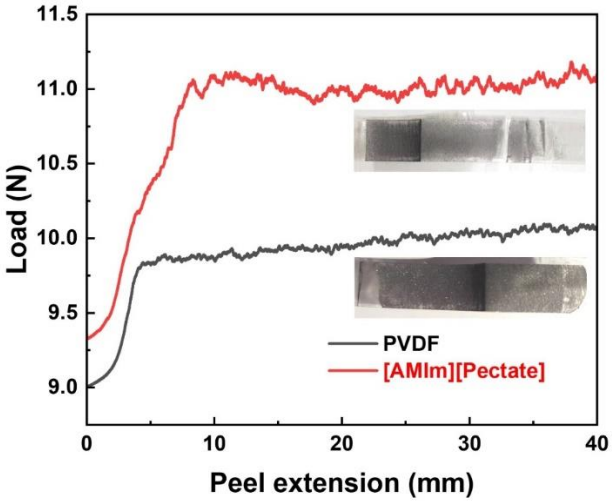

Figure 2.4. Adhesion strength profiles of PVDF (black line) and [AMIm][pectate] (red line) anodes after the peeling test.

The mechanical peeling test serves as a method for characterizing the adhesive properties of binders between electrode materials and copper foil. Enhanced adhesiveness is important to increase the structural stability of anodes, thereby improving adhesion between the anode and current collector. As shown in **Figure 2.4**, the peeling force of [AMIm][Pectate]-based anode was 11.1 N, surpassing that of PVDF counterpart 10.3 N. This disparity can potentially be

attributed to the substantial presence of -OH groups and carboxylate anions ($-COO^-$) within [AMIm][Pectate] polymer. These groups engender van der Waals force among molecules, improving the interconnection between active and conductive substances. Also, $-COO^-$ anions can coordinate with different polymer chains to form a network structure, further enhancing the ability to hold anode tightly.[33–35]

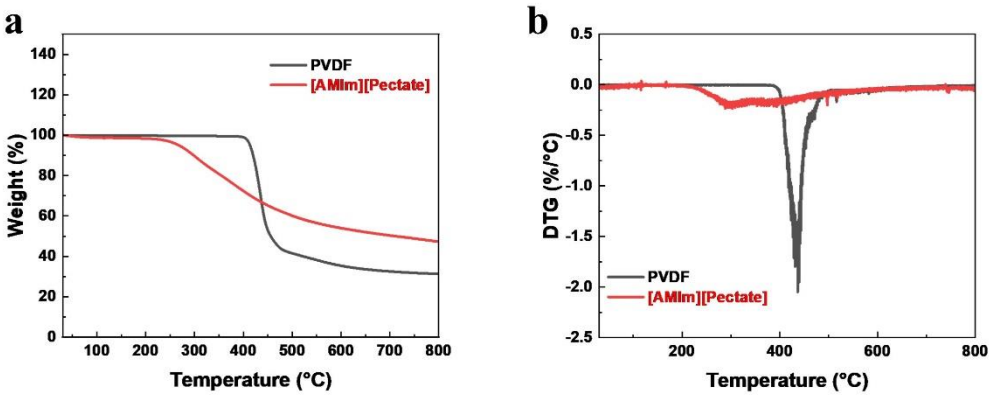

Figure 2.5. (a) TG and (b) DTG curves of PVDF and [AMIm][Pectate].

In addition to mechanical property testing, TGA was conducted to evaluate the thermal stability of PVDF and [AMIm][Pectate], helping to determine suitable operating temperatures for battery safety, as shown in **Figure 2.5a**. The results indicate that PVDF undergoes a 57% weight loss due to decomposition between 387 and 497 °C, with a peak loss at 437 °C. In contrast, [AMIm][Pectate] exhibits a gradual 38% weight loss between 213 and 493 °C, without a distinct decomposition peak. Although [AMIm][Pectate] has a lower decomposition onset temperature than PVDF, its gradual degradation minimizes sudden weight loss, enhancing battery safety, as depicted in **Figure 2.5b**. Additionally, considering the reliable operating temperatures specified by manufacturers, 213 °C is sufficient for typical battery lifespans.

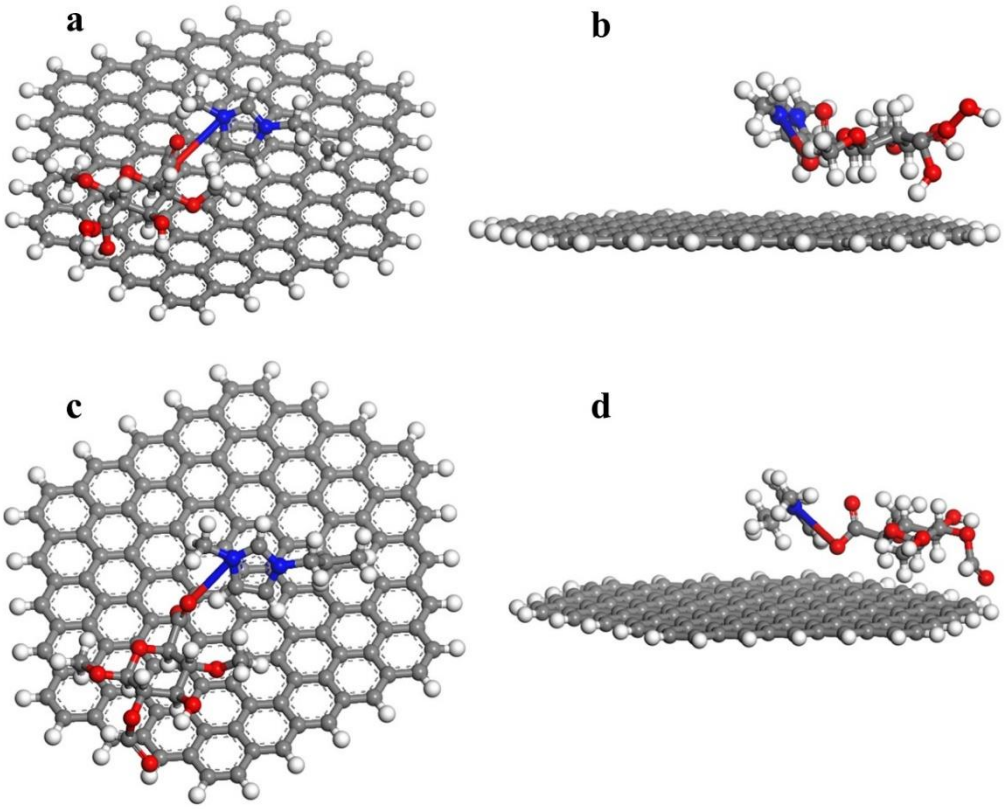

Figure 2.6. Structures of (a) front and (b) side views of the combined system between graphite and [AMIm][Pectate], and (c) front and (d) side views of the combined system between graphite and [PMIm][Pectate], as generated using Materials Studio.

Prior to cell preparation, to examine the effect of allyl substituent on the interaction of [AMIm][Pectate] with graphite, interaction energy ($E_{interaction}$) of [AMIm][Pectate] with graphite (**Figure 2.6a** and **2.6b**) was computed[36] and comparison was made with binder system without allyl substituent, i.e. 1-methyl-3-propyl-imidazolium (**Figure 2.6c** and **2.6d**). The energy was computed through Materials Studio, with the results in **Table 2.1**. The results indicate that $E_{Interacion}$ between graphite and [AMIm][Pectate] is -90.31 KJ/mol, slightly higher than that of [PMIm][Pectate], at -89.05 KJ/mol. This suggests that the existence of allyl group

is beneficial for connecting synthesized binder and graphite layer. However, since the difference value between $E_{Graphite+[AMIm][Pectate]}$ and $E_{Graphite+[PMIm][Pectate]}$ is small, the influence of allyl group remains limited.

Table 2.1. The energy of different materials. ($E_{Interacion} = E_{A+B} - (E_A + E_B)$).

$E_{Graphite}$	-4967.1943 Ha	$E_{Graphite}$	-4967.1943 Ha
$E_{[AMIm][Pectate]}$	-1296.1358 Ha	$E_{[PMIm][Pectate]}$	-1297.3678 Ha
$E_{Graphite+[AMIm][Pectate]}$	-6263.3645 Ha	$E_{Graphite+[PMIm][Pectate]}$	-6264.5962 Ha
$E_{Interacion}$	-0.0344 Ha=	$E_{Interacion}$	-0.00341 Ha=
	-90.31 $KJmol^{-1}$		-89.05 $KJmol^{-1}$

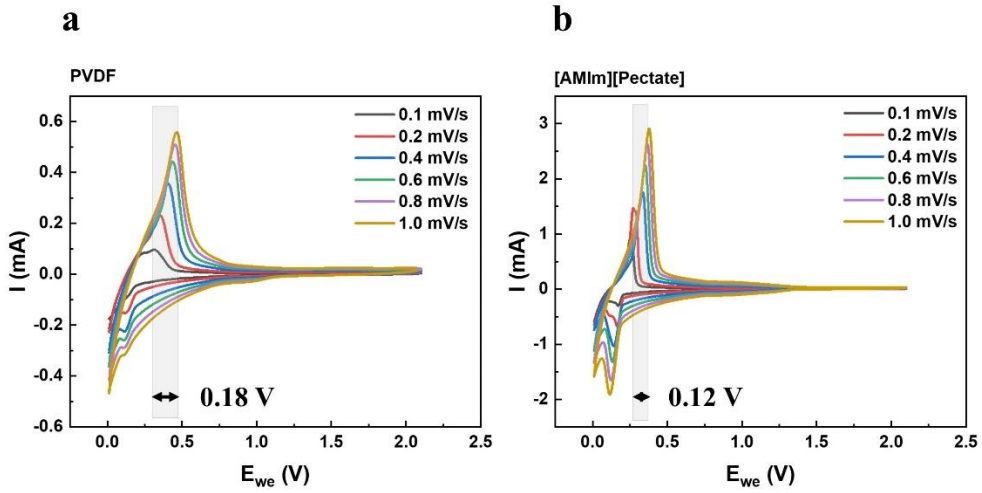

Figure 2.7. CV at different scan rates with (a) PVDF and (b) [AMIm][Pectate] as the binders for graphite anodes in 1M $LiPF_6$/EC: DEC.

To evaluate electrochemical performance of cells, CV measurements were performed at various scan rates, as depicted in **Figure 2.7a** and **2.7b**. Herein, the delithiation overpotentials are investigated by comparing the performance of [AMIm][Pectate] and PVDF based anodic half-cells. Notably, the delithiation overpotential exhibited by [AMIm][Pectate]-based anodic half-cell was found to be at 0.12 V, presenting a lower value compared to PVDF counterpart (0.18 V). Usually, the lower overpotential signifies improved kinetics and reduced energy

losses, thereby enhancing electrochemical efficiency. Additionally, the current range of the synthesized [AMIm][Pectate] binder is approximately 5-6 times higher than that of PVDF-based sample due to its ability to significantly enhance the interaction between the electrode and electrolyte. Higher current responses in CV studies indicate that [AMIm][Pectate] binder-based anode exhibits greater electrochemical activity and faster Li^+ diffusion, which are essential for higher capacity storage and long-term cycling stability. Furthermore, [AMIm][Pectate]-based sample maintains high currents response across multiple scan rates, demonstrating its ability to retain high capacity even at fast charge-discharge rates. This characteristic is particularly advantageous for high-power applications.[7,37–39]

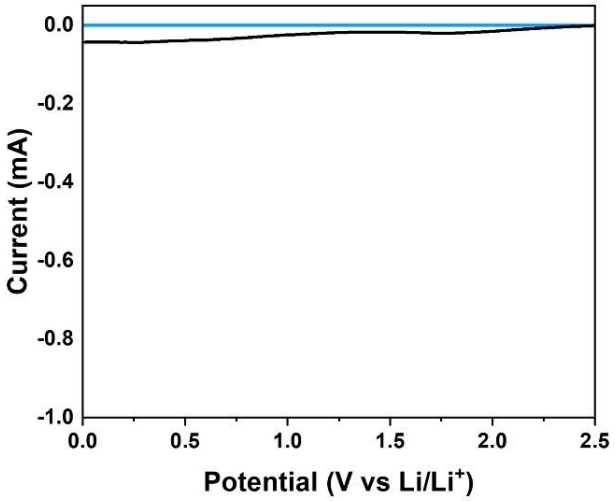

Figure 2.8. LSV of Li/[AMIm][Pectate] half-cell in 1M $LiPF_6$/EC: DEC from 2.5 V to 0.01 V at a scan rate of 0.2 mVs^{-1}.

To assess the electrochemical stability of [AMIm][Pectate] binder under cycling-induced electrochemical stress, LSV was performed on Li/[AMIm][Pectate] half-cell. The test was conducted from 2.5 V to 0.01 V at a scan rate of 0.2 mV/s, as shown in **Figure 2.8**. The results indicate that after voltage application, only weak negative currents were observed relative to

the baseline (X=0), with no significant reduction peaks detected. This suggests that neither the bulky anion $[Pectate]^-$ nor the cation $[AMIm]^+$ undergoes significant degradation during cycling between 0.01 V and 2.1 V, demonstrating the long-term stability of [AMIm][Pectate] under electrochemical stress.

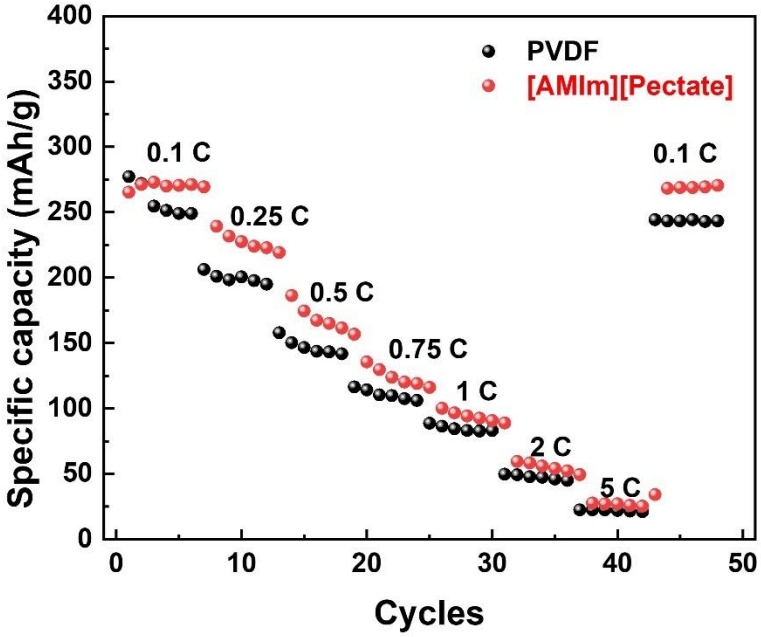

Figure 2.9. Cycling test of PVDF and [AMIm][Pectate] based half-cells with rate between 0.1 C and 5 C.

Figure 2.9 depicts the cycling test of two anodic half-cells with rates ranging from 0.1 C to 5 C (1 C = 372 mA/g). Rate capability, as a crucial way to assess battery performance, offers insights into Li^+ transport efficiency at varied rates and the impact of diverse charging and discharging rates on battery life. [AMIm][Pectate] based half-cell exhibited superior discharge capacity compared to PVDF counterpart across different discharge currents. Even under the high-rate charging and discharging condition, 5 C, the capacity demonstrated resilience, rebounded to 275 mAh/g at the low-rate condition (0.1 C) after 40 cycles.[40,41]

Long cycling, as a valuable method for assessing battery life, offers significant insights for subsequent research and optimization. **Figure 2.10a** presents a comparative analysis of

specific capacity and coulombic efficiency between anodic half cells employing PVDF and [AMIm][Pectate] binders, operated at the charge-discharge rate of 1 C within the voltage range of 0.01 to 2.1 V. The results indicated the cells required 100-200 cycles to reach their high capacities. This is because graphite anode materials undergo repeated volume expansion and contraction to improve lithium-ion transport efficiency gradually. During the initial cycle, the cells were in a relatively “inactive state”, with limited lithium diffusion pathways. However, as cycling progressed, the anode structure had been electrochemically “activated”, achieving an optimized state for lithium-ion storage and transport. Also, graphite-based anodes exhibited gradual electrolyte wettability, which limited lithium diffusion. Hence, in the first cycle of CV, lithiation-delithiation was limited. With repeated voltage scans, accessibility to active sites increased due to improved wettability. The utilization of [AMIm][Pectate] binder within the cell manifested the highest capacity of 239.8 mAh/g, in contrast to commercial PVDF binder, which showed 208 mAh/g. Over 1000 cycles, the specific capacity of [AMIm][Pectate]-based cell reduced to 178.9 mAh/g, while PVDF counterpart diminishes to 131.9 mAh/g. Consequently, [AMIm][Pectate]-based cell exhibited a capacity retention of 74.6% after 1000 cycles, surpassing the 63.4% retention in PVDF-based cell. In addition, the coulombic efficiency of [AMIm][Pectate]-based anodic half-cell demonstrated stability till 500 cycles. In contrast, the coulombic efficiency of PVDF binder-based anodic half-cell exhibited fluctuations, indicative of inferior stability. This observed stability in [AMIm][Pectate]-based anode is attributed to maintaining mechanical integrity of anode structure. The internal transformations of anodes were investigated using differential capacity analyses based on delithiation capacity data, as depicted in **Figure 2.10b** and **2.10c**. A comparative study of these zoom-in peaks between [AMIm][Pectate] and PVDF based binder half cells reveals that with the increase of cycles, the magnitudes of both samples diminished concurrently. However, the peaks of PVDF-based sample exhibited shifts towards lower voltages, while the peaks of

[AMIm][Pectate] sample displayed no obvious shift. These shifts indicated the extent of available lithium depletion over long cycling periods.[42] Specifically, the degradation of PVDF is more likely than [AMIm][Pectate]-based anode. PVDF-based anode was aggravated by lithium deposition on the anode surface and intercalation of electrolyte solvents within the anode structure, resulting in lower specific capacity.

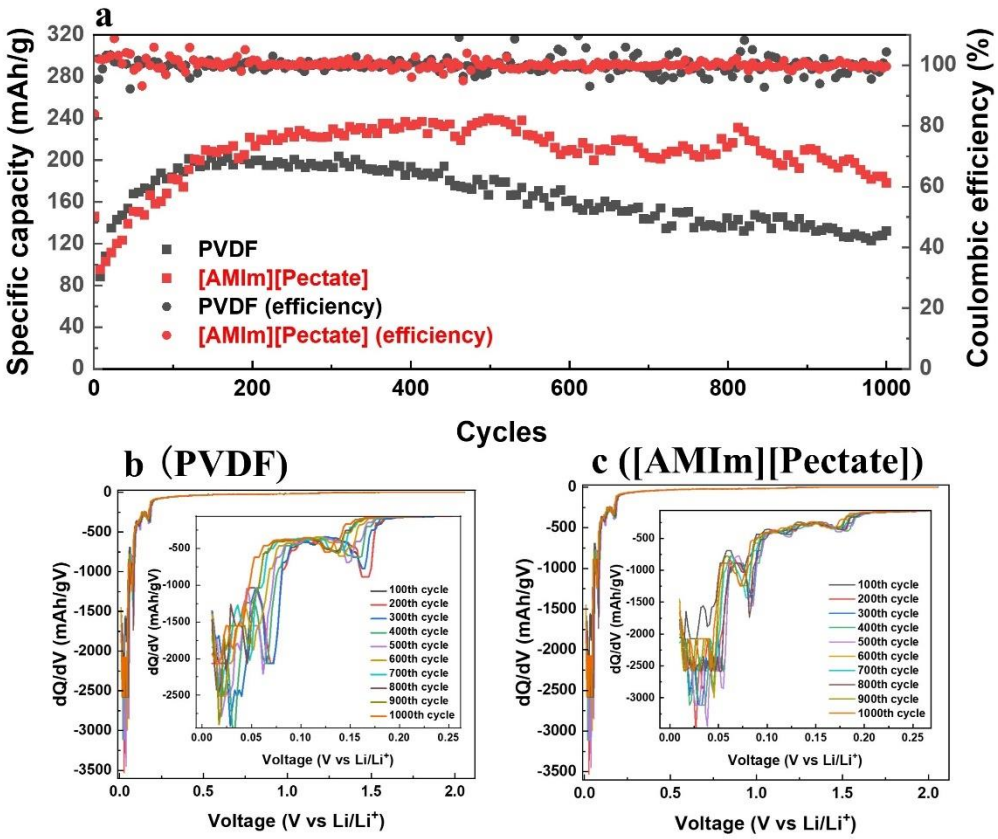

Figure 2.10. (a) Long cycling specific capacity and coulombic efficiency comparison between PVDF and [AMIm][Pectate] based half-cells at 1 C; Differential capacity vs voltage plots (dQ/dV) of (b) PVDF and (c) [AMIm][Pectate] binders based half-cells.

Additionally, to determine whether [AMIm][Pectate] influenced lithiation–delithiation process, dV/dQ analysis was performed using data from **Figure 2.11a** and **2.11b** after the cells underwent 5 charge-discharge cycles at 0.1 C, as shown in **Figure 2.11c** and **2.11d**. The results

show peaks at 76, 189, and 258 mAh/g in case of PVDF-based half-cell and 88, 216, and 306 mAh/g in case of [AMIm][Pectate] indicating that the formation of LiC_{36}/LiC_{24}, LiC_{12}, and LiC_6 respectively. At these peak positions, [AMIm][Pectate]-based anode exhibits an increased capacity of 12 mAh/g, 15 mAh/g, and 20 mAh/g compared to PVDF, demonstrating that [AMIm][Pectate] positively impacts Li^+ storage due to its superior electrochemical properties. As lithiation progresses, [AMIm][Pectate] exhibits a greater ability to stabilize graphite, facilitating enhanced Li^+ intercalation.

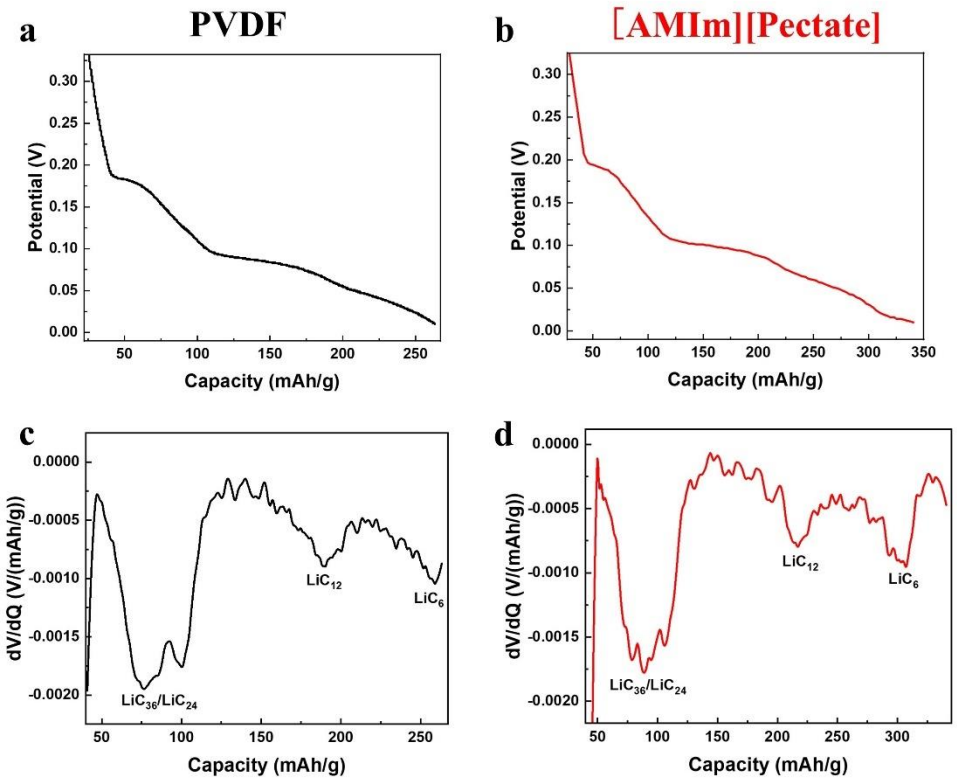

Figure 2.11. Lithiation voltage profiles at 0.1 C of (a) PVDF and (b) [AMIm][Pectate] based anodes; dV/dQ plots for the lithiation cycle at 0.1 C of (c) PVDF and (d) [AMIm][Pectate] anodes.

Furthermore, to verify the peak formations, [AMIm][Pectate] anodes held at 0.2, 0.4, and 2.1 V after lithiation were analyzed via XRD, as shown in **Figure 2.12**. The results clearly indicate the formation of LiC_{36}, LiC_{24}, LiC_{12}, and LiC_6 at peaks of 26.06°, 25.4°, 25.0°, and

23.8°, respectively, in the anode at 0.2 V, compared to those at 0.4 V and 2.1 V. Similarly, previous research has reported that PVDF-based graphite anodes also exhibit the formation of LiC_{12} and LiC_6 phases after lithiation, as confirmed by XRD, with peak positions closely matching those observed for [AMIm][Pectate]-based samples.[43,44]

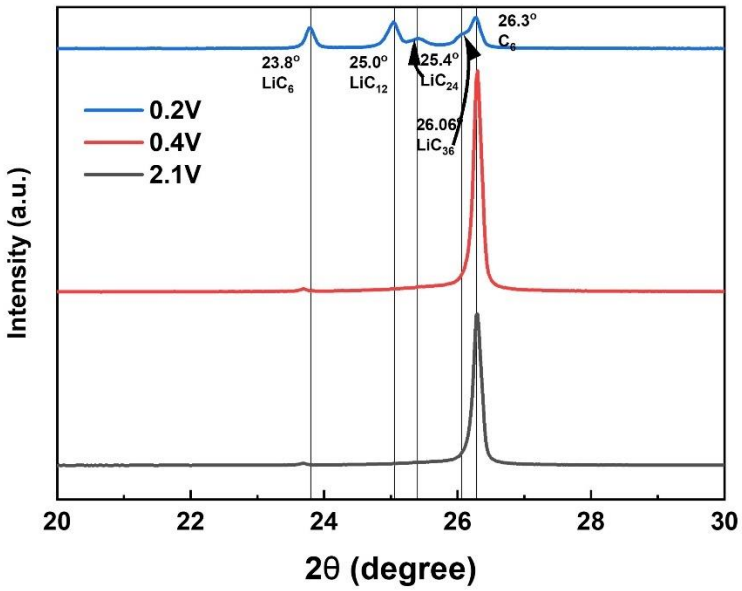

Figure 2.12. XRD comparison of the anodes at 0.2 V, 0.4 V, and 2.1 V after lithiation.

To investigate the impact of SEI formation on the internal resistance of cells, PEIS was conducted. A comparative analysis of Nyquist plots of half cells was undertaken both before and after the initial CV test at the scan rate of 0.1 mV/s, as illustrated in **Figure 2.13a**. Based on the results, it is evident that after SEI formation during the first CV cycle, the polarization resistances of both PVDF and [AMIm][Pectate] based anodes significantly decreased. Also, the polarization resistance of [AMIm][Pectate] was lower than that of PVDF based anode, which indicates the tendency for rapider electrochemical reactions occurring at the interface between [AMIm][Pectate] based electrode and electrolytes. Furthermore, by examining the points of Warburg impedance in Nyquist plots after CV test, Warburg constants were

determined in **Figure 2.13b**. Then, employing Equation 1, lithium diffusion coefficient (D_{Li}) was computed,[45,46] yielding values of 7.15×10^{-13} S/cm^2 and 1.20×10^{-13} S/cm^2 for [AMIm][Pectate] and PVDF based samples, respectively. A higher D_{Li} enhances lithium-ion transport, enabling more efficient access to active material sites, which helps mitigate capacity degradation and improve long cycling stability.[47]

$$D_{Li} = \frac{R^2T^2}{2A^2n^4F^4C^2\,\sigma^2} \qquad \textit{Equation 1}$$

Where: R is gas constant, T is absolute temperature, A is anode area, n is electrons number, F is Faraday constant, C is lithium-ions concentration, and σ is Warburg factor, obtained from slopes in **Figure 2.13b**.

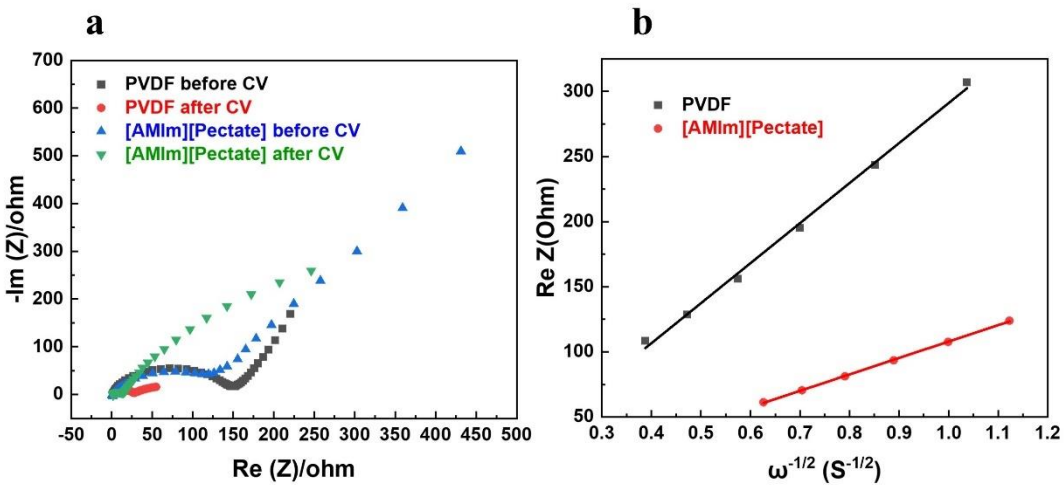

Figure 2.13. (a) Nyquist plots of anodic half cells with PVDF and [AMIm][Pectate] binders before and after CV at 0.1 mVs^{-1}; (b) Re vs $\omega^{-1/2}$ of PVDF and [AMIm][Pectate] based anode samples.

To explore SEI formation more intuitively, the initial cycles of CV analysis was performed at a scan rate of 0.1 mV/s, as shown in **Figure 2.14**. Within the reduction process, distinct peaks associated with SEI formation were observed between 0.56 V and 0.94 V for PVDF and between 0.49 V and 0.85 V for [AMIm][Pectate]. Based on Randles-Sevcik Equation, as shown in Equation 2, the electrode surface areas of these two samples were calculated by incorporating

D_{Li} values obtained from **Figure 2.13b** and peak currents during the redox process in **Figure 2.14**. The calculated electrode surface areas of PVDF and [AMIm][Pectate]-based samples are 5.82×10^5 cm² and 9.72×10^4 cm², respectively. A higher surface area in PVDF anode results in increased lithium consumption during SEI formation. Additionally, greater surface exposure to liquid electrolytes leads to more undesirable side reactions, accelerating capacity degradation. In contrast, [AMIm][Pectate] anode, with a lower surface area, exhibits greater structural stability, reducing the risk of material cracking.

$$I_p = (2.69\times10^5)\, n^{3/2} A C_{Li} D_{Li}^{1/2} v^{1/2} \qquad \textit{Equation 2}$$

Where: I_p is peak current, n is number of electrons transferred, A is electrode surface area, C_{Li} is the concentration in the electrode, D_{Li} is lithium diffusion coefficient, and v is scan rate.

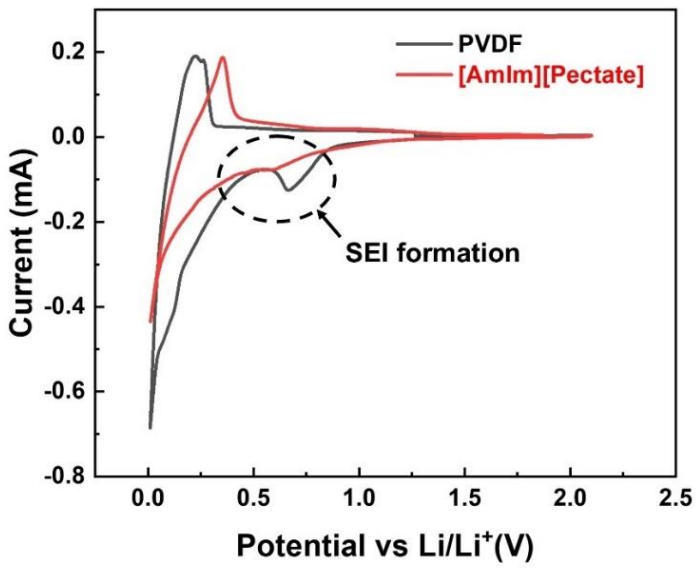

Figure 2.14. First CV cycles of PVDF and [AMIm][Pectate] based half-cells between 0.01 V and 2.1 V.

DEIS, as another way for elucidating internal phenomena within LIBs, facilitates the estimation of various impedance parameters, including anode internal resistance (R_{Int}), charge transfer resistance (R_{CT}), SEI resistance (R_{SEI}), and diffusion resistance (R_{Dif}).[48] In **Figure**

2.15a and **2.15b**, Nyquist plots comparing [AMIm][Pectate] and PVDF cells are presented across different potentials during the discharge process. Utilizing appropriate equivalent electric circuit models (EECMs), circuit fitting was conducted to get tables, as delineated in **Table 2.2** and **Table 2.3**. Particularly noteworthy is the observation that R_{SEI} associated with [AMIm][Pectate] demonstrates a diminution compared to PVDF counterpart, as illustrated in **Figure 2.16**. A lower R_{SEI} minimizes voltage drops and polarization, beneficial for improving energy efficiency and coulombic efficiency of cells. Furthermore, when combined with insights from SEI formation analysis in **Figure 2.14**, these findings confirm that SEI layer in [AMIm][Pectate]-based anode exhibits superior electrochemical performance than PVDF counterpart.[49,50]

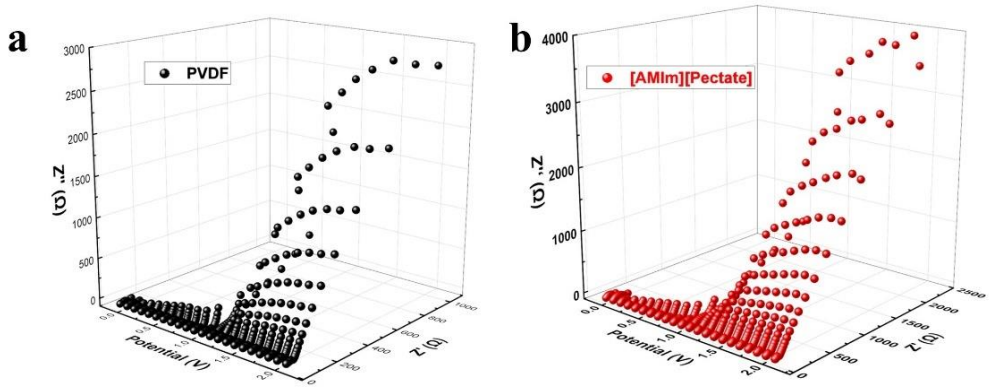

Figure 2.15. DEIS Nyquist profiles of (a) PVDF and (b) [AMIm][Pectate] based anodic hall cells with discharging.

Table 2.2. Circuit fitting data for PVDF for discharging cycle at different potentials.

Potential (V)	R_{Int}	R_{CT}	R_{SEI}	R_{Dif}	W	Chsq	Equivalent circuit
0.11	2.264	13.02	5.812	33.61	1.64E-01	1.22E-04	RL(QR)(QR)(QR)W
0.21	2.36	27.59	12.54	192.2	0.2019	8.22E-05	RL(QR)(QR)(QR)W
0.31	2.304	22.7	12.26	7.95E+08	1.48E-01	3.83E-05	RL(QR)(QR)(QR)W
0.41	3.152	28.06	8.436	2.26E+16	1.34E+13	2.02E-03	RL(QR)(QR)(QR)W
0.51	2.275	23.92	11.93	8010	1.15E-01	3.07E-05	RL(QR)(QR)(QR)W

0.61	2.368	25.31	11.96	1.04E+14	0.1075	3.38E-05	RL(QR)(QR)(QR)W
0.71	2.363	26.49	11.53	1.96E+06	1.10E-01	6.00E-05	RL(QR)(QR)(QR)W
0.91	2.313	30.42	11	2.87E+17	9.82E-02	3.34E-04	RL(QR)(QR)(QR)W
1.01	2.651	35.31	8.674	3.23E+12	8.00E-02	1.08E-03	RL(QR)(QR)(QR)W
1.11	2.218	23.49	12.65	41.46	3.11E-04	1.29E-04	RL(QR)(QR)(QR)(CRW)
1.21	2.297	20.67	12.04	3.27E+12	1.28E-02	5.01E-03	RL(QR)(QR)(QR)W
1.3	2.215	130.1	24.15	2753	4.09E+08	1.67E-03	RL(QR)(QR)(QR)W
1.4	2.26	25.53	12.13	1.07E+04	4.08E-02	5.73E-05	RL(QR)(QR)(QR)W
1.5	2.278	25.34	12.19	1.83E+05	3.41E-02	4.74E-05	RL(QR)(QR)(QR)W
1.6	3.238	25.84	12.41	2.11E+04	3.49E-03	2.84E-05	RL(QR)(QR)(QR)W
1.7	3.156	26.35	12.79	2255	3.58E-02	4.02E-05	RL(QR)(QR)(QR)W
1.8	2.906	26.69	12.75	2.24E+04	3.72E-01	4.08E-05	RL(QR)(QR)(QR)W
1.9	2.84	30.9	11.81	3.12E+04	1.02E+14	2.38E-04	RL(QR)(QR)(QR)W
2	2.711	26.48	12.65	1.60E+04	3.38E-02	5.78E-05	RL(QR)(QR)(QR)W
2.1	2.729	26.52	12.85	1.31E+04	3.19E-02	1.11E-04	RL(QR)(QR)(QR)W

Table 2.2. Circuit fitting data for [AMIm][Pectate] for discharging cycle at different potentials.

Potential (V)	R_{Int}	R_{CT}	R_{SEI}	R_{Dif}	W	Chsq	Equivalent circuit
0.11	1.819	29.06	1.394	106.3	1.24E-01	2.88E-04	RL(QR)(QR)(QR)W
0.21	1.82	51.5	1.448	191.3	1.329	9.88E-04	RL(QR)(QR)(QR)W
0.31	1.695	32.01	7.22	63.34	0.1321	5.85E-04	RL(QR)(CR)(CR)W
0.41	1.653	36.03	6.428	125.9	0.1117	6.35E-04	RL(QR)(CR)(CR)W
0.51	1.599	36.46	6.44	1055	8.40E+10	9.57E-04	RL(QR)(QR)(QR)W
0.61	1.598	37.6	10.41	7998	4.60E+04	9.73E-04	RL(QR)(QR)(QR)W
0.71	1.6	36.28	2.305	75.14	0.07495	9.93E-04	RL(QR)(CR)(CR)W
0.91	1.546	18.61	8.684	40.16	0.02481	5.14E-03	RL(QR)(CR)(CR)W
1.01	1.74	22.68	3.62	79.88	1.98E-02	2.70E-03	RL(QR)(QR)(QR)W
1.11	1.542	25.03	4.163	156.2	0.01227	1.88E-03	RL(QR)(CR)(CR)W
1.21	1.713	12.65	6.15	4.40E+02	6.84E-03	5.38E-04	RL(QR)(QR)(QR)W
1.3	1.755	19.24	5.6	4630	7.32E+08	5.43E-04	RL(QR)(QR)(QR)W
1.4	1.728	20.13	5.45	26530	3.94E-01	1.94E-04	RL(QR)(QR)(QR)W
1.5	1.687	13.73	9.583	6.66E+04	0.003146	4.41E-04	RL(QR)(QR)(CR)W
1.6	1.75	20.03	5.51	80050	4.77E+03	2.66E-04	RL(QR)(QR)(QR)W
1.7	1.679	14.21	10.45	9.71E+04	2.50E+07	4.90E-04	RL(QR)(QR)(CR)W
1.8	1.581	31.88	11.46	45.73	2.22E+05	2.06E-03	RL(QR)(QR)(QR)W
1.9	1.709	19.29	6.59	5.66E+03	1.18E+06	2.57E-04	RL(QR)(QR)(QR)W
2	1.61	32.32	10	35090	2.66E+03	2.25E-03	RL(QR)(QR)(QR)W
2.1	1.745	19.42	6.192	3.60E+04	1.38E+08	3.88E-04	RL(QR)(QR)(QR)W

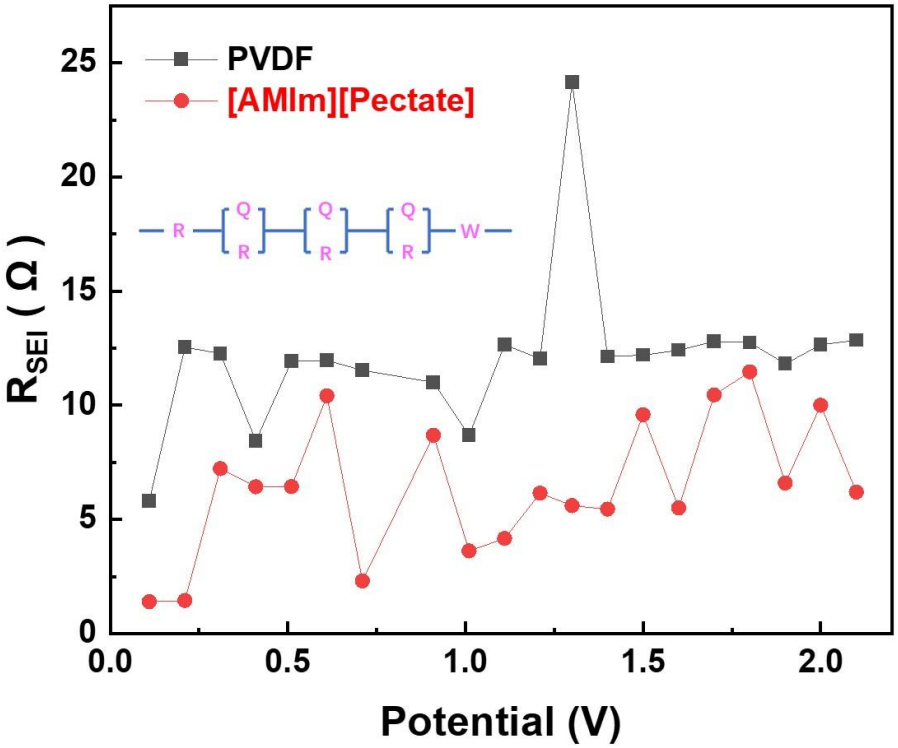

Figure 2.16. SEI resistance vs potential plots of PVDF and [AMIm][Pectate] based anodic half cells.

To explore the electrochemical performance across varying thermal environments, Nyquist plots were executed within the temperature range of 20~60 °C, as shown in **Figure 2.17a** and **2.17b**. The first semicircle relates to the interface resistance between graphite electrodes and liquid electrolytes, R_{CT}. Notably, an inverse relationship is discerned between temperature elevation and the magnitude of R_{CT} semicircle, wherein higher temperatures correspond to lower R_{CT}. This observed increment in charge transfer with rising temperature can be attributed to the reduction in interfacial impedance, thereby decreasing the energetic barriers of Li^+ transport. Consequently, an increased resistance would generate heightened impedance to Li^+ migration, ultimately leading to diminished electrochemical efficacy within batteries. After applying appropriate EECMs for circuit fitting in **Table 2.4** and **2.5**, log (R_{CT}^{-1}) versus 1000/T was plotted, yielding the graphical representation in **Figure 2.18**. According

to Arrhenius Equation, as shown in Equation 3, the activation energy (E_a) governing Li^+ desolvation was calculated through slopes. It is noteworthy that E_a for PVDF and [AMIm][Pectate] are 56.04 and 48.37 kJ/mol, respectively. This disparity in E_a suggests a lower energy barrier associated with [AMIm][Pectate] sample, which essentially helps to accelerate Li^+ migration kinetics, conferring superior electrochemical performance.[51,52]

$$k = Ae^{\frac{-E_a}{RT}} \qquad \textit{Equation 3}$$

Where: k is the rate constant of reaction, A is the pre-exponential factor, R is the gas constant, and T is the absolute temperature.

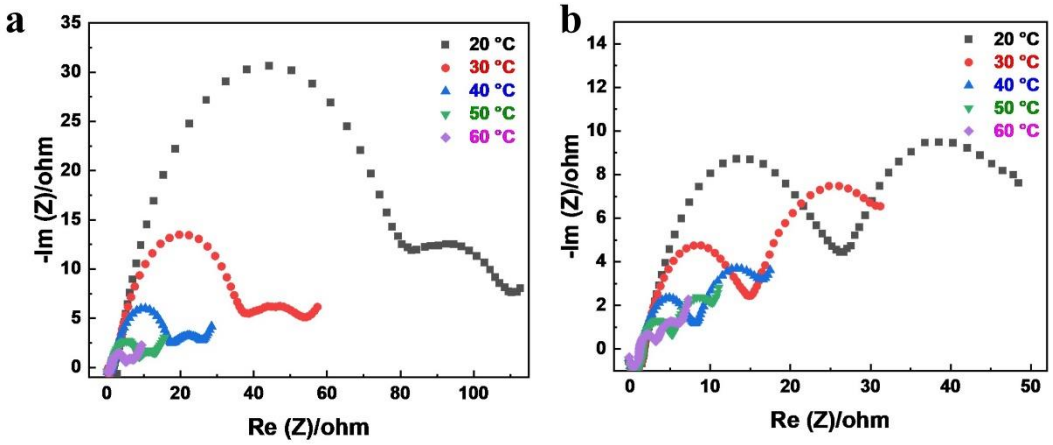

Figure 2.17. Nyquist EIS profiles of (a) PVDF and (b) [AmIm][Pectate] based anode cells at 20, 30, 40, 50, 60 °C.

Table 2.4. Circuit fitting data for Nyquist plots of PVDF-based anode at different temperatures.

Temperature (℃)	R_{Int}	R_{CT}	R_{SEI}	W	Chsq	Equivalent circuit
20	1.589	61.14	38.55	7.98E-02	2.34E-03	R(QR)(CR)W
30	1.689	38.91	9.686	1.49E-01	1.86E-03	R(QR)(CR)W
40	1.297	17.54	5.091	2.04E-01	1.53E-03	R(QR)(CR)W
50	1.121	8.066	2.816	2.686	8.96E-04	R(QR)(CR)W
60	1.011	4.231	1.53	3.66E+00	1.09E-03	R(QR)(CR)W

Table 2.5. Circuit fitting data for Nyquist plots of [AMIm][Pectate]-based anode at different temperatures.

Temperature (°C)	R_{Int}	R_{CT}	R_{SEI}	W	Chsq	Equivalent circuit
20	1.825	25.33	14.03	0.1346	8.25E-04	R(QR)(CR)W
30	1.155	1105	7.431	8.75E+10	3.00E-03	R(QR)(CR)W
40	1.055	43.21	3.601	2.07E+09	2.96E-03	R(QR)(CR)W
50	1.401	2.376	2.14	2.70E+14	2.75E-03	R(QR)(CR)W
60	1.284	4.881	1.283	6.92E-01	1.81E-03	R(QR)(CR)W

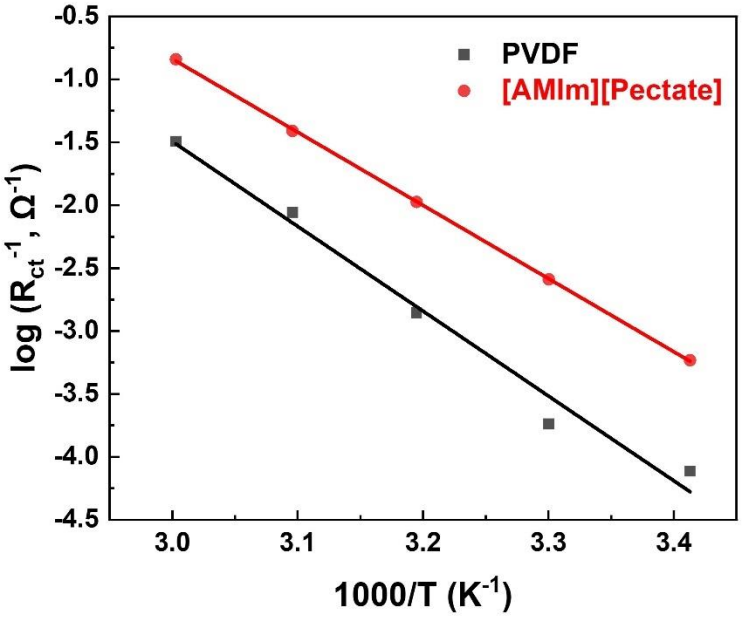

Figure 2.18. Arrhenius plots for charge transfer resistance (R_{CT}).

After long cycling, the cells were disassembled to discern chemical transformations occurring on the anode surface through XPS. Analysis of PVDF and [AMIm][Pectate] based samples, as depicted in **Figure 2.19a-f**, revealed the presence of F, O, and C elements. In PVDF-based sample, the F 1s spectrum exhibited discernible peaks corresponding to C-F and Li_xPF_y, $Li_xPO_yF_z$ bonds, with C-F peak notably prominent. However, this prominence is disadvantageous for Li^+ transport through SEI. The abundant C-F distribution on the surface of PVDF-based sample is electrochemical inactive, creating a barrier that hinders Li^+

intercalation into the anode. This obstruction impairs Li^+ transport, leading to reduced capacity and rate performance. Within the O 1s spectrum, $Li_xPO_yF_z$, C=O, $LiCO_3$, and C-O bonds were observed, primarily resulting from electrolyte decomposition. Similarly, the C 1s spectrum displayed peaks attributed to C-F, C=O, C-O, $LiCO_3$, as well as C-C, C-H, and C=C bonds, indicative of the decomposition of electrolyte and electrochemical reactions of graphite anode. Contrastingly, in [AMIm][Pectate]-based sample, in addition to Li_xPFy and $Li_xPO_yF_z$ bonds, LiF bond was discerned within the F 1s spectrum, facilitating Li^+ transport. LiF, as a well-known ionic conductor, enhances the ionic conductivity of SEI layer, ensuring its stability while preventing further electrolyte decomposition. The O 1s spectrum demonstrated negligible disparity between PVDF and [AMIm][Pectate]-based samples, albeit the intensity of the C-O peak was notably higher than that of C=O, possibly attributed to the prevalence of C-O moieties within the [AMIm][Pectate] binder. Within the C 1s spectrum, the bond profiles in [AMIm][Pectate] resemble those observed in PVDF-based sample, except for the absence of C-F bond.[53–56]

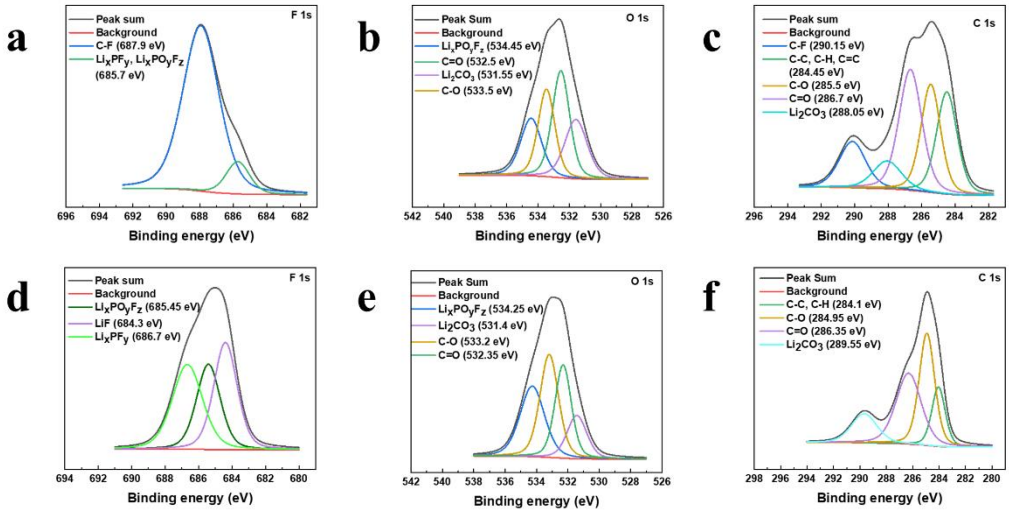

Figure 2.19. XPS spectra of PVDF sample (a) F 1s, (b) O 1s, (c) C 1s and [AMIm][Pectate] sample of (d) F 1s, (e) O 1s, (f) C.

SEM images of the surface and cross-section, as presented in **Figure 2.20a-f**, provide a clear comparison between PVDF and [AMIm][Pectate] based anodes after 1000 cycles. In PVDF sample, conspicuous features included obvious cracking (**Figure 2.20a** and **2.20b**) and delamination (**Figure 2.20c**), whereas [AMIm][Pectate] sample exhibited sustained structural integrity (**Figure 2.20d-f**). The preservation of structural integrity in [AMIm][Pectate] holds notable implications, ensuring the retention of high capacity throughout prolonged charge-discharge cycles. Moreover, this extends the operational lifespan of cells, thereby mitigating the depletion of natural resources and minimizing waste accumulation.

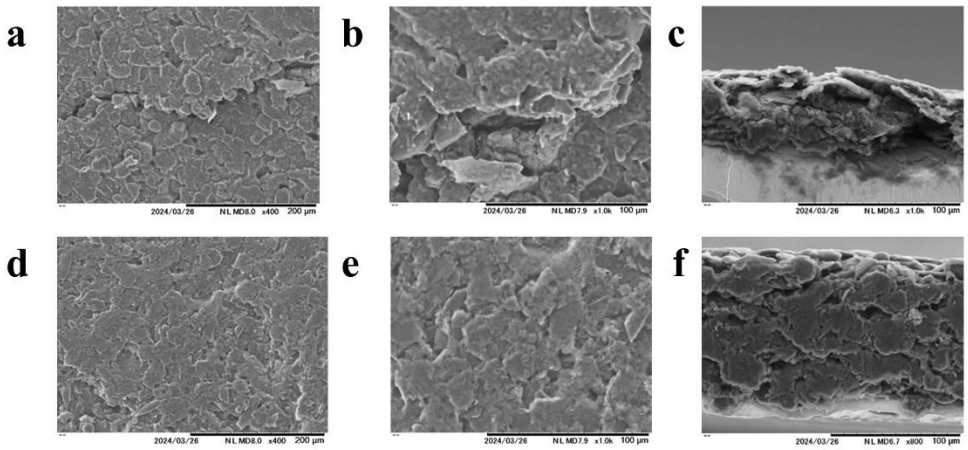

Figure 2.20. SEM images in different magnifications. (a) 400× surface, (b) 1000× surface, (c) 1000× cross-section of PVDF-based anode and (d) 400× surface, (e) 1000× surface and (f) 1000× cross-section [AMIm][Pectate]-based anode.

2.4 Conclusion

The utilization of [AMIm][Pectate] as a binder instead of PVDF within graphite anodes not only showed superior mechanical strength conducive to the preservation of structural integrity but also manifested remarkable electrochemical attributes post-SEI formation. These attributes encompass diminished delithiation overpotential, lower SEI resistance, reduced

charge transfer resistance, and decreased activation energy of lithiation, collectively augmenting the facilitation of Li^+ diffusion and enhancing the overall charge-discharge efficiency. Moreover, this study underscores the feasibility of utilizing biomaterial pectic acid as the polymer backbone to maintain structural stability of anodes. The employment of [AMIm][Pectate] as a water-soluble binder economizes the anode preparation timeline and avoids the utilization of environmentally harmful NMP solvent. These advantages align with the sustainable advancement of LIBs, supporting the transition toward green energy solutions and contributing to global net-zero emissions goals.

References

(1) He, B.; Zheng, H.; Tang, K.; Xi, P.; Li, M.; Wei, L.; Guan, Q. A Comprehensive Review of Lithium-Ion Battery (LiB) Recycling Technologies and Industrial Market Trend Insights. *Recycling.* **2024**, *9* (1), 9. https://doi.org/10.3390/recycling9010009.

(2) Wei, Q.; Wu, Y.; Li, S.; Chen, R.; Ding, J.; Zhang, C. Spent Lithium Ion Battery (LIB) Recycle from Electric Vehicles: A Mini-Review. *Science of the Total Environment*. **2023**, 866. https://doi.org/10.1016/j.scitotenv.2022.161380.

(3) Bai, H.; Song, Z. Lithium-Ion Battery, Sodium-Ion Battery, or Redox-Flow Battery: A Comprehensive Comparison in Renewable Energy Systems. *Journal of Power Sources.* **2023**, *580*. 233426. https://doi.org/10.1016/j.jpowsour.2023.233426.

(4) Wang, E.; Nie, J.; Wang, Y. Government Subsidy Strategies for the New Energy Vehicle Power Battery Recycling Industry. *Sustainability.* **2023**, *15* (3), 2090. https://doi.org/10.3390/su15032090.

(5) Serhan, M.; Sprowls, M.; Jackemeyer, D.; Long, M.; Perez, I. D.; Maret, W.; Tao, N.; Forzani, E. Total Iron Measurement in Human Serum with a Smartphone. *IEEE Journal of Translational Engineering in Health and Medicine.* **2019**, 99: 1-1. https://doi.org/10.1039/x0xx00000x.

(6) Patnaik, K. S.; Mantripragada, B. S.; Punyasloka, S.; Matsumi, N. Advancing Lithium-Ion Battery Performance with Heteroatom-Based Anode Architectures for Fast Charging and High Capacity. *Chemical Communications.* **2025**. *61* (7). https://doi.org/10.1039/D4CC04776A.

(7) Mishra, S. N.; Punyasloka, S.; Mantripragada, B. S.; Pradhan, A.; Matsumi, N. Enabling Ultrafast Charging in Graphite Anodes Using BIAN-Based Conjugated Polymer/Lithium Polyacrylate as a Binder. *ACS Applied Energy Materials.* **2023**, *8* (6), 3360-3368. https://doi.org/10.1021/acsaem.3c02129.

(8) Shi, Y.; Zhou, X.; Yu, G. Material and Structural Design of Novel Binder Systems for High-Energy, High-Power Lithium-Ion Batteries. *Acc. Chem. Res.* **2017**, *50* (11), 2642-2652. https://doi.org/10.1021/acs.accounts.7b00402.

(9) Kumagai, S.; Abe, Y.; Tomioka, M.; Kabir, M. Suitable Binder for Li-Ion Battery Anode Produced from Rice Husk. *Sci. Rep.* **2021**, *11* (1), 15784. https://doi.org/10.1038/s41598-021-95297-9.

(10) Wang, R.; Feng, L.; Yang, W.; Zhang, Y.; Zhang, Y.; Bai, W.; Liu, B.; Zhang, W.; Chuan, Y.; Zheng, Z.; Guan, H. Effect of Different Binders on the Electrochemical Performance of Metal Oxide Anode for Lithium-Ion Batteries. *Nanoscale Research Letters.* **2017**, *12*. https://doi.org/10.1186/s11671-017-2348-6.

(11) Park, J. H.; Kim, S. H.; Ahn, K. H. Role of Carboxymethyl Cellulose Binder and Its Effect on the Preparation Process of Anode Slurries for Li-Ion Batteries. *Colloids and Surfaces A: Physicochemical and Engineering Aspects.* **2023**, *664*. https://doi.org/10.1016/j.colsurfa.2023.131130.

(12) Eshetu, G. G.; Mecerreyes, D.; Forsyth, M.; Zhang, H.; Armand, M. Polymeric Ionic Liquids for Lithium-Based Rechargeable Batteries. *Molecular Systems Design and Engineering*. **2019**, *4* (2), 294-309. https://doi.org/10.1039/c8me00103k.

(13) Grygiel, K.; Lee, J. S.; Sakaushi, K.; Antonietti, M.; Yuan, J. Thiazolium Poly(Ionic Liquid)s: Synthesis and Application as Binder for Lithium-Ion Batteries. *ACS Macro Letters.* **2015**, *4* (12), 1312-1316. Https://doi.org/10.1021/acsmacrolett.5b00655.

(14) Vauthier, S.; Alvarez-Tirado, M.; Guzmán-González, G.; Tomé, L. C.; Cotte, S.; Castro, L.; Guéguen, A.; Mecerreyes, D.; Casado, N. High-Performance Pyrrolidinium-Based Poly(Ionic Liquid) Binders for Li-Ion and Li-Air Batteries. *Materials Today Chemistry.* **2023**, *27*, 101293. https://doi.org/10.1016/j.mtchem.2022.101293.

(15) Lee, J. S.; Sakaushi, K.; Antonietti, M.; Yuan, J. Poly(Ionic Liquid) Binders as Li^+ Conducting Mediators for Enhanced Electrochemical Performance. *RSC Advances.* **2015**, *5* (104), 85517-85522. https://doi.org/10.1039/c5ra16535k.

(16) Von Zamory, J.; Bedu, M.; Fantini, S.; Passerini, S.; Paillard, E. Polymeric Ionic Liquid Nanoparticles as Binder for Composite Li-Ion Electrodes. *Journal of Power Sources.* **2013**, *240*, 745-752. https://doi.org/10.1016/j.jpowsour.2013.04.127.

(17) Mizumo, T.; Marwanta, E.; Matsumi, N.; Ohno, H. Allylimidazolium Halides as Novel Room Temperature Ionic Liquids. *Chemistry Letters.* **2004**, *33* (10), 1360-1361. https://doi.org/10.1246/cl.2004.1360.

(18) Jayakumar, T. P.; Badam, R.; Matsumi, N. Allylimidazolium-Based Poly(Ionic Liquid) Anodic Binder for Lithium-Ion Batteries with Enhanced Cyclability. *ACS Applied Energy Materials.* **2020**, *3* (4), 3337-3346. https://doi.org/10.1021/acsaem.9b02376.

(19) Patra, A.; Matsumi, N. Densely Imidazolium Functionalized Water Soluble Poly(Ionic Liquid) Binder for Enhanced Performance of Carbon Anode in Lithium/Sodium-Ion Batteries. *Advanced Energy Materials.* **2024**, *15* (5). https://doi.org/10.1002/aenm.202403071.

(20) Walkinshaw, M. D.; Arnott, S. Conformations and Interactions of Pectins II. Models for Junction Zones in Pectinic Acid and Calcium Pectate Gels. *J. Mol. Biol.* **1981**, *153* (4), 1075-85. doi: 10.1016/0022-2836(81)90468-x.

(21) Li, J.; Wu, Z.; Jiao, Z.; Wang, Y.; Wang, Z.; Guo, M.; Li, G.; Wang, L.; Zhang, P. A Rapid Crosslinking Injectable Polygalacturonic Acid Barrier Modified with Zwitterion Bottlebrush for Preventing Postoperative Adhesion. *Chemical Engineering Journal.* **2024**, *482*, 148932. https://doi.org/10.1016/j.cej.2024.148932.

(22) Minzanova, S. T.; Mironov, V. F.; Arkhipova, D. M.; Khabibullina, A. V.; Mironova, L. G.; Zakirova, Y. M.; Milyukov, V. A. Biological Activity and Pharmacological Application of Pectic Polysaccharides: A Review. *Polymers*. **2018**, *10* (12), 1407. https://doi.org/10.3390/polym10121407.

(23) Alkorta, I.; Garbisu, C.; Llama, M. J.; Serra, J. L. Industrial applications of pectic enzymes: a review. *Process Biochemistry.* **1998**, *33* (1), 21-28. http://dx.doi.org/10.1016/S0032-9592(97)00046-0.

(24) Andrade, J. R.; Raphael, E.; Pawlicka, A. Plasticized Pectin-Based Gel Electrolytes. *Electrochimica Acta.* **2009**, *54* (26), 6479-6483. https://doi.org/10.1016/j.electacta.2009.05.098.

(25) Liu, R.; Gao, M.; Zhang, J.; Li, Z.; Chen, J.; Liu, P.; Wu, D. An Ionic Liquid Promoted Microwave-Hydrothermal Route towards Highly Photoluminescent Carbon Dots for Sensitive and Selective Detection of Iron(III). *RSC Advances.* **2015**, *5* (31), 24205-24209. https://doi.org/10.1039/c5ra00089k.

(26) Song, H.; Zhang, J.; Niu, Y.; Wang, Z. Phase Transition and Rheological Behaviors of Concentrated Cellulose/Ionic Liquid Solutions. *Journal of Physical Chemistry B.* **2010**, *114* (18), 6006-6013. https://doi.org/10.1021/jp1013863.

(27) Zhang, B.; Zou, T.; Lu, Y. H.; Wang, J. W. Stimulation of Artemisinin Biosynthesis in Artemisia Annua Hairy Roots by Oligogalacturonides. *African Journal of Biotechnology.* **2010**, *9* (23), 3437-3442. https://doi.org/10.4314/ajb.v9i23.

(28) Abreu, J.; Santos, C.; Abreu, C.; Corrêa, A.; Lima, L. Sugar fractionation and pectin content during the ripening of guava cv. Pedro Sato. *Food Science and Technology.* **2012**, *32* (1), 156-162. 10.1590/S0101-20612012005000029.

(29) Lacroix, C.; Sultan, E.; Fleury, E.; Charlot, A. Functional Galactomannan Platform from Convenient Esterification in Imidazolium-Based Ionic Liquids. *Polymer Chemistry.* **2012**, *3* (2), 538-546. https://doi.org/10.1039/c2py00512c.

(30) Jiang, J.; Xiao, Y.; Huang, W.; Gong, P.; Peng, S.; He, J.; Fan, M.; Wang, K. An Insight into the Influence of Hydrogen Bond Acceptors on Cellulose/1-Allyl-3-Methyl Imidazolium Chloride Solution. *Carbohydrate Polymers.* **2017**, *178*, 295-301. https://doi.org/10.1016/j.carbpol.2017.08.006.

(31) Ji, X.; Yan, Y.; Hou, C.; Shi, M.; Liu, Y. Structural Characterization of a Galacturonic Acid-Rich Polysaccharide from Ziziphus Jujuba Cv. Muzao. *International Journal of Biological Macromolecules.* **2020**, *147*, 844-852. https://doi.org/10.1016/j.ijbiomac.2019.09.244.

(32) Badam, R.; Shibuya, M.; Mantripragada, B. S.; Ohira, M.; Zhou, L.; Matsumi, N. BIAN-Based Durable Polymer Metal Complex as a Cathode Material for Li–O2 Battery Applications. *Polymer Journal.* **2022**, *54* (11), 1355-1366. https://doi.org/10.1038/s41428-022-00699-9.

(33) Vogel, J. E.; Sederholm, J. G.; Shumway, E. M.; Abello, G. J.; Trask, S. E.; Wheeler, D. R.; Mazzeo, B. A. Li-Ion Battery Electrode Contact Resistance Estimation by Mechanical Peel Test. *Journal of The Electrochemical Society.* **2022**, *169*. 10.1149/1945-7111/ac8504.

(34) Gaikwad, A. M.; Arias, A. C. Understanding the Effects of Electrode Formulation on the Mechanical Strength of Composite Electrodes for Flexible Batteries. *ACS Appl. Mater. Interfaces.* **2017**, *9* (7), 6390-6400. https://doi.org/10.1021/acsami.6b14719.

(35) Gupta, A.; Badam, R.; Mantripragada, B. S.; Mishra, S. N.; Matsumi, N. Ultra-Durability and Reversible Capacity of Silicon Anodes with Crosslinked Poly-BIAN Binder in Lithium-Ion Secondary Batteries for

Sturdy Performance. *Advanced Sustainable Systems.* **2024**, *54* (11), 1-12. https://doi.org/10.1002/adsu.202400263.

(36) Mantripragada, B. S.; Badam, R.; Matsumi, N. BIAN-Based Porous Organic Polymer as a High-Performance Anode for Lithium-Ion Batteries. *ACS Applied Energy Materials.* **2022**, *5* (6), 6903-6912. https://doi.org/10.1021/acsaem.2c00530.

(37) Kim, T.; Choi, W.; Shin, H. C.; Choi, J. Y.; Kim, J. M.; Park, M. S.; Yoon, W. S. Applications of Voltammetry in Lithium Ion Battery Research. *Journal of Electrochemical Science and Technology*. **2020**, *11* (1), 14-25. https://doi.org/10.33961/jecst.2019.00619.

(38) Pradhan, A.; Badam, R.; Miyairi, R.; Takamori, N.; Matsumi, N. Extreme Fast Charging Capability in Graphite Anode via a Lithium Borate Type Biobased Polymer as Aqueous Polyelectrolyte Binder. *ACS Materials Letters.* **2023**, *5* (2), 413-420. https://doi.org/10.1021/acsmaterialslett.2c00999.

(39) Mantripragada, B. S.; Patnaik, K. S.; Patra, A.; Punyasloka, S.; Matsumi, N. Nano-Engineering Strategies for High-Performance Batteries and Capacitors. *Nano-Engineering at Functional Interfaces for Multi-Disciplinary Applications.* **2025**, 311-337. https://doi.org/https://doi.org/10.1016/B978-0-443-21691-6.00014-7.

(40) Yesibolati, N.; Umirov, N.; Koishybay, A.; Omarova, M.; Kurmanbayeva, I.; Zhang, Y.; Zhao, Y.; Bakenov, Z. High Performance Zn/$LiFePO_4$ Aqueous Rechargeable Battery for Large Scale Applications. *Electrochimica Acta.* **2014**, *152*, 505-511. https://doi.org/10.1016/j.electacta.2014.11.168.

(41) Huang, G.; Xu, S.; Lu, S.; Li, L.; Sun, H. Micro-/Nanostructured Co_3O_4 Anode with Enhanced Rate Capability for Lithium-Ion Batteries. *ACS Appl. Mater. Interfaces.* **2014**, *6* (10), 7236-7243. https://doi.org/10.1021/am500452t.

(42) Sarkar, A.; Shrotriya, P.; Nlebedim, I. C. Anodic Interfacial Evolution in Extremely Fast Charged Lithium-Ion Batteries. *ACS Applied Energy Materials.* **2022**, *5* (3), 3179-3188. https://doi.org/10.1021/acsaem.1c03803.

(43) Haik, O.; Ganin, S.; Gershinsky, G.; Zinigrad, E.; Markovsky, B.; Aurbach, D.; Halalay, I. On the Thermal Behavior of Lithium Intercalated Graphites. *Journal of The Electrochemical Society.* **2011**, *158* (8), A913-A923. https://doi.org/10.1149/1.3598173.

(44) Allart, D.; Montaru, M.; Gualous, H. Model of Lithium Intercalation into Graphite by Potentiometric Analysis with Equilibrium and Entropy Change Curves of Graphite Electrode. *Journal of The Electrochemical Society.* **2018**, *165* (2), A380-A387. https://doi.org/10.1149/2.1251802jes.

(45) Mantripragada, B. S.; Patnaik, K. S.; Higashimine, K.; Badam, R.; Matsumi, N. Energy Efficient and Fast Charging Nitrogen Doped Carbon Anodes Derived from BIAN-Melamine Based Porous Organic Polymer for Lithium-Ion Batteries. *Batteries & Supercaps.* **2024**, *7* (4). https://doi.org/10.1002/batt.202300515.

(46) Patnaik, K. S.; Mantripragada, B. S.; Badam, R.; Higashimine, K.; Zhong, X.; Kaneko, T.; Matsumi, N. Bio-Based Poly(Benzimidazole-Co-Amide)-Derived N, O Co-Doped Carbons as Fast-Charging Anodes for Lithium-Ion Batteries. *Nanoscale Advances.* **2024**, *6* (20), 5181-5192. https://doi.org/10.1039/d4na00416g.

(47) Choi, W.; Shin, H. C.; Kim, J. M.; Choi, J. Y.; Yoon, W. S. Modeling and Applications of Electrochemical Impedance Spectroscopy (Eis) for Lithium-Ion Batteries. *Journal of Electrochemical Science and Technology*. **2020**, *11* (1), 1-13. https://doi.org/10.33961/jecst2019.00528.

(48) Mantripragada, B. S.; Patnaik, K. S.; Higashimine, K.; Badam, R.; Matsumi, N. POP Based Nitrogen Containing Anodic Materials for High Capacity and Fast Charge-Discharge Applications in LIB. *Electrochemistry Communications.* **2023**, *157*, 107616. https://doi.org/10.1016/j.elecom.2023.107616.

(49) Azaki, N. J.; Ahmad, A.; Hassan, N. H.; Abdah, M. A. A. M.; Su'ait, M. S.; Ataollahi, N.; Lee, T. K. Poly(Methyl Methacrylate) Grafted Natural Rubber Binder for Anodes in Lithium-Ion Battery Applications. *ACS Applied Polymer Materials.* **2023**, *5* (7), 4953-4965. https://doi.org/10.1021/acsapm.3c00532.

(50) Mekonnen, Y.; Sundararajan, A.; Sarwat, A. I. A Review of Cathode and Anode Materials for Lithium-Ion Batteries. In *Conference Proceedings - IEEE SOUTHEASTCON*; Institute of Electrical and Electronics Engineers Inc., 2016; Vol. 2016-July. https://doi.org/10.1109/SECON.2016.7506639.

(51) Zheng, H.; Qu, Q.; Zhang, L.; Liu, G.; Battaglia, V. S. Hard Carbon: A Promising Lithium-Ion Battery Anode for High Temperature Applications with Ionic Electrolyte. *RSC Advances.* **2012**, *2* (11), 4904-4912. https://doi.org/10.1039/c2ra20536j.

(52) Kurc, B.; Pigłowska, M. An Influence of Temperature on the Lithium Ions Behavior for Starch-Based Carbon Compared to Graphene Anode for LIBs by the Electrochemical Impedance Spectroscopy (EIS). *Journal of Power Sources.* **2021**, *485* (2), 229323. https://doi.org/10.1016/j.jpowsour.2020.229323.

(53) Niehoff, P.; Passerini, S.; Winter, M. Interface Investigations of a Commercial Lithium Ion Battery Graphite Anode Material by Sputter Depth Profile X-Ray Photoelectron Spectroscopy. *Langmuir.* **2013**, *29* (19), 5806-5816. https://doi.org/10.1021/la400764r.

(54) Li, P.; Feng, W.; Dong, X.; Wang, Y.; Xia, Y. A New Strategy of Constructing a Highly Fluorinated Solid-Electrolyte Interface towards High-Performance Lithium Anode. *Advanced Materials Interfaces.* **2020**, *7* (11), 2000154. https://doi.org/10.1002/admi.202000154.

(55) Malmgren, S.; Ciosek, K.; Hahlin, M.; Gustafsson, T.; Gorgoi, M.; Rensmo, H.; Edström, K. Comparing Anode and Cathode Electrode/Electrolyte Interface Composition and Morphology Using Soft and Hard X-Ray Photoelectron Spectroscopy. *Electrochimica Acta.* **2013**, *97*, 23-32. https://doi.org/10.1016/j.electacta.2013.03.010.

(56) Zhang, G.; Wei, X.; Han, G.; Dai, H.; Zhu, J.; Wang, X.; Tang, X.; Ye, J. Lithium Plating on the Anode for Lithium-Ion Batteries during Long-Term Low Temperature Cycling. *Journal of Power Sources.* **2021**, *484* (2). https://doi.org/10.1016/j.jpowsour.2020.229312.

Chapter 3 [Choline][Pectate] Eco-Friendly Polymer as a High-Performing Binder for Lithium-Ion Battery Electrodes

3.1 Introduction

Lithium-ion batteries (LIBs) have become ubiquitous in modern life, powering everything from small portable devices to large-scale energy storage systems since Sony commercialized them at the end of 20th century.[1] Poly(vinylidene fluoride) (PVDF) is widely used as a binder in LIB electrodes due to its excellent chemical and electrochemical stability and strong adhesion properties.[2,3] However, growing environmental concerns and evolving governmental policies have spurred increased research into greener raw materials and production processes in recent years.[4,5] PVDF requires the use of environmentally hazardous solvents, such as N-methyl-2-pyrrolidone (NMP), for mixture with active and conductive materials in electrode preparation processes, and the presence of fluorine complicates the recycling of waste LIBs.[6] Consequently, water-soluble binders with outstanding stability and mechanical properties are being developed to achieve longer cycle life and address environmental challenges in LIB manufacturing.[7]

Currently, various aqueous binders, including carboxymethyl cellulose (CMC),[8] styrene-butadiene rubber (SBR),[9] poly(acrylic acid) (PAA),[10] chitosan,[11] and sodium alginate (SA),[12] have been extensively studied.[13] These binders are rich in carboxyl (-COOH) and hydroxyl (-OH) polar groups, which enhance their interaction with electrode materials. Among them, CMC-SBR combination maximizes the benefits of CMC's superior dispersion capability in electrode slurry and SBR's inherent flexibility, resulting in enhanced mechanical strength of electrodes.[14] This collaboration significantly improves cycle stability and overall performance of LIBs compared to conventional PVDF binder.[15] However, at room and low temperatures, CMC/SBR-based electrodes suffer from higher electrochemical resistance compared to PVDF-

based counterparts, which hinder lithium-ion (Li^+) intercalation and deintercalation.[16,17] Additionally, under rapid current fluctuations, CMC/SBR-based electrodes struggle to accommodate dynamic changes, leading to electrolyte decomposition and capacity fade.[18] To address these challenges, various strategies have been explored, such as cross-linking with PAA,[19] optimizing CMC/SBR ratio, and chemically modifying CMC structure.[20] Despite ongoing efforts, the intrinsic limitations of materials themselves remain challenging to overcome, prompting researchers to explore alternative binders.

Poly(ionic liquid)s (PILs), as innovative materials that integrate ionic liquids into polymer chains, have been extensively explored as binders and solid electrolytes in LIBs. They offer a combination of the high ionic conductivity of ionic liquids and the mechanical robustness of polymeric structures.[21] The application of PILs has been shown to improve key electrochemical properties of electrode, such as interfacial stability and ionic transport. For instance, Jayakumar et al.[22] synthesized an allylimidazolium-based PIL for graphite anodes, demonstrating that, compared to conventional PVDF binder, PIL-based anode exhibited lower interfacial and diffusion resistance, thereby enhancing charge-discharge efficiency. Similarly, Grygiel et al.[23] developed thiazolium-based PILs with different counter anions via radical polymerization, resulting in electrodes that maintained long-term charge-discharge stability at both 1 C and 5 C. Furthermore, Hernández-Sánchez et al.[24] designed choline-based PIL, which endowed the electrode with excellent mechanical properties, leading to improved coulombic efficiency and high specific capacity retention over extended cycling. Imidazolium- and pyridinium-based ionic liquids have been explored as battery electrolytes and catalysts for organic transformations. However, their high cost and limited biodegradability present challenges.[25] In

contrast, choline-based ionic liquids offer advantages such as low cost in industry scale, thermal stability, non-toxicity, and biocompatibility, reducing the overall cost of battery cycling.[26] Additionally, choline-based ionic liquids exhibit excellent ionic conductivity, wide electrochemical stability window, and effective corrosion inhibition.[27,28]

At present, the synthesis of PILs primarily involves methods such as the addition polymerization of ionic monomers, polycondensation reactions of monomers with corresponding functional groups, and direct polymer modification.[29] These approaches have led to the development of a diverse range of PILs with varying thermal stability and ionic conductivity, enabling their use in different applications. However, each method presents certain challenges. The preparation of monomers for addition polymerization usually requires ion exchange, quaternization, or protonation, which necessitate strict reaction conditions. Polycondensation reactions demand high-purity monomers, as functional parts containing ionic groups can trigger side reactions that compromise the final product's properties. Meanwhile, polymer modification typically requires high temperatures and long time with low conversion, making it unsuitable for large-scale production.[30]

Given the limitations of PILs synthesis and the growing need for eco-friendly materials suitable for electrode properties, some researchers have paid their attention to polygalacturonic acid (pectic acid). Pectic acid primarily consists of α-(1,4)-linked d-galacturonic acid units, structurally resembling the β-(1,4)-linked d-glycosidic units of sodium CMC (Na-CMC). Its ability to form extensive hydrogen bonds enhances adhesion properties, improving the connection between Si/graphite electrode materials and binders.[31] Additionally, as the fully demethylated form of pectin, pectic acid has demonstrated outstanding potential as a binder in

LIB anodes. Ndour et al.[32] enzymatically synthesized and utilized it as a binder in Si/graphite anodes, reporting an extraordinary capacity of 2275 mAh/g after 49 cycles, significantly outperforming CMC-based anodes (245 mAh/g). This superior performance is attributed to demethylated pectin's ability to buffer the substantial volume changes occurring during lithiation-delithiation process, thereby increasing anode stability and cycling performance.

The present study synthesized a PIL, [Choline][Pectate], by neutralizing polymer pectic acid with ionic liquid [Choline][OH] and compared with CMC-SBR binder. The water-soluble CMC-SBR binder combines the excellent dispersion capability of CMC with the flexibility of SBR, resulting in improved mechanical strength of the electrode compared to PVDF. Additionally, this synergistic system supports good cycling stability and overall battery performance. However, CMC-SBR exhibits higher electrochemical resistance than PVDF-based sample, which limits its effectiveness. Thus, the objective of Chapter 3 is to synthesize a water-soluble binder with superior electrochemical performance compared to CMC-SBR. This PIL leverages the combined advantages of [Pectate] cation's bulky part and [Choline] anions to enhance overall performance. Furthermore, its electrochemical properties and practical feasibility were evaluated through a comparative analysis.

3.2 Experimental

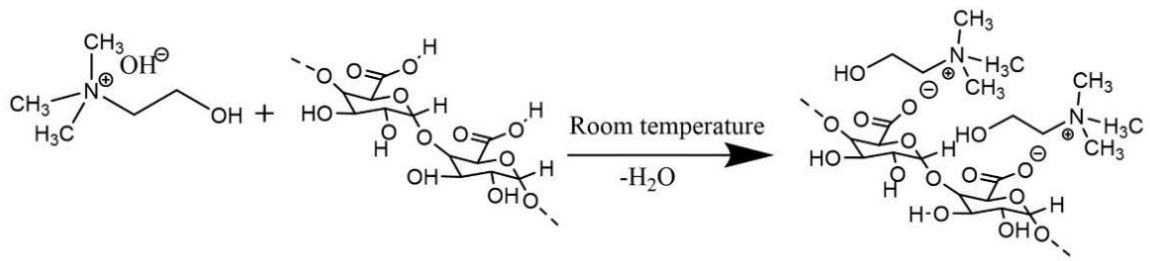

Scheme 3.1. Synthesis of [Choline][Pectate] through the neutralization between [Choline][OH] and pectic acid.

Pectic acid (Sigma-Aldrich, USA, M_w 25,000-50,000) was heated under vacuum at 80 ℃ for 24 hours. A solution containing 2 mmol of [Choline][OH] (Sigma-Aldrich, USA) was added to 100 mL of distilled water, followed by 1 mmol (176 mg) of pectic acid. The neutralization reaction proceeded at room temperature for 12 hours, as illustrated in **Scheme 3.1**. Subsequently, water was evaporated under vacuum at 70 ℃, yielding the product. The obtained product was purified using ethanol: methanol (3:1, volume ratio) solvent mixture and dried under vacuum at 60 ℃, resulting in the final product of 168.9 mg with a 96% yield. A small amount of dried sample was dissolved in distilled water, and pH value was measured at 7.19, as shown in **Figure 3.1**.

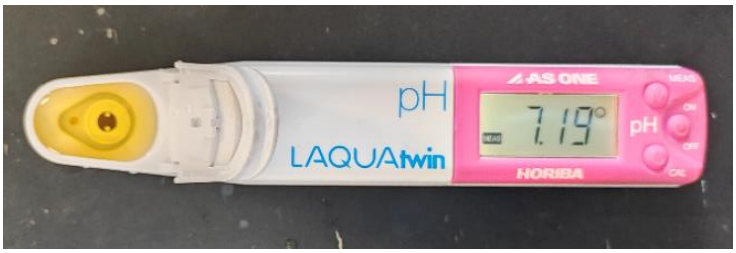

Figure 3.1. Measured pH of [Choline][Pectate] dissolved in distilled water.

Fourier transform infrared (FTIR) spectra of pectic acid, [Choline][OH], and [Choline][Pectate] was characterized via PerkinElmer 100 instrument with a resolution 2 cm^{-1} for 10 scans in attenuated total reflectance (ATR) mode. Nuclear magnetic resonance (NMR) measurements were conducted through Bruker Advance II-400 MHz for ^{1}H-NMR and 100 MHz for ^{13}C-NMR respectively.

A mixture containing 80 wt% graphite, 10 wt% Super P, and 10 wt% [Choline][Pectate] was prepared in distilled water. Separately, another mixture comprising 80 wt% graphite, 10 wt% Super P, 5 wt% CMC (Na-CMC, Sigma-Aldrich, USA), and 5 wt% SBR (NIPPON A&L INC., Japan) was also prepared in distilled water using SK-350TII Kakuhunter planetary motion mixer to ensure uniform dispersion. The slurry was then coated onto copper foil (The Nilaco Corporation, Japan) and subjected to vacuum drying at 80 °C for 2 hours to remove water. For full-cell preparation, the anode sheets were initially left at room temperature for 8 hours, followed by an additional 2 hours drying step at 80 °C under vacuum. Finally, the dried anode sheets were cut into 15 mm diameter discs for cell assembly. The loading mass of active materials in anodes ranged from 1.13 to 2.15 mg/cm^2 for half-cells and was 5.7 mg/cm^2 for full cells.

The half-cells (CR2025) were assembled using CMC/SBR and [Choline][Pectate]-based graphite anodes as working electrodes, 13 mm lithium foil discs (Honjo Chemical Corporation, Japan) as counter electrodes, polypropylene (PP) membranes (Celgard 2500) as separators, and 1.0 M lithium hexafluorophosphate ($LiPF_6$) in a 1:1 (volume ratio) mixture of ethylene carbonate (EC) and diethyl carbonate (DEC) (Sigma-Aldrich, USA) as the liquid electrolyte. Electrochemical measurements, including cyclic voltammetry (CV) and potentiostatic/dynamic electrochemical impedance spectroscopy (PEIS/DEIS), were performed using an electrochemical workstation (Bio-Logic Co. Ltd). The full-cell configuration used the same components as half-cells, except for the cathode, which was $LiNi_{1/3}Co_{1/3}Mn_{1/3}O_2$ (NCM). For CV analysis, the first scan of half-cells was conducted at 0.1 mV/s over a potential range of 0.1 V to 2.1 V. To determine overpotentials, additional CV tests

were performed at scan rates of 0.1, 0.2, 0.4, 0.6, 0.8, and 1.0 mV/s within the same voltage range. PEIS and DEIS were carried out from 1.0 MHz to 0.1 Hz, with DEIS measurements at 0.1 V intervals over the 0.1 V to 2.1 V range.

After long cycling at 1 C, 2 C, and 5 C, the half-cells were disassembled for morphologial analysis of the anodes using S-4500 scanning electron microscope (SEM). Elemental analysis of synthesized binder was conducted, and after long cycling at 1 C, 2 C, and 5 C, chemical bonds on the anode surface were examined and compared using S-Probe TM 2803 X-ray photoelectron spectroscopy (XPS).

3.3 Result and discussion

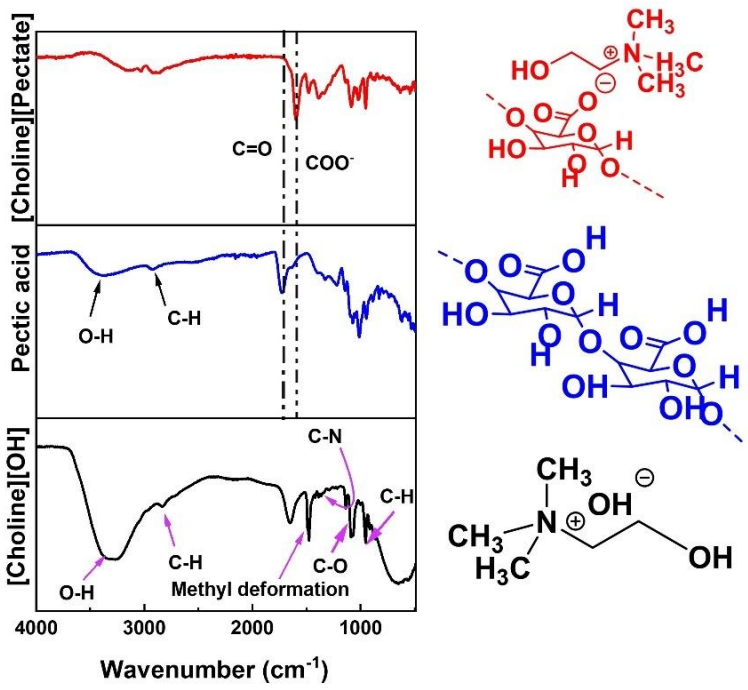

Figure 3.2. ATR-IR spectra of [Choline][OH], pectic acid, and [Choline][Pectate].

After confirming the synthesis of product [Choline][Pectate]-based on pH testing of its solution in distilled water, the functional groups of [Choline][OH], pectic acid, and [Choline][Pectate] were analyzed using FTIR spectroscopy, as shown in **Figure 3.2**. Prior to neutralization, the FTIR spectra of [Choline][OH] displayed characteristic peaks at 3346 cm^{-1}, 2865 cm^{-1}, 1471 cm^{-1}, 1354 cm^{-1}, 1080 cm^{-1}, and 967 cm^{-1}, corresponding to O-H stretching, aliphatic C-H stretching, methyl deformation, C-N stretching, C-O stretching in alcohols, and C-H deformation in -CH_2- groups, respectively.[33] For pectic acid, peaks observed at 3378 cm^{-1}, 2931 cm^{-1}, 1715 cm^{-1}, and 1608 cm^{-1} were attributed to O-H stretching, C-H stretching, C=O stretching of COOH groups, and COO^- stretching vibration, respectively.[34] Notably, the peak for C=O stretching was strong, whereas COO^- peak was relatively weak. Following neutralization, significant changes were observed in FTIR spectra of [Choline][Pectate]: the intensity of C=O peak sharply decreased and nearly disappeared, while COO^- peak became markedly stronger. Meanwhile, other characteristic peaks of [Choline][OH] and pectic acid remained visible in [Choline][Pectate] spectra. These observations confirm that a reaction occurred between -COOH groups of pectic acid and -OH groups of [Choline][OH], leading to [Choline][Pectate] formation.

To further explore the molecular structure of synthesized binder [Choline][Pectate], both ^{1}H-NMR and ^{13}C-NMR spectroscopy were employed, as illustrated in **Figures 3.3a** and **3.3b**. Chemical shifts in ^{1}H-NMR were 5.70 ppm (1H, **H**O-CH_2), 5.00 ppm (1H, C-C**H**(COO^-)-O), 4.34 ppm (2H, C(OH)-CH(O**H**)-C, C-CH(O**H**)-C(OH)), 3.98 ppm (2H, HO-C**H**$_2$-CH_2), 3.91 ppm (1H, C(OH)-C**H**-CH(COO^-)), 3.67 ppm (1H, O-C**H**-C(OH)), 3.59 ppm (1H, C-CH(O**H**)-C(OH)), 3.52 ppm (1H, C(OH)-C**H**(OH)-C), 3.45 ppm (2H, CH_2-C**H**$_2$-N), and 3.12 ppm (9H, N(C**H**$_3$)$_3$).[35,36] Chemical shifts in ^{13}C-NMR were 175.40, 99.25, 78.07, 71.26, 67.39, 64.35, 60.39, 55.68, and 53.89 ppm.[37] Collectively, FTIR and NMR results provide strong evidence for the successful synthesis and structural confirmation of [Choline][Pectate]. Furthermore, the

interaction energy between [Choline][Pectate] and graphite were computed by modelling the interaction between a monomer of [Choline][Pectate] and graphene sheet (Figure 10). The energy of interaction between [Choline][Pectate] and graphene sheet was calculated to be -188.25 kcal/mol. Whereas energy of interaction between PVDF and graphene sheet was calculated to be -7.52 kcal/mol and CMC and graphene sheet was calculated to be -20.33 kcal/mol. These calculations indicate the stronger interaction between [Choline][Pectate] and graphite in comparison with commercial binders such as PVDF and CMC.

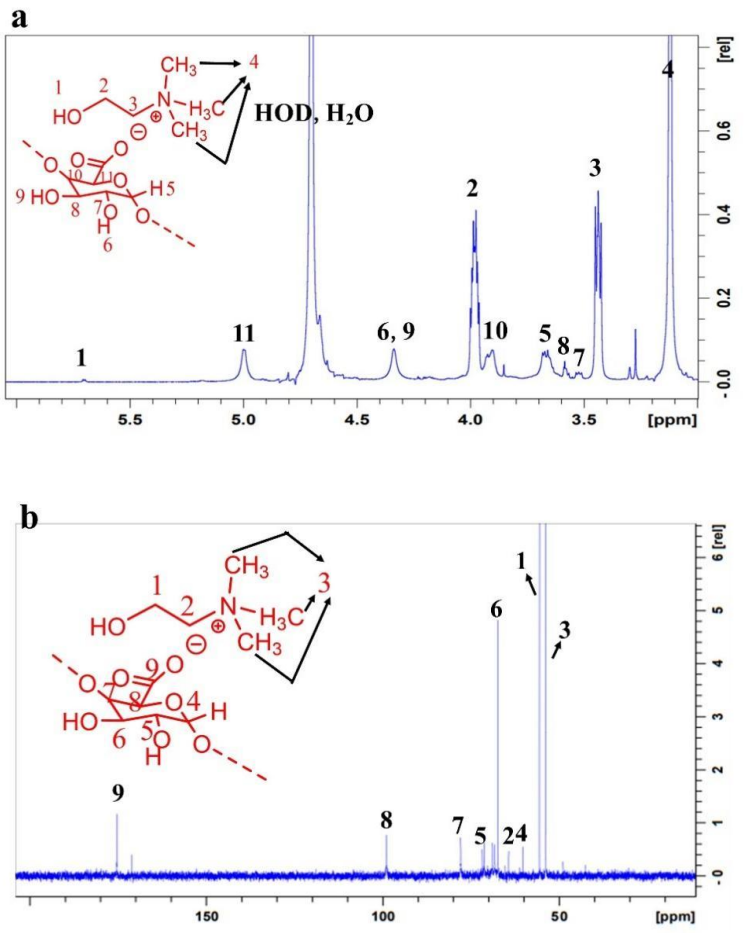

Figure 3.3. (a) ^{1}H-NMR and (b) ^{13}C-NMR of [Choline][Pectate] in D_2O.

To investigate the formation of SEI film on the surface of anodes, the first and second CV curves of CMC/SBR and [Choline][Pectate]-based anodic half-cells were compared, as shown

in **Figure 3.4a** and **3.4b**. In both samples, SEI formation was observed at around 0.6-0.7 V during the lithiation process, resulting from electrolyte decomposition. This SEI layer helps protect the electrodes from further electrolyte decomposition while enhancing ionic conductivity.[38] After SEI formation, the peak anodic current of [Choline][Pectate]-based sample in the second CV cycle was higher than that of CMC/SBR-based sample. However, the peak cathodic current of [Choline][Pectate] electrode was nearly the same as that of CMC/SBR-based electrode. This indicates that [Choline][Pectate]-based anode exhibits greater reversibility in lithiation/delithiation process compared to CMC/SBR. Additionally, a higher peak current suggests that [Choline][Pectate]-based anode has higher electrochemical activity, which is beneficial for efficient charge-discharge process.[39]

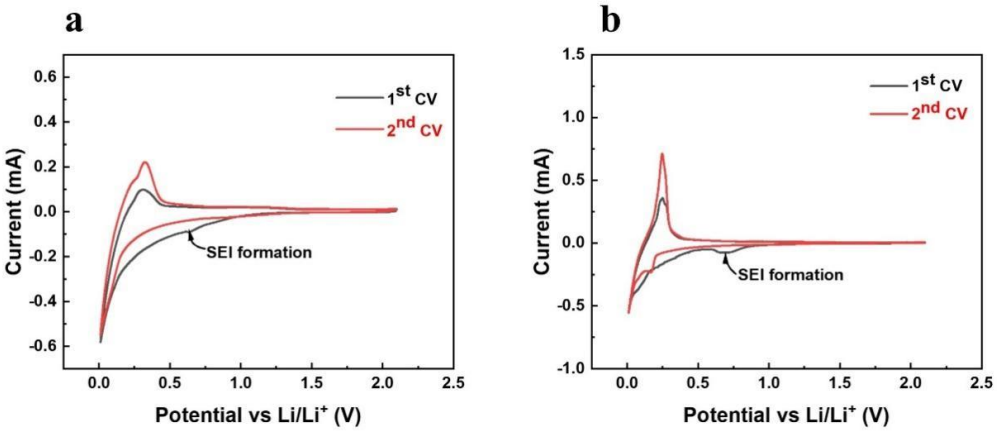

Figure 3.4. First and second CV curves of (a) CMC-SBR and (b) [Choline][Pectate] at a scan rate of 0.1 mV/s.

Nyquist plots of anodic half-cells before and after the first CV at a scan rate of 0.1 mV/s were analyzed to explore the influence of SEI formation from an impedance perspective, as depicted in **Figure 3.5a**. Prior to SEI formation, the initial interfacial resistance indicated by the semicircle diameter, was lower for [Choline][Pectate]-based half-cell compared to CMC-SBR counterpart. After SEI formation, the semicircle diameters for both samples decreased

significantly, suggesting improved charge transfer kinetics. Notably, [Choline][Pectate] cell displayed a smaller semicircle than CMC-SBR, indicating a more efficient interfacial process and the possible activation of additional surface sites on the graphite anode. Furthermore, the 45° linear tail observed in the low-frequency region after CV represents Warburg impedance, which reflects Li^+ diffusion condition after SEI formation.[40–42] The corresponding Warburg coefficients, determined in **Figure 3.5b**, were used to calculate Li^+ diffusion coefficient (D_{Li^+}) based on the following equation.

$$D_{Li} = \frac{R^2T^2}{2A^2n^4f^4C^2\,\sigma^2} \qquad \textit{Equation}$$

Where: R is gas constant, T is absolute temperature, A is anode area, n is electrons number, f is Faraday constant, C is lithium-ions concentration, and σ is Warburg coefficient, calculated from slopes in **Figure 3.5b**.

The results showed that [Choline][Pectate]-based anode exhibited a higher D_{Li^+} (1.6×10^{-11} S/cm^2) compared to that of CMC-SBR-based anode (6.6×10^{-13} S/cm^2). This improvement can be attributed to the formation of a more conductive SEI layer on [Choline][Pectate] anode, which facilitates faster Li^+ transport.

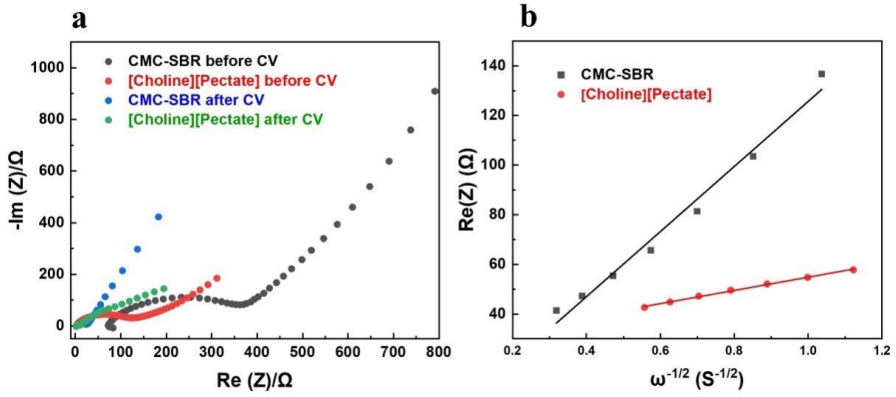

Figure 3.5. (a) Nyquist plots of anodic half-cells with CMC-SBR and [Choline][Pectate] binders before and after CV at a scan rate of 0.1 mV/s and (b) Re vs $\omega^{-1/2}$ of CMC-SBR and [Choline][Pectate]-based anodes.

CV was performed after the anodic half-cells underwent 100 charge-discharge cycles at 0.5 C, as detailed in **Figure 3.6a** and **3.6b**. This pre-cycling step was necessary to activate the anode structure and raise Li^+ transport pathways. CV results revealed that [Choline][Pectate]-based anode exhibited higher peak currents, particularly at elevated scan rates, indicating improved charge transfer kinetics and electrochemical activity. Although the overpotentials of CMC-SBR and [Choline][Pectate] samples were same (~0.40 V), the oxidation overpotential of [Choline][Pectate] anode (0.12 V) was notably lower than that of CMC-SBR-based anode (0.18 V). This reduced overpotential suggests that the interface between [Choline][Pectate] binder and active material facilitated more efficient Li^+ transport, with less energy loss during delithiation from graphite layers.[14,43,44] Furthermore, the anodic peaks observed in CMC-SBR sample were broader than those of [Choline][Pectate], likely due to uneven CMC-SBR binder distribution within the electrode. This inhomogeneity might lead to Li^+ extraction across the anode surface non-uniformly, resulting in slower and less synchronized redox reactions.

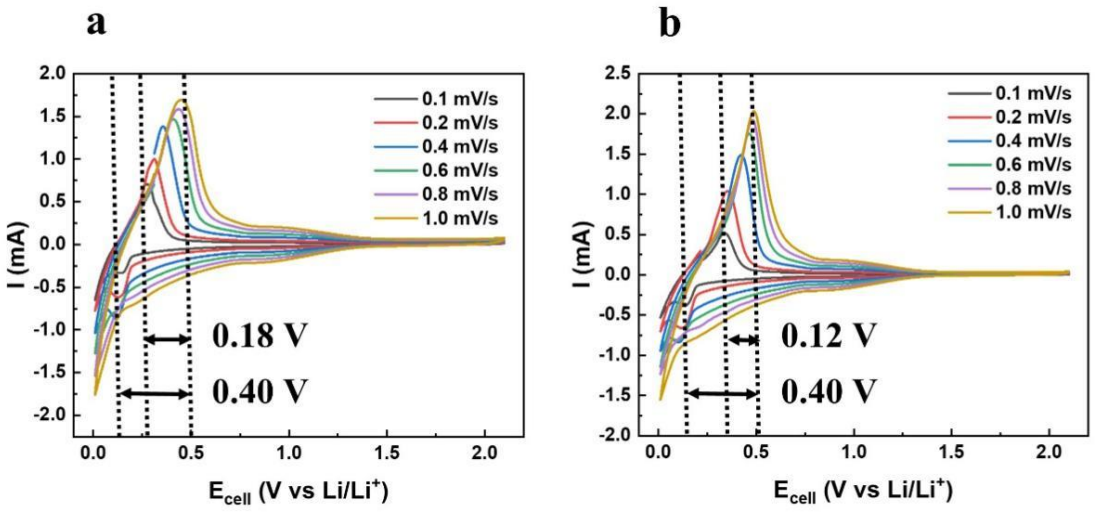

Figure 3.6. CV at different scan rates with (a) CMC-SBR and (b) [Choline][Pectate] as the binders for graphite anodes in 1M $LiPF_6$/EC: DEC.

The interaction energy between [Choline][Pectate] and graphite were computed by modelling the interaction between a monomer of [Choline][Pectate] and graphene sheet (**Figure 3.7**). The energy of interaction between [Choline][Pectate] and graphene sheet was calculated to be -188.25 kcal/mol. Whereas energy of interaction between PVDF and graphene sheet was calculated to be -7.52 kcal/mol and CMC and graphene sheet was calculated to be -20.33 kcal/mol. These calculations indicate the stronger interaction between [Choline][Pectate] and graphite in comparison with commercial binders such as PVDF and CMC.

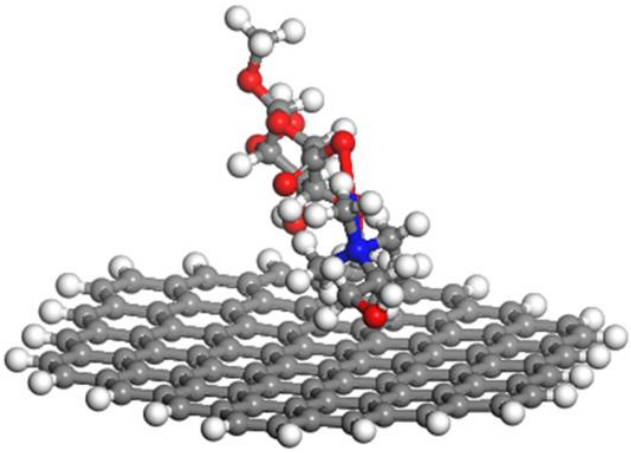

Figure 3.7 Interaction energy calculations of [Choline][Pectate] and graphite.

Figure 3.8 illustrated the rate capabilities of CMC-SBR and [Choline][Pectate]-based half-cells, tested at current densities of 0.1 C, 1 C, 2 C, and 5 C after 150 precycling cycles at 0.25 C. [Choline][Pectate]-based cell achieved specific capacities of approximately 350, 310, 190, and 75 mAh/g, respectively, which were consistently higher than those of CMC-SBR-based cell (approximately 320, 200, 125, and 25 mAh/g). After high-rate cycling at 5 C, both cells recovered their original capacities at 0.1 C, reaching 350 mAh/g for [Choline][Pectate] and 320 mAh/g for CMC-SBR, indicating good reversibility. Throughout this rate study, [Choline][Pectate]-based anode demonstrated superior electrochemical performance,

attributed to several synergistic factors: the formation of a more conductive SEI film, enhanced electrochemical activity, and higher D_{Li}^{+}, as supported by the results in **Figure 3.4b**, **3.5b**, and **3.6b**. The introduction of $[Choline]^{+}$ cations into the polymer may enhance interfacial properties by promoting uniform SEI formation due to their inherent electrochemical stability. Moreover, the chemical tunability of $[Choline]^{+}$, specially through modifying anion pairs, can improve compatibility with the liquid electrolyte, thereby increasing the wettability of porous graphite anode.[45–47]

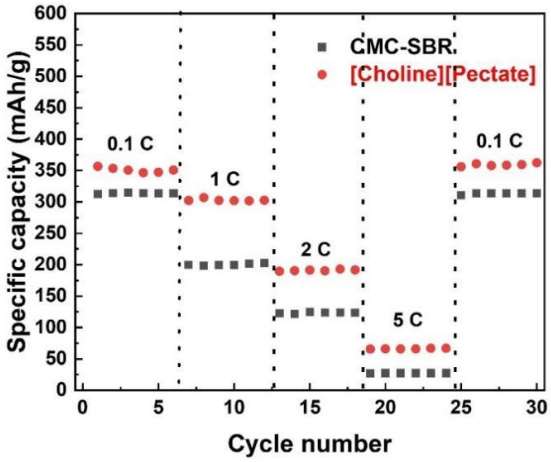

Figure 3.8. Cycling performance of CMC-SBR and [Choline][Pectate]-based half-cells at the current densities of 0.1 C, 1 C, 2 C, and 5 C (after 150 precycling cycles at 0.25 C).

Long cycling studies offered valuable insights into the stability, durability, and overall electrochemical performance of the electrodes under practical operating conditions. **Figures 3.9a**, **3.9b**, and **3.9c** presented the discharge capacities and coulombic efficiencies of CMC-SBR and [Choline][Pectate] based half-cells over 700 cycles at 1 C and 2 C, and 900 cycles at 5 C. At 1 C, [Choline][Pectate]-based cell achieved the highest capacity of 368.6 mAh/g, significantly higher than 211.6 mAh/g for CMC-SBR cell. After 700 cycles, capacities declined to 211.3 mAh/g and 80.2 mAh/g, corresponding to capacity retentions of 57.3% and 29.9%, respectively. At 2 C, the highest capacities were 268.3 mAh/g for [Choline][Pectate] and 139.2

mAh/g for CMC-SBR. After 700 cycles, these decreased to 174.8 mAh/g and 76.8 mAh/g, with capacity retentions of 65.2% and 55.2%, respectively. At the higher rate of 5 C, [Choline][Pectate] still outperformed CMC-SBR with the highest capacity of 82.3 mAh/g versus 30.3 mAh/g. After 900 cycles, the capacities were 67.3 mAh/g and 28.4 mAh/g, reflecting capacity retentions of 81.2% and 93.7%, respectively. Importantly, regardless of current rate, both systems exhibited stable coulombic efficiencies close to 100% throughout the entire cycling period, indicating high reversibility and minimal side reactions.

During long cycling, both types of half-cells exhibited a characteristic trend: an initial rise in specific capacity, followed by a gradual decline. This behavior was commonly attributed to the progressive activation of Li^+ storage sites during the early cycles, followed by structural and interfacial degradation over time. Compared with CMC-SBR, [Choline][Pectate]-based cell exhibited both higher peak capacity and capacity retention at 1 C and 2 C. This signified that $[Pectate]^-$ anions not only possessed great electrochemical stability but might also contribute to improved Li^+ transport through reversible coordination with Li^+ during lithiation and delithiation. Additionally, the abundance of -OH groups within $[Pectate]^-$ structure likely promoted stronger intermolecular interactions, such as Van der Waals forces, thereby improving mechanical cohesion among electrode materials and reinforcing structural integrity during extended cycling. As a result, [Choline][Pectate]-based cell maintained excellent performance even after 900 cycles at 5 C. Interestingly, although CMC-SBR cell exhibited higher capacity retention than [Choline][Pectate] at 5 C, its specific capacity remained significantly lower. This might be due to CMC-SBR's limited ability to accommodate large Li^+ fluxes at high current densities, which led to uneven site activation and faster deactivation of some active regions. Consequently, while a portion of CMC-SBR-based anode remained functional over time, its total storage capability was compromised.[48–50]

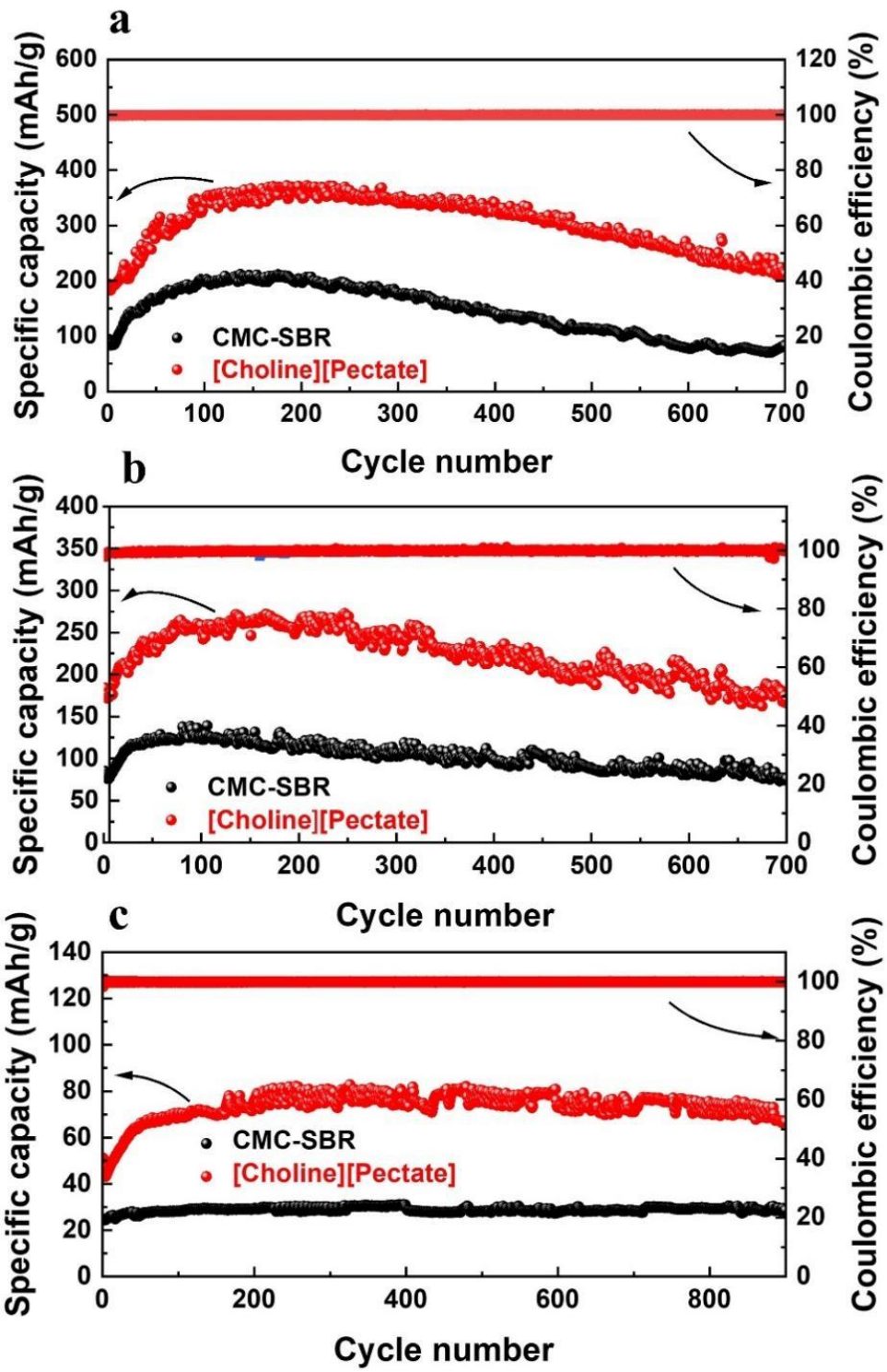

Figure 3.9. Long cycling specific capacity and coulombic efficiency comparisons between CMC-SBR and [Choline][Pectate] based half-cells at (a) 1 C, (b) 2 C, and (c) 5 C.

To delve into the rate of change in capacity with voltage, differential capacity versus voltage (dQ/dV) plots were analyzed for anodic half-cells with CMC-SBR and [Choline][Pectate] binders, as shown in **Figure 3.10**. In the case of CMC-SBR-based electrode (**Figure 3.10a**), dQ/dV plot at 100 cycle displayed a sharp and intense peak, indicating a highly reactive phase.[51] However, as cycling progressed to 300, 500, and 700 cycles, the peaks became notably broader and less intense. This decline in peak intensity suggests a loss of active material and structural degradation of the electrode, likely accompanied by the breakdown of SEI layer and increased anode resistance. The rapid reduction in peak intensity underscores the inability of CMC-SBR binder to maintain structural integrity during cycling. Additionally, the observed shift of peak positions toward higher voltages implies Li^+ depletion, possibly due to undesirable side reactions. In contrast, [Choline][Pectate]-based half-cell (**Figure 3.10b**) exhibited relatively stable peak intensities and positions over cycling at 1 C, indicating better preservation of active materials and minimal SEI deterioration. This stability can be attributed to the enhanced mechanical and electrochemical properties provided by [Choline][Pectate] binder, resulting in lower anode degradation and improved capacity retention.[52,53]

At 2 C (**Figure 3.10c**), CMC-SBR-based electrode still showed identifiable peaks, but their intensity diminished significantly, and the peak positions again shifted to higher voltages-consistent with trends observed at 1 C. Conversely, [Choline][Pectate]-based cell (**Figure 3.10d**) also showed a reduction in peak intensity due to capacity fading, but the peak positions remained relatively unchanged, suggesting minimal Li^+ depletion. Under high current density (5 C), CMC-SBR electrode (**Figure 3.10e**) exhibited no discernible oxidation peaks, indicating severe degradation and loss of electrochemical activity. Meanwhile, [Choline][Pectate] electrode (**Figure 3.10f**) maintained distinct oxidation peaks, demonstrating robust structural stability and better performance even under high-rate conditions.

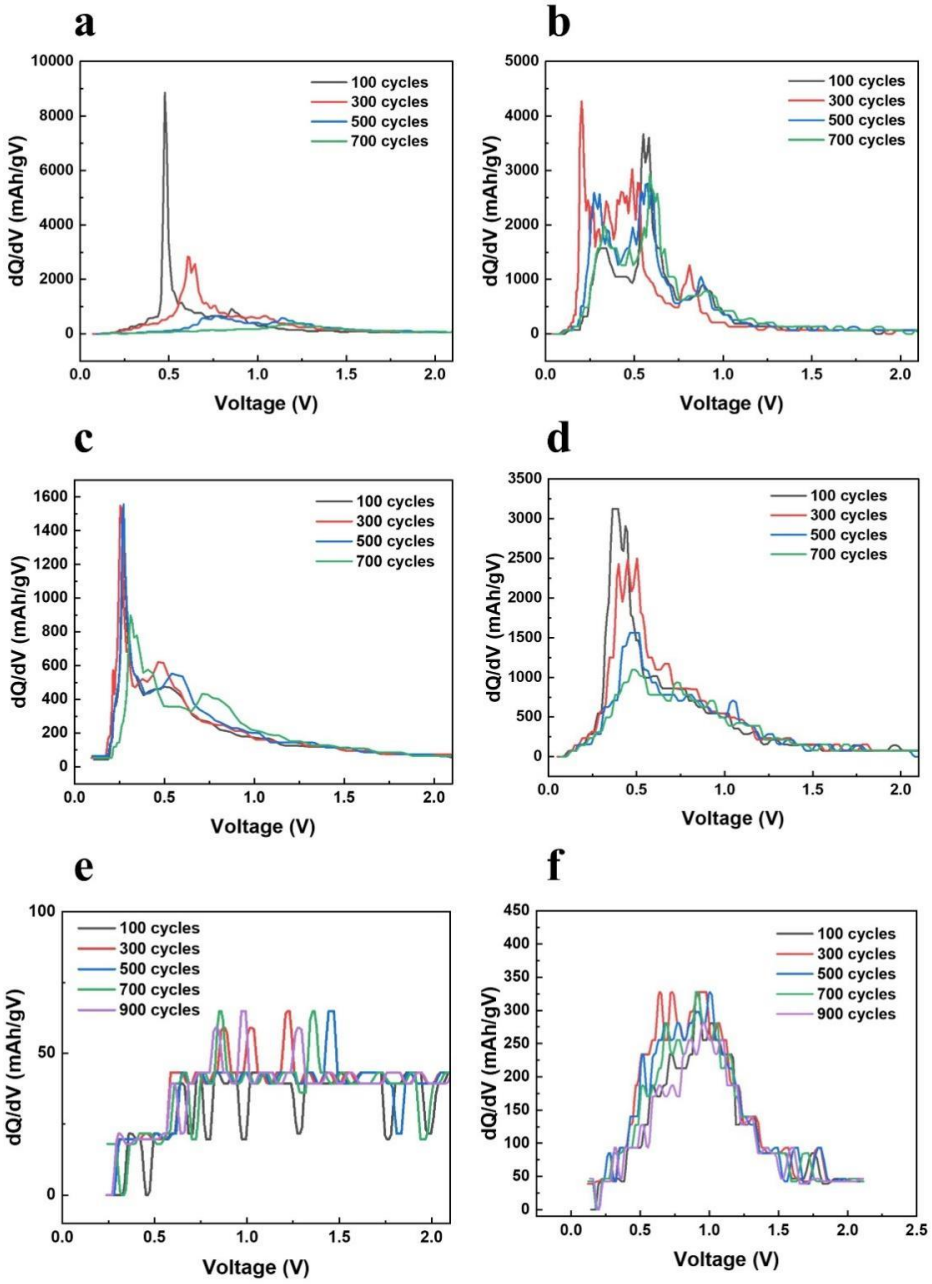

Figure 3.10. Differential capacity vs voltage (dQ/dV) plots of (a) CMC-SBR, (b) [Choline][Pectate] at 1 C, (c) CMC-SBR, (d) [Choline][Pectate] at 2 C, and (e) CMC-SBR, (f) [Choline][Pectate] at 5 C, based on long cycling data of anodic half-cell (charge process).

After 700 charge-discharge cycles at 1C, real-time impedance changes of cells were monitored using DEIS. Fitting data provided insights into key resistance components of half-

cells: anode internal resistance (R_{Int}), SEI resistance (R_{SEI}), and charge transfer resistance (R_{CT}) at various potentials. **Figures 3.11a** and **3.11b** showed DEIS Nyquist plots for CMC-SBR and [Choline][Pectate] based cells, respectively, during the lithiation process. Using corresponding equivalent electrical circuit models (EECMs), the resistance values were simulated, as summarized in **Tables 3.1** and **3.2**.

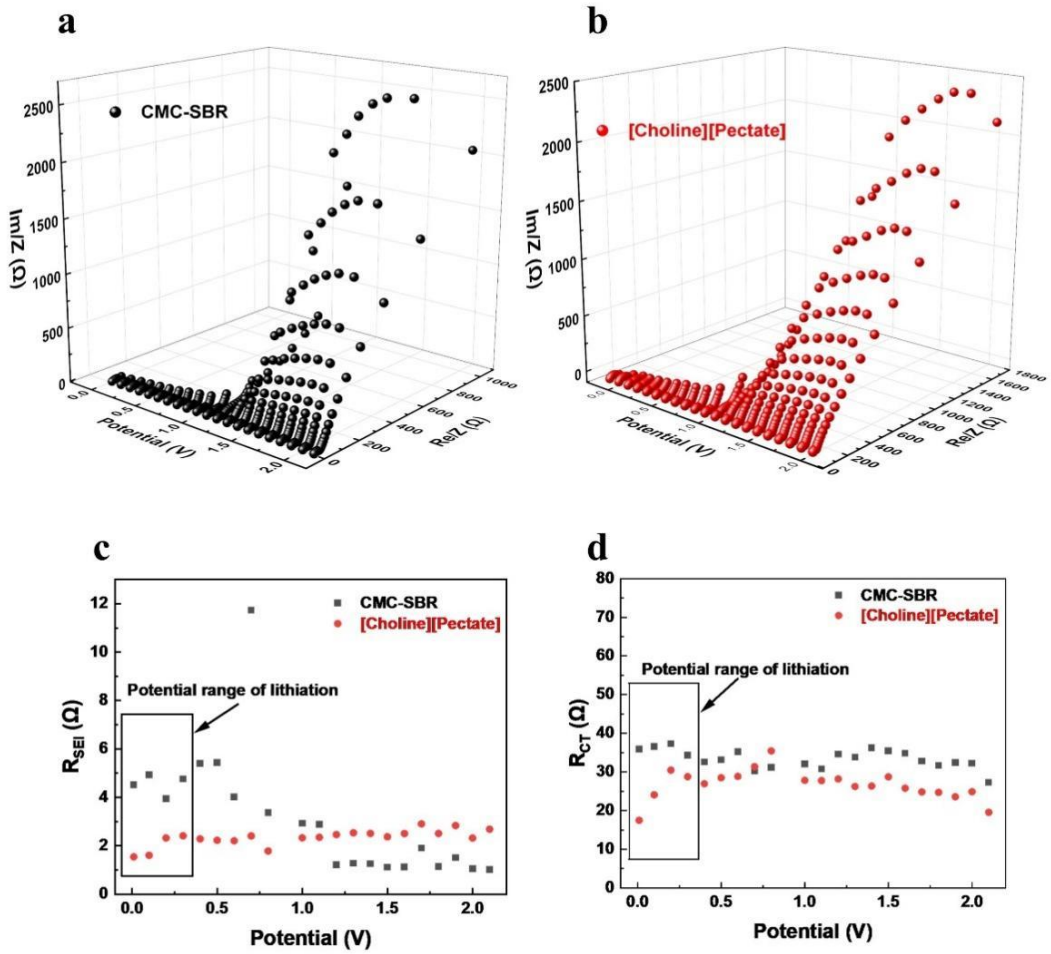

Figure 3.11. DEIS Nyquist profiles of (a) CMC-SBR and (b) [Choline][Pectate] based anodic hall cells; (c) SEI resistance (R_{SEI}) vs potential plots and (d) charge transfer resistance (R_{CT}) of CMC-SBR and [Choline][Pectate] based half-cell (during lithiation).

As shown in **Figure 3.11c**, when the potential decreased from 2.1 V to 1.1 V, R_{SEI} of CMC-SBR electrode was lower than that of [Choline][Pectate] electrode. However, below 1.0 V, especially in the critical lithiation range for graphite (0.25-0.01 V), R_{SEI} of CMC-SBR anode increased significantly, exceeding that of [Choline][Pectate]. This suggests the instability of SEI layer on CMC-SBR anode surface at low potentials. Importantly, this increased resistance in the lithiation range indicates that CMC-SBR anode is less effective at facilitating Li^+ intercalation. In contrast, [Choline][Pectate] anode maintained low and stable R_{SEI} values across the full potential range (2.1 V to 0.1 V), highlighting its superior SEI stability. Furthermore, as shown in **Figure 3.11d**, R_{CT} values for CMC-SBR cell were consistently higher than those of [Choline][Pectate] cell, except at 0.7 V and 0.8 V, further underscoring the improved electrochemical performance of [Choline][Pectate]-based half-cell.[54]

Table 3.1. Circuit fitting data for the anodic half-cell with CMC-SBR binder for discharging cycles at different potentials.

Potential	R_{Int}	R_{SEI}	R_{CT}	EECMs
0.01	3.598	4.516	35.88	R(QR)(QR)(CRW)
0.1	3.603	4.935	36.56	R(QR)(QR)(CRW)
0.2	3.727	3.94	37.3	R(QR)(QR)(CRW)
0.3	3.611	4.759	34.3	R(QR)(QR)(QRW)
0.4	3.726	5.398	32.59	R(QR)(QR)(QRW)
0.5	3.592	5.432	33.12	R(QR)(QR)(CRW)
0.6	3.617	4.008	35.19	R(QR)(QR)(CRW)
0.7	3.33	11.73	30.18	R(QR)(QR)(CRW)
0.8	3.674	3.364	31.15	R(QR)(QR)(QR)(CRW)
1	3.656	2.927	32.09	R(QR)(QR)(QR)(QRW)
1.1	3.65	2.881	30.79	R(QR)(QR)(QR)(QRW)
1.2	3.629	1.214	34.59	R(QR)(QR)(CRW)
1.3	3.664	1.272	33.78	R(QR)(QR)(QR)
1.4	3.673	1.253	36.25	R(QR)(QR)(QRW)
1.5	3.642	1.111	35.43	R(QR)(QR)(QRW)

1.6	3.634	1.116	34.83	R(QR)(QR)(QR)
1.7	3.629	1.897	32.82	R(QR)(QR)(QRW)
1.8	3.614	1.134	31.65	R(QR)(QR)(QR)(CR)
1.9	3.557	1.506	32.4	R(QR)(QR)(QRW)
2	3.509	1.046	32.24	R(QR)(QR)(QR)
2.1	3.557	1.004	27.26	R(QR)(QR)(QR)W

Table 3.2. Circuit fitting data for the anodic half-cell with [Choline][Pectate] binder for discharging cycles at different potentials.

Potential	R_{Int}	R_{SEI}	R_{CT}	EECMs
0.01	1.509	1.538	17.49	R(QR)(QR)(CRW)
0.1	1.499	1.604	24.09	R(QR)(QR)(CRW)
0.2	1.488	2.322	30.48	R(QR)(QR)(QR)(CR)
0.3	1.472	2.41	28.79	R(QR)(QR)(QR)
0.4	1.475	2.28	26.95	R(QR)(QR)(QRW)
0.5	1.483	2.224	28.5	R(QR)(QR)(CRW)
0.6	1.465	2.2046	28.85	R(QR)(QR)(QRW)
0.7	1.513	2.401	31.36	R(QR)(QR)(QRW)
0.8	1.471	1.781	35.43	R(QR)(QR)(QRW)
1	1.513	2.327	27.82	R(QR)(QR)(QR)(QRW)
1.1	1.521	2.348	27.77	R(QR)(QR)(QR)(QRW)
1.2	1.511	2.459	28.2	R(QR)(QR)(QR)(CR)
1.3	1.543	2.531	26.25	R(QR)(QR)(QR)
1.4	1.548	2.504	26.35	R(QR)(QR)(CR)
1.5	1.544	2.37	28.73	R(QR)(QR)(QCR)
1.6	1.558	2.503	25.8	R(QR)(QR)(QR)
1.7	1.524	2.902	24.85	R(QR)(QR)(QR)
1.8	1.562	2.504	24.7	R(QR)(QR)(QR)
1.9	1.558	2.835	23.58	R(QR)(QR)(QRW)
2	1.538	2.315	24.89	R(QR)(QR)(QRW)
2.1	1.542	2.683	19.56	R(QR)(QR)(QR)

Through various electrochemical characterizations, the excellent performance of [Choline][Pectate] was verified. To evaluate its behavior under low-temperature conditions, [Choline][Pectate]-based half-cell was subjected to charge-discharge cycling at a current

density of 0.5 mA, with tests conducted at 5 °C and 0 °C. As illustrated in **Figure 3.12**, the specific capacities of the cell at 5 °C and 0 °C were 50 mAh/g and 36.5 mAh/g, respectively-values notably lower than those observed at room temperature. Nilsson's research also showed similar results, at -10 °C, the capacity of graphite-based cell was lower than 40 and 20 mAh/g at 0.1 C and 1 C, respectively.[55] This capacity decay is primarily ascribed to sluggish Li^+ diffusion kinetics and elevated internal resistance at low temperatures, which impede charge transfer processes and interfacial reaction rates. Importantly, despite these reductions in capacity, the cell remained functional, demonstrating that [Choline][Pectate] binder sustains sufficient ionic conductivity and electrode structural integrity even under thermally challenging environments. However, instead of modifying graphite anode half-cells, optimizing the electrolyte represents a more efficient and straightforward approach to enhancing the low-temperature performance of batteries. When electrolytes are modified through appropriate methods, the battery capacity could reach 200 mAh/g at -20 °C, maintaining high capacity retention even after 100 charge-discharge cycles.[56]

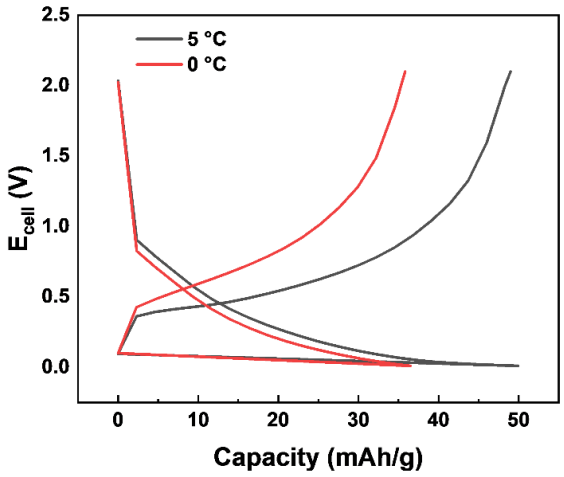

Figure 3.12. Cycling test of [Choline][Pectate] based half-cells at 5 °C and 0 °C (current density= 0.5 mA=0.75 C).

After demonstrating the excellent electrochemical performance of [Choline][Pectate]-based graphite anode, it was integrated into a full cell with NCM cathode to assess its potential for practical applications. As shown in **Figure 3.13**, [Choline][Pectate]-based full cell exhibited stable specific capacity and coulombic efficiency at 0.05C over 160 cycles. The capacity initially increased slightly, reaching a peak of 1.54 mAh (270.2 mAh/g), before gradually declining. After 100 cycles, the cell retained a capacity of 1.25 mAh (219.3 mAh/g), corresponding to a capacity retention of 81.2%. After 160 cycles, the capacity was 1.11 mAh (194.7 mAh/g), with a capacity retention of 72.5%. These results indicated that [Choline][Pectate] effectively maintains structural stability and electrochemical performance during charge-discharge cycling. The initial coulombic efficiency was 73.5%, which rapidly increased to nearly 100% and remained stable throughout the testing period, indicating highly reversible electrochemical reactions and the formation of a robust SEI film that efficiently protected the electrode from degradation.[57, 58]

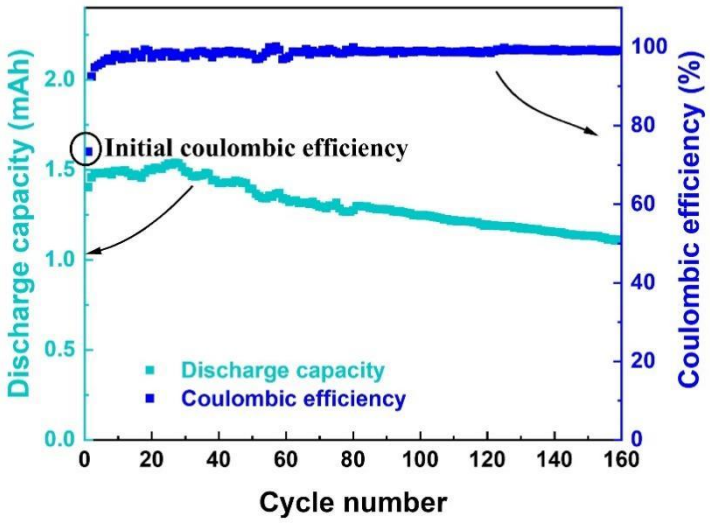

Figure 3.13. Long cycling discharge capacity and coulombic efficiency of [Choline][Pectate]-based full cell at 0.05C (active material 5.7 mg/cm^2).

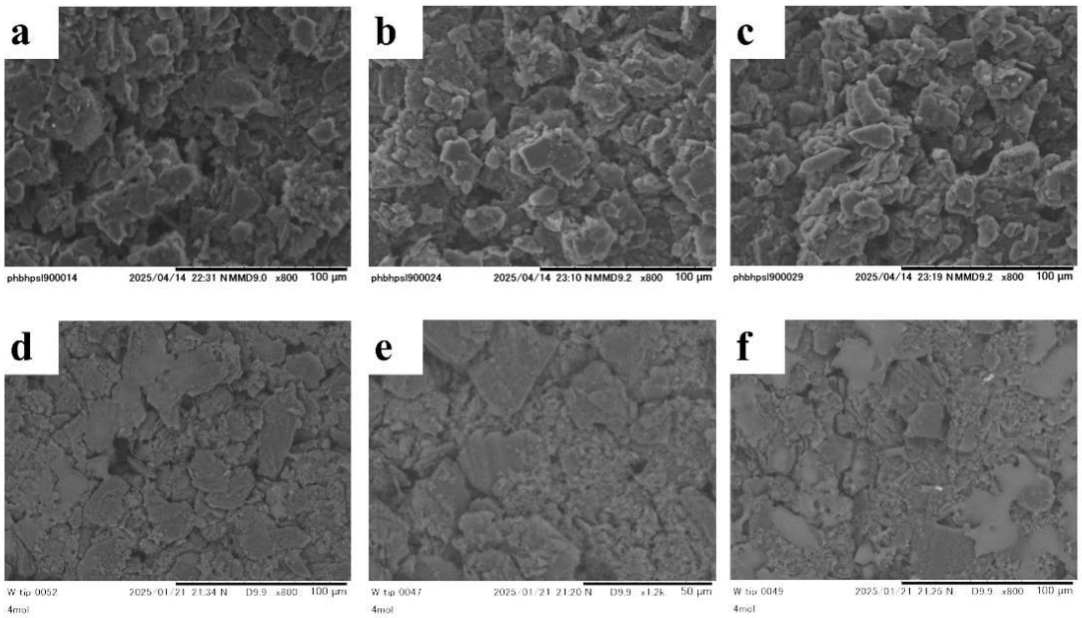

Figure 3.14. SEM of CMC-SBR-based anodes after long cycling at (a) 1 C, (b) 2 C, and (c) 5 C, and [Choline][Pectate]-based anodes after long cycling at (d) 1 C, (e) 2 C, (f) 5 C.

After long cycling at 1 C, 2 C, and 5 C, the cells were disassembled to examine the morphological differences in the anodes by SEM, as displayed in **Figure 3.14**. CMC-SBR-based anode at 1 C (**Figure 3.14a**) exhibited a relatively dense surface with aggregated particle clusters and visible cracking, indicative of moderate structural degradation. As the current density increased to 2 C and 5 C (**Figures 3.14b** and **3.14c**), the surface became increasingly disrupted, characterized by pronounced particle detachment, severe cracking, and porous morphologies, which signified a substantial loss of structural integrity at higher rates. In contrast, [Choline][Pectate]-based anode demonstrated significantly improved morphological stability. At 1 C (**Figure 3.14d**), the surface was uniform, compact, and largely free of cracks, suggesting effective structural stability and strong binder cohesion. When subjected to higher current densities of 2 C and 5 C (**Figures 3.14e** and **3.14f**), the electrode surface remained

relatively smooth and continuous, with only minor morphological changes compared to the 1 C condition. These SEM observations are consistent with the electrochemical results, reinforcing the conclusion that [Choline][Pectate] binder offers superior mechanical stability and resistance to degradation. This enables enhanced cycling performance, particularly under high-rate conditions.[59]

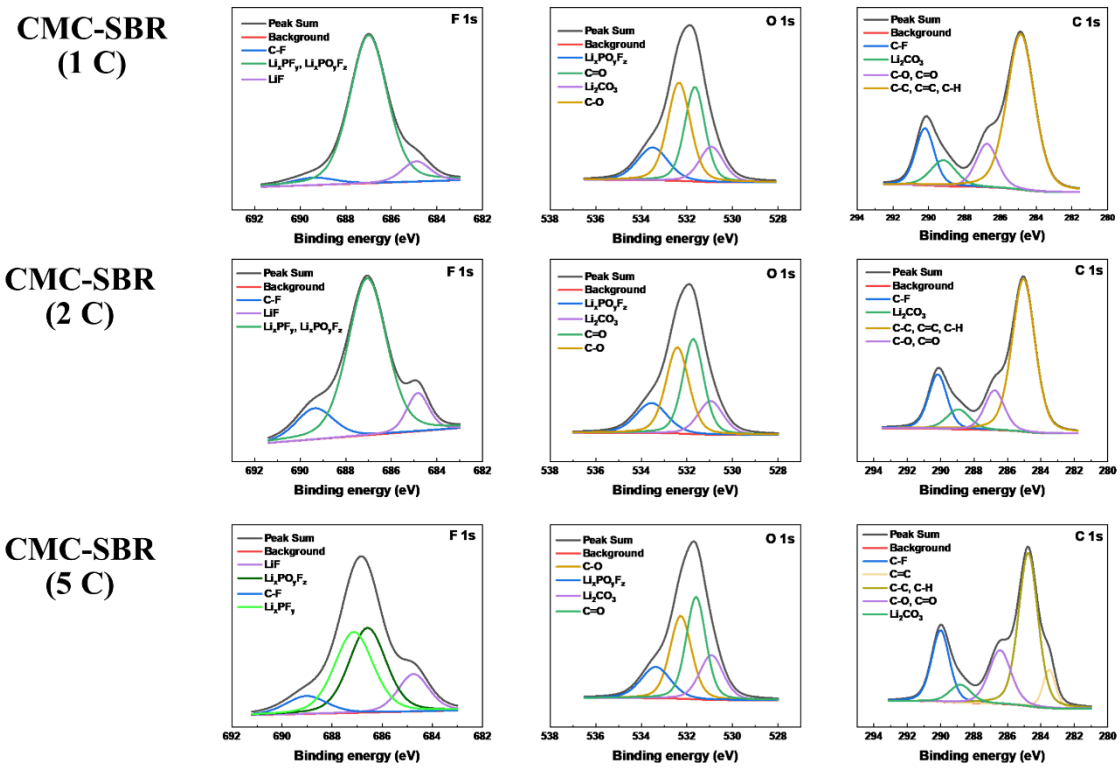

Figure 3.15. F 1s, O 1s, and C 1s XPS spectra of cycled electrode with CMC-SBR binder.

To draw insights into the surface chemistry, SEI composition, and the stability of the anodes under various cycling rates, XPS analysis was conducted. **Figures 3.15** and **3.16** present F 1s, O 1s, and C 1s spectra of cycled electrodes using CMC-SBR and [Choline][Pectate] binders at 1 C, 2 C, and 5 C. In F 1s spectra, peaks corresponding to LiF, $Li_xPO_yF_z$, Li_xPF_y and

C-F were identified. Among these, LiF, $Li_xPO_yF_z$, and Li_xPF_y were key SEI components, with LiF contributing significantly to both chemical and mechanical stability. The presence of C-F was attributed to reactions between the lithium salt and the electrode. As current density increased, the intensity of LiF, $Li_xPO_yF_z$, and Li_xPF_y peaks also rose, indicating enhanced electrolyte decomposition at higher current densities. Notably, [Choline][Pectate]-based electrodes exhibited more stable F-containing species with no C-F signal, suggesting superior resistance to electrolyte degradation.[60]

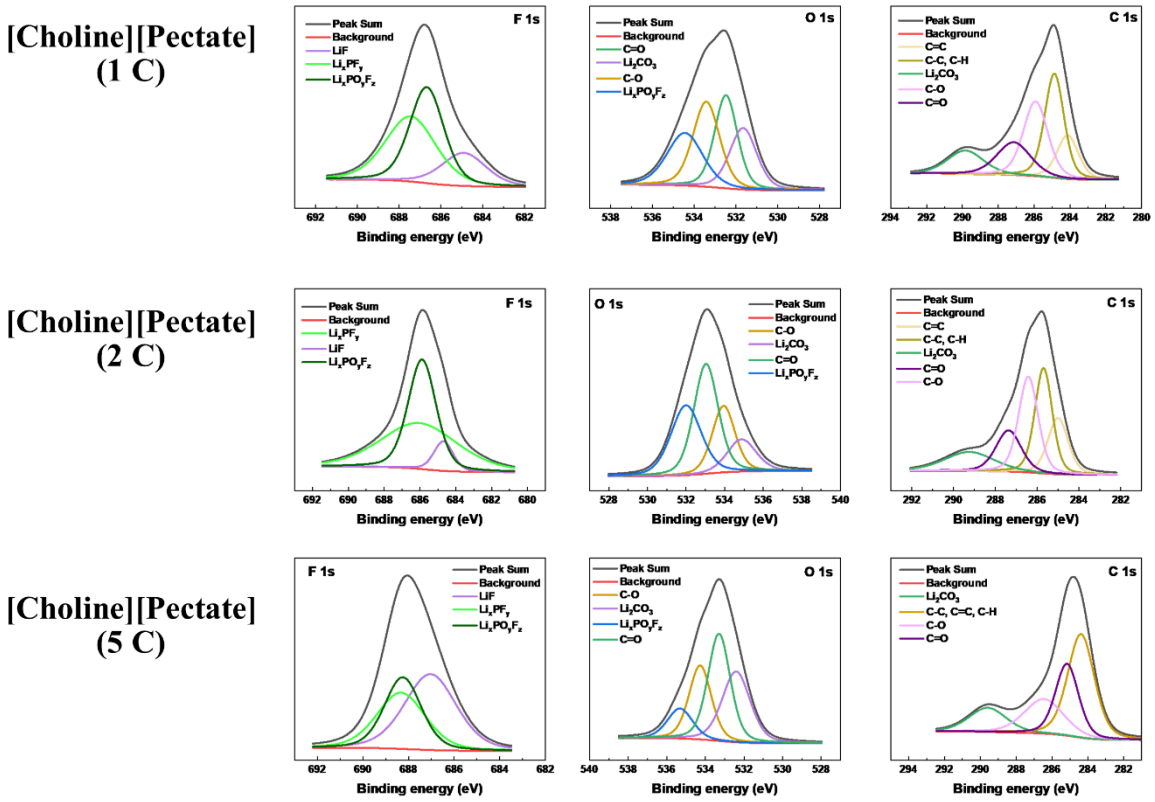

Figure 3.16. F 1s, O 1s, and C 1s XPS spectra of cycled electrode with [Choline][Pectate] binder.

In O 1s spectra, peaks corresponding to Li_2CO_3, $Li_xPO_yF_z$, C=O, and C-O were observed. Li_2CO_3 and $Li_xPO_yF_z$ were indicative of electrolyte decomposition and SEI formation, while C=O and C-O arose mainly from the binders themselves and fewer decomposition byproducts.

Compared to CMC-SBR-based samples, which displayed stronger C=O and C-O signals, [Choline][Pectate] electrodes showed relatively weaker binder-related peaks and more prominent SEI-related peaks, indicating improved electrochemical stability and more uniform SEI formation.[61]

In C 1s spectra, characteristic peaks corresponding to C-C/C-H, C-O, C=O, and Li_2CO_3 were observed. For CMC-SBR electrodes, Li_2CO_3 peak intensity increased at high current density (5 C), indicating more pronounced SEI formation and side reactions at higher rates. In contrast, [Choline][Pectate] electrodes exhibited a more stable and uniform SEI composition, characterized by lower carbonate accumulation and fewer decomposition byproducts. These findings suggest that [Choline][Pectate] binder effectively promotes the formation of a robust and consistent SEI across varying current densities, thereby enhancing interfacial stability.[62]

3.4 Conclusion

In this study, a water-soluble PIL, [Choline][Pectate], as a novel binder for electrodes was proposed to enhance the overall performance of LIBs. The use of [Choline][Pectate] eliminates the need for toxic organic solvents during anode preparation and, owing to its biodegradability, further reduces the environmental impact associated with waste LIBs. Additionally, the incorporation of $[Choline]^+$ cation contributes to improved electrochemical performance, including a lower delithiation overpotential, higher D_{Li}^+, and reduced R_{CT}. Meanwhile, $[Pectate]^-$ anion, serving as a polymeric backbone, ensures both electrochemical and structural stability of the anode. As a result, half-cells utilizing [Choline][Pectate] exhibit higher specific capacity and superior capacity retention compared to those using CMC-SBR binders. Notably, at high current densities (2 C and 5 C), [Choline][Pectate]-based anodes effectively mitigate

Li^+ depletion and suppress undesirable side reactions during long cycling, maintaining high capacity and offering promising potential for fast-charging and high-power applications. Furthermore, the excellent performance of [Choline][Pectate]-based anodes in the full-cell configuration with NCM cathode highlights their practical viability for real-world applications.

References

(1) Li, M.; Lu, J.; Chen, Z.; Amine, K. 30 Years of Lithium-Ion Batteries. *Advanced Materials*. **2018**, *30* (33). https://doi.org/10.1002/adma.201800561.

(2) Lingappan, N.; Kong, L.; Pecht, M. The Significance of Aqueous Binders in Lithium-Ion Batteries. *Renewable and Sustainable Energy Reviews*. **2021**, *147*, 111227. https://doi.org/10.1016/j.rser.2021.111227.

(3) Zhong, X.; Han, J.; Chen, L.; Liu, W.; Jiao, F.; Zhu, H.; Qin, W. Binding Mechanisms of PVDF in Lithium Ion Batteries. *Applied Surface Science.* **2021**, *553* (4), 149564. https://doi.org/10.1016/j.apsusc.2021.149564.

(4) Lux, S. F.; Schappacher, F.; Balducci, A.; Passerini, S.; Winter, M. Low Cost, Environmentally Benign Binders for Lithium-Ion Batteries. *Journal of The Electrochemical Society.* **2010**, *157* (3), A320-A325. https://doi.org/10.1149/1.3291976.

(5) Wu, Q.; Ha, S.; Prakash, J.; Dees, D. W.; Lu, W. Investigations on High Energy Lithium-Ion Batteries with Aqueous Binder. *Electrochimica Acta.* **2013**, *114*, 1-6. https://doi.org/10.1016/j.electacta.2013.09.068.

(6) Courtel, F. M.; Niketic, S.; Duguay, D.; Abu-Lebdeh, Y.; Davidson, I. J. Water-Soluble Binders for MCMB Carbon Anodes for Lithium-Ion Batteries. *Journal of Power Sources.* **2011**, *196* (4), 2128-2134. https://doi.org/10.1016/j.jpowsour.2010.10.025.

(7) Yoon, J.; Lee, J.; Kim, H.; Kim, J.; Jin, H. J. Polymeric Binder Design for Sustainable Lithium-Ion Battery Chemistry. *Polymers*. **2024**, *16* (2), 254. https://doi.org/10.3390/polym16020254.

(8) Qiu, L.; Yang, W.; Hu, X. B.; Li, W. S. High Performance Study of Lithium Carboxymethylcellulose as Water-Soluble Binder for Lithium Supplementation in Lithium Batteries. *Starch-Staerke.* **2022**, *74* (7-8). https://doi.org/10.1002/star.202200049.

(9) Buqa, H.; Holzapfel, M.; Krumeich, F.; Veit, C.; Novák, P. Study of Styrene Butadiene Rubber and Sodium Methyl Cellulose as Binder for Negative Electrodes in Lithium-Ion Batteries. *Journal of Power Sources.* **2006**, *161* (1), 617-622. https://doi.org/10.1016/j.jpowsour.2006.03.073.

(10) Magasinski, A.; Zdyrko, B.; Kovalenko, I.; Hertzberg, B.; Burtovyy, R.; Huebner, C. F.; Fuller, T. F.; Luzinov, I.; Yushin, G. Toward Efficient Binders for Li-Ion Battery Si-Based Anodes: Polyacrylic Acid. *ACS Applied Materials & Interfaces.* **2010**, *2* (11), 3004-3010. https://doi.org/10.1021/am100871y.

(11) Chen, C.; Lee, S. H.; Cho, M.; Kim, J.; Lee, Y. Cross-Linked Chitosan as an Efficient Binder for Si Anode of Li-Ion Batteries. *ACS Applied Materials & Interfaces.* **2016**, *8* (4), 2658-2665. https://doi.org/10.1021/acsami.5b10673.

(12) Zhang, S.; Ren, S.; Han, D.; Xiao, M.; Wang, S.; Meng, Y. Aqueous Sodium Alginate as Binder: Dramatically Improving the Performance of Dilithium Terephthalate-Based Organic Lithium Ion Batteries. *Journal of Power Sources.* **2019**, *438*, 227007. https://doi.org/10.1016/j.jpowsour.2019.227007.

(13) Hou, J.; Qu, S.; Yang, M.; Zhang, J. Materials and Electrode Engineering of High Capacity Anodes in Lithium Ion Batteries. *Journal of Power Sources*. **2020**, *450* (2), 227697. https://doi.org/10.1016/j.jpowsour.2019.227697.

(14) Wang, R.; Feng, L.; Yang, W.; Zhang, Y.; Zhang, Y.; Bai, W.; Liu, B.; Zhang, W.; Chuan, Y.; Zheng, Z.; Guan, H. Effect of Different Binders on the Electrochemical Performance of Metal Oxide Anode for Lithium-Ion Batteries. *Nanoscale Research Letters.* **2017**, *12* (1). https://doi.org/10.1186/s11671-017-2348-6.

(15) Lee, J. H.; Lee, S.; Paik, U.; Choi, Y. M. Aqueous Processing of Natural Graphite Particulates for Lithium-Ion Battery Anodes and Their Electrochemical Performance. *Journal of Power Sources.* **2005**, *147* (1-2), 249-255. https://doi.org/10.1016/j.jpowsour.2005.01.022.

(16) Chen, B.; Zhang, Z.; Xiao, M.; Wang, S.; Huang, S.; Han, D.; Meng, Y. Polymeric Binders Used in Lithium Ion Batteries: Actualities, Strategies and Trends. *ChemElectroChem*. **2024**, *11* (14). https://doi.org/10.1002/celc.202300651.

(17) Yen, J. P.; Chang, C. C.; Lin, Y. R.; Shen, S. T.; Hong, J. L. Effects of Styrene-Butadiene Rubber/Carboxymethylcellulose (SBR/CMC) and Polyvinylidene Difluoride (PVDF) Binders on Low Temperature Lithium Ion Batteries. *Journal of The Electrochemical Society.* **2013**, *160* (10), A1811-A1818. https://doi.org/10.1149/2.083310jes.

(18) Dobryden, I.; Montanari, C.; Bhattacharjya, D.; Aydin, J.; Ahniyaz, A. Bio-Based Binder Development for Lithium-Ion Batteries. *Materials*. **2023**, *16* (16), 5553. https://doi.org/10.3390/ma16165553.

(19) Shin, D.; Park, H.; Paik, U. Cross-Linked Poly(Acrylic Acid)-Carboxymethyl Cellulose and Styrene-Butadiene Rubber as an Efficient Binder System and Its Physicochemical Effects on a High Energy Density Graphite Anode for Li-Ion Batteries. *Electrochemistry Communications.* **2017**, *77*, 103-106. https://doi.org/10.1016/j.elecom.2017.02.018.

(20) Müllner, S.; Michlik, T.; Reichel, M.; Held, T.; Moos, R.; Roth, C. Effect of Water-Soluble CMC/SBR Binder Ratios on Si-RGO Composites Using Mm- and Nm-Sized Silicon as Anode Materials for Lithium-Ion Batteries. *Batteries.* **2023**, *9* (5), 248. https://doi.org/10.3390/batteries9050248.

(21) Yuan, J.; Mecerreyes, D.; Antonietti, M. Poly(Ionic Liquid)s: An Update. *Progress in Polymer Science*. **2013**, *38* (7), 1009-1036. https://doi.org/10.1016/j.progpolymsci.2013.04.002.

(22) Jayakumar, T. P.; Badam, R.; Matsumi, N. Allylimidazolium-Based Poly(Ionic Liquid) Anodic Binder for Lithium-Ion Batteries with Enhanced Cyclability. *ACS Applied Energy Materials.* **2020**, *3* (4), 3337-3346. https://doi.org/10.1021/acsaem.9b02376.

(23) Grygiel, K.; Lee, J. S.; Sakaushi, K.; Antonietti, M.; Yuan, J. Thiazolium Poly(Ionic Liquid)s: Synthesis and Application as Binder for Lithium-Ion Batteries. *ACS Macro Letters.* **2015**, *4* (12), 1312-1316. https://doi.org/10.1021/acsmacrolett.5b00655.

(24) Hernández-Sánchez, A.; Alcaraz-Espinoza, J. J.; Thomas, C. S.; Jiménez-Regalado, E.; Mayrén, A.; González, I.; Sánchez, G. R. Choline Based Poly-Ionic Liquid as Outstanding Binder for Li[Sbnd]S Batteries. *Journal of Energy Storage.* **2025**, *106*. 114746. https://doi.org/10.1016/j.est.2024.114746.

(25) Moosavi, M.; Banazadeh, N.; Torkzadeh, M. Structure and Dynamics in Amino Acid Choline-Based Ionic Liquids: A Combined QTAIM, NCI, DFT, and Molecular Dynamics Study. *Journal of Physical Chemistry B.* **2019**, *123* (18), 4070-4084. https://doi.org/10.1021/acs.jpcb.9b01799.

(26) Yong, T.; Zhang, L.; Wang, J.; Mai, Y.; Yan, X.; Zhao, X. Novel Choline-Based Ionic Liquids as Safe Electrolytes for High-Voltage Lithium-Ion Batteries. *Journal of Power Sources.* **2016**, *328*, 397-404. https://doi.org/10.1016/j.jpowsour.2016.08.044.

(27) Lee, T. H. W. *Thermophysical and Electrochemical Properties Measurements of Novel Choline-Based Ionic Liquids. THESIS*. **2025**, University of Nottingham Malaysia. https://eprints.nottingham.ac.uk/id/eprint/80023.

(28) Mobin, M.; Aslam, R.; Salim, R.; Kaya, S. An Investigation on the Synthesis, Characterization and Anti-Corrosion Properties of Choline Based Ionic Liquids as Novel and Environmentally Friendly Inhibitors for Mild Steel Corrosion in 5% HCl. *Journal of Colloid and Interface Science*. **2022**, *620* (1), 293-312. https://doi.org/10.1016/j.jcis.2022.04.036.

(29) Zhang, R.; Ahmed, A.; Yu, B.; Cong, H.; Shen, Y. Preparation, Application and Development of Poly(Ionic Liquid) Microspheres. *Journal of Molecular Liquids*. **2022**, *362* (11), 119706. https://doi.org/10.1016/j.molliq.2022.119706.

(30) Shaplov, A. S.; Ponkratov, D. O.; Vygodskii, Y. S. Poly(Ionic Liquid)s: Synthesis, Properties, and Application. *Polymer Science - Series B*. **2016**, 58 (2), 73-142. https://doi.org/10.1134/S156009041602007X.

(31) Eftekhari, A.; Shakerian, M.; Majeed, H. J.; Eftekhari, M.; Rezazadeh, N. Pectic Acid–Graphene Oxide Nanocomposite as an Adsorbent in Vortex-Assisted Dispersive Solid-Phase Extraction for Preconcentration of Copper Ion Followed by Flame Atomic Absorption Spectrometry. *Polymer Bulletin*. **2020**, *77* (6), 2821-2836. https://doi.org/10.1007/s00289-019-02884-y.

(32) Ndour, M.; Bonnet, J., P.; Cavalaglio, S.; Lombard, T.; Safran, J.; Pau-Roblot, C.; Bonnet, V. Enzymatically demethylated pectins: From fruit waste to an outstanding polymer binder for silicon-based anodes of Li-ion batteries. *New Journal of Chemistry*. 2023, *47* (37), 17499-17507. https://doi.org/10.1039/D3NJ02736H.

(33) Vajekar, S. N.; Shankarling, G. S. Highly Efficient Green Synthesis of the Photochromic Spironaphthoxazines Using an Eco-Friendly Choline Hydroxide Catalyst. *Synthetic Communications*. **2020**, *50* (3), 338-347. https://doi.org/10.1080/00397911.2019.1694690.

(34) Demir, D.; Ceylan, S.; Göktürk, D.; Bölgen, N. Extraction of Pectin from Albedo of Lemon Peels for Preparation of Tissue Engineering Scaffolds. *Polymer Bulletin*. **2021**, *78* (4), 2211-2226. https://doi.org/10.1007/s00289-020-03208-1.

(35) Delso, I.; Lafuente, C.; Muñoz-Embid, J.; Artal, M. NMR Study of Choline Chloride-Based Deep Eutectic Solvents. *Journal of Molecular Liquids*. **2019**, *290*, 111236. https://doi.org/10.1016/j.molliq.2019.111236.

(36) Veroutis, E.; Merz, S.; Eichel, R. A.; Granwehr, J. Intra- and Inter-Molecular Interactions in Choline-Based Ionic Liquids Studied by 1D and 2D NMR. *Journal of Molecular Liquids*. **2021**, *322* (80), 114934. https://doi.org/10.1016/j.molliq.2020.114934.

(37) Huamani-Palomino, R. G.; M., P. R.; Oliveira, G.; Kock, F. V. C.; Venâncio, T.; Córdova, B. M. Structural Elucidation of Pectin Extracted from Cocoa Pod Husk (Theobroma Cacao L.): Evaluation of the Degree of Esterification Using FT-IR and 1H NMR. *Biomass Conversion and Biorefinery*. **2023**, *15*, 2047-2061. https://doi.org/10.1007/s13399-023-04082-3.

(38) Patra, A.; Matsumi, N. Densely Imidazolium Functionalized Water Soluble Poly(Ionic Liquid) Binder for Enhanced Performance of Carbon Anode in Lithium/Sodium-Ion Batteries. *Advanced Energy Materials*. **2024**, *15* (5). https://doi.org/10.1002/aenm.202403071.

(39) Peled, E.; Menkin, S. Review—SEI: Past, Present and Future. *Journal of The Electrochemical Society*. **2017**, *164* (7), A1703-A1719. https://doi.org/10.1149/2.1441707jes.

(40) Zheng, B.; Zhou, W.; Liu, H.; Chen, S.; Gao, P.; Wang, Z.; Liu, J. Surface Chemistry Induced Robust SEI on Graphite Surface via Soft Carbon Coating Enables Fast Lithium Storage. *Carbon*. **2024**, *218* (31), 118729. https://doi.org/10.1016/j.carbon.2023.118729.

(41) Zhu, X.; Cao, B.; Yan, C.; Tang, C.; Chen, A.; Zhang, Q. Advances in Coating Strategies for Graphite Anodes in Lithium-Ion Batteries. *Acta Physico-Chimica Sinica*. **2025**, 100096. https://doi.org/10.1016/j.actphy.2025.100096.

(42) Li, C.; Deng, Y.; Wang, K.; Li, S.; Meng, X.; Chen, M.; Liao, Y.; Xing, L.; Xu, M. Q.; Li, W. Insight into the Enforced Stability of the Solid Electrolyte Interphase on the Graphite Anode by Prelithiation. *Journal of Physical Chemistry Letters*. **2024**, *15* (35), 9105-9112. https://doi.org/10.1021/acs.jpclett.4c01891.

(43) Jeong, H. T.; Kim, W. J. Enhancing Durability and Capacity Retention of Ultrafine-Grained Aluminum Foil Anodes in Lithium-Ion Batteries. *ACS Applied Materials & Interface* . **2024**, *16* (11), 13662-13673. https://doi.org/10.1021/acsami.3c17359.

(44) Schweigart, P.; Hua, W.; Sánchez, P. A.; Lian, C.; Nylund, I.; Wragg, D.; Lai, S. Y.; Cova, F.; Svensson, A. M.; Blanco, M. V. Deciphering the Impact of Current, Composition, and Potential on the Lithiation Behavior of Si-Rich Silicon-Graphite Anodes. *Small*. **2025**, *21* (4). https://doi.org/10.1002/smll.202406615.

(45) Xu, K. Electrolytes and Interphases in Li-Ion Batteries and Beyond. *Chemical Reviews*. **2014**, *114* (23), 11503-11618. https://doi.org/10.1021/cr500003w.

(46) Mantripragada, B. S.; Patnaik, K. S.; Higashimine, K.; Badam, R.; Matsumi, N. POP Based Nitrogen Containing Anodic Materials for High Capacity and Fast Charge-Discharge Applications in LIB. *Electrochemistry Communications*. **2023**, *157*, 107616. https://doi.org/10.1016/j.elecom.2023.107616.

(47) Varma, A.; Badam, R.; James, A. L.; Higashimine, K.; Jasuja, K.; Matsumi, N. Titanium Diboride-Based Hierarchical Nanosheets as Anode Material for Li-Ion Batteries. *ACS Applied Nano Materials*. **2022**, *5* (11), 16154-16163. https://doi.org/10.1021/acsanm.2c03054.

(48) Zheng, H.; Zhang, L.; Liu, G.; Song, X.; Battaglia, V. S. Correlationship between Electrode Mechanics and Long-Term Cycling Performance for Graphite Anode in Lithium Ion Cells. *Journal of Power Sources*. **2012**, *217*, 530-537. https://doi.org/10.1016/j.jpowsour.2012.06.045.

(49) Mao, C.; Wood, M.; David, L.; An, S. J.; Sheng, Y.; Du, Z.; Meyer, H. M.; Ruther, R. E.; Wood, D. L. Selecting the Best Graphite for Long-Life, High-Energy Li-Ion Batteries. *Journal of The Electrochemical Society*. **2018**, *165* (9), A1837-A1845. https://doi.org/10.1149/2.1111809jes.

(50) Sun, C.; Ji, X.; Weng, S.; Li, R.; Huang, X.; Zhu, C.; Xiao, X.; Deng, T.; Fan, L.; Chen, L.; Wang, X.; Wang, C.; Fan, X. 50C Fast-Charge Li-Ion Batteries Using a Graphite Anode. *Advanced Materials*. **2022**, *34* (43). https://doi.org/10.1002/adma.202206020.

(51) Gautam, M.; Mishra, G. K.; Bhawana, K.; Kalwar, C. S.; Dwivedi, D.; Yadav, A.; Mitra, S. Relationship between Silicon Percentage in Graphite Anode to Achieve High-Energy-Density Lithium-Ion Batteries. *ACS Applied Materials & Interfaces*. **2024**, *16* (35), 45809-45820. https://doi.org/10.1021/acsami.4c10178.

(52) Maruyama, S. Operando Raman Observation of Lithium-Ion Battery Graphite Composite Electrodes with Various Densities and Thicknesses. *Electrochimica Acta*. **2024**, *498*, 144611. https://doi.org/10.1016/j.electacta.2024.144611.

(53) Güneren, A.; Nada, A. A.; Šišková, A. O.; Mosnáčková, K.; Kleinová, A.; Mosnáček, J.; Lenčéš, Z. Novel Alginate-Based Binders for Silicon–Graphite Anodes in Lithium-Ion Batteries: Effect of Binder Chemistry on the Electrochemical Performance. *Journal of Applied Electrochemistry*. **2024**, *54* (6), 1409-1423. https://doi.org/10.1007/s10800-023-02038-z.

(54) Tian, C.; Li, Y.; Gong, Y.; Wu, C.; Bai, Y. Insights and Applications of Electrochemical Techniques and Devices in Rechargeable Batteries. *ACS Applied Energy Materials*. **2025**, *8* (8), 4915-4931. https://doi.org/10.1021/acsaem.4c03347.

(55) Nilsson, J. F. Low temperature Li-ion battery ageing. *Thesis*. Diva-portal.org/smash/get/diva2:805776/FULLTEXT01.pdf.

(56) Rakhatkyzy, M., Belgibayeva, A., Kalimuldina, G., Nurpeissova, A., & Bakenov, Z. (2023). Enhancing low-temperature characteristics of graphite anode by comprehensive modification of electrolyte. *Electrochemistry Communications.* **2023**, 157(000), 7.

(57) Li, Y.; Bettge, M.; Polzin, B.; Zhu, Y.; Balasubramanian, M.; Abraham, D. P. Understanding Long-Term Cycling Performance of Li 1.2 Ni 0.15 Mn 0.55 Co 0.1 O 2 –Graphite Lithium-Ion Cells. *Journal of the Electrochemical Society*. **2013**, *160* (5), A3006-A3019. https://doi.org/10.1149/2.002305jes.

(58) Wu, J.; Cao, Y.; Zhao, H.; Mao, J.; Guo, Z. The Critical Role of Carbon in Marrying Silicon and Graphite Anodes for High-Energy Lithium-Ion Batteries. *Carbon Energy*. **2019**, *1* (1), 57-76. https://doi.org/10.1002/cey2.2.

(59) Takamori, N.; Yamazaki, T.; Furukawa, T.; Jayakumar, T. P.; Badam, R.; Matsumi, N. Facile Stabilization of Microsilicon Oxide Based Li-Ion Battery Anode Using Poly(Vinylphosphonic Acid). *ACS Applied Energy Materials*. **2024**, *7* (4), 1403-1410. https://doi.org/10.1021/acsaem.3c02127.

(60) Lu, M.; Cheng, H.; Yang, Y. A Comparison of Solid Electrolyte Interphase (SEI) on the Artificial Graphite Anode of the Aged and Cycled Commercial Lithium Ion Cells. *Electrochimica Acta*. **2008**, *53* (9), 3539-3546. https://doi.org/10.1016/j.electacta.2007.09.062.

(61) Zhang, G.; Wei, X.; Han, G.; Dai, H.; Zhu, J.; Wang, X.; Tang, X.; Ye, J. Lithium Plating on the Anode for Lithium-Ion Batteries during Long-Term Low Temperature Cycling. *Journal of Power Sources*. **2021**, *484* (2). https://doi.org/10.1016/j.jpowsour.2020.229312.

(62) Liu, Y.; Yang, S.; Guo, H.; Wang, Z.; Liu, J.; Chen, N.; Gong, X. Low LUMO Energy Carbon Molecular Interface to Suppress Electrolyte Decomposition for Fast Charging Natural Graphite Anode. *Energy Storage Materials*. 2024, *73*, 103806. https://doi.org/10.1016/j.ensm.2024.103806.

Chapter 4 Conclusion

This thesis, from the perspective of sustainable development, addresses the limitations of conventional water-soluble binders in maintaining the high performance of lithium-ion batteries (LIBs) during long charge-discharge cycling. To tackle this issue, two novel water-soluble poly(ionic liquid) (PIL) binders were synthesized by neutralizing a biodegradable polymer, polygalacturonic acid (pectic acid), with two ionic liquids: 1-allyl-3-methylimidazolium hydroxide ([AMIm][OH]) and choline hydroxide ([Choline][OH]). This process resulted in the formation of [AMIm][Pectate] and [Choline][Pectate]. The electrochemical properties of these PILs were systematically investigated and demonstrated excellent potential as high-performance anode binders for LIBs.

Chapter 1 provides an overview of recent trends in battery technologies, with a focus on the status and development of LIBs. It highlights the shared goals of the field: to produce batteries that are more environmentally friendly, safer, and longer-lasting. Within this context, the chapter explores the role and importance of anode binders-starting from conventional binders such as polyvinylidene fluoride (PVDF), polyacrylonitrile (PAN), polytetrafluoroethylene (PTFE), carboxymethyl cellulose (CMC), and polyacrylic acid (PAA), to newer alternatives including carboxymethyl cellulose-styrene-butadiene rubber (CMC-SBR), chitosan, alginate, and PILs. The chapter also discusses various strategies proposed to overcome the shortcomings of existing binders, such as enhancing mechanical adhesion, combining with conductive additives or other binders, introducing self-healing capabilities, and developing PIL-based binders, all of which inspired the experimental investigations presented in Chapters 2 and 3.

Chapter 2 explores the performance of [AMIm][Pectate] binder in comparison with widely used PVDF. The PIL binder exhibited superior electrochemical characteristics, including lower delithiation overpotential, enhanced Li^+ transport, reduced SEI resistance, and lower activation energy. Additionally, it demonstrated improved anode stability during long cycling at 1 C. The findings reveal that $[AMIm]^+$ cation significantly contributes to improved electrochemical performance, while $[Pectate]^-$ polymer backbone plays a crucial role in maintaining structural stability. These results represent the first phase of a novel approach to utilizing pectic acid, with its abundant hydroxyl (-OH) groups, as a functional, biodegradable binder in LIBs.

Chapter 3 builds upon the findings of Chapter 2 by shifting the comparison from a non-water-soluble binder (PVDF) to a commonly used water-soluble binder (CMC-SBR). Additionally, the ionic liquid component is changed from [AMIm][OH] to [Choline][OH]. The resulting [Choline][Pectate] binder also showed excellent electrochemical and structural stability, even under higher current densities (2 C and 5 C). Compared to CMC-SBR, [Choline][Pectate] binder was more effective in preventing anode degradation and preserving electrochemical activity during long cycling.

In terms of cation size and structure, $[Choline]^+$ is smaller and more compact, and it can move more easily in the anode during charging and discharging. In contrast, the larger and more flat $[AMIm]^+$ can impede Li^+ transport through steric hindrance, as shown in **Figure 4.1**. This behavior is supported by the measured lithium-ion diffusion coefficients. The higher diffusivity in [Choline]-based system suggests more efficient Li^+ transport and improved activation of storage sites within graphite layers, thereby enhancing the anode's capacity.

Additionally, [Choline][Pectate] shows a lower SEI resistance, indicating a thinner or more stable SEI film. This facilitates lithiation and delithiation, further contributing to its higher capacity. Moreover, the presence of a hydroxyl group in $[Choline]^+$ increases its hydrophilicity, enhancing electrode wettability in liquid electrolytes and promoting a more uniform Li^+ flux at the electrode-electrolyte interface. In conclusion, [Choline][Pectate] offers better electrochemical properties and compatibility, leading to higher capacity at higher current densities.

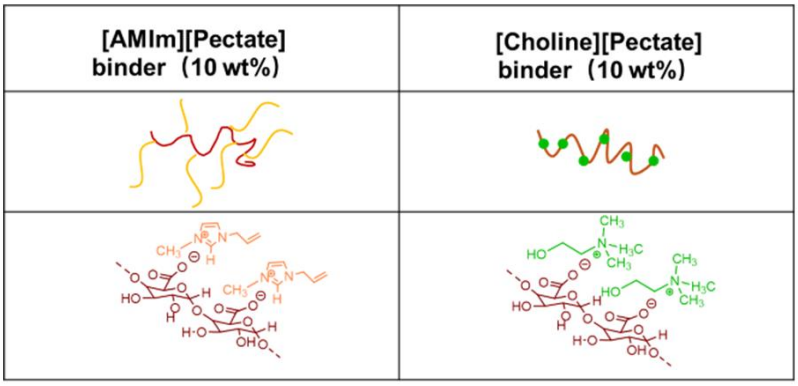

Figure 4.1. Structure comparison between [AMIm][Pectate] and [Choline][Pectate].

The anode material used in this study was graphite, with a theoretical capacity of 372 mAh/g. The results indicate that pectate-based PIL binders are highly effective in this system and hold strong potential for future application in high-capacity anodes, such as silicon (Si), which offers a theoretical capacity of 3597 mAh/g. In fast-charging applications, the high ionic conductivity of [AMIm][Pectate] and [Choline][Pectate] could facilitate rapid Li^+ transport, decreasing charging time and minimizing heat generation. For large-scale energy storage systems integrated into power grid, the biodegradability and sustainability of water-soluble

pectate-based binders would not impose any burden on the environment. At the same time, their stability at high current densities makes them suitable for grid-level applications that require frequent charge-discharge processes.

Looking ahead, future research could focus on optimizing the molecular structure of pectate-based binders to further improve electrochemical properties and mechanical strength simultaneously. In addition, exploring their compatibility with emerging cathode materials could unlock new research directions of pectate-based PIL. The scalability of these binders from lab to industrial production will also be significant for commercialization.

This thesis presents a sustainable and innovative strategy for improving LIB performance through the development of pectic acid-derived PIL binders. By leveraging the biodegradability and functional versatility of pectic acid in combination with ionic liquids, the study introduces a new class of water-soluble binders that significantly enhance electrochemical performance and anode stability. The findings not only contribute to the advancement of environmentally responsible battery technologies but also open new possibilities for high-efficiency energy storage applications in both consumer electronics and large-scale power systems.